2016

Conformations and Dynamics of Semi-Flexible Polymers

Aiqun Huang
University of Central Florida

CONFORMATIONS AND DYNAMICS OF SEMI-FLEXIBLE POLYMERS

by

Aiqun Huang
B.Eng. Chemical Engineering, Zhengzhou University, China, 2008
M.S. Physics, Nanjing University, China, 2011
M.S. Physics, University of Central Florida, Orlando, FL, USA, 2013

A dissertation submitted in partial fulfillment of the requirements
for the degree of Doctor of Philosophy
in the Department of Physics
in the College of Sciences
at the University of Central Florida
Orlando, Florida

Fall Term
2016

Major Professor: Aniket Bhattacharya

ABSTRACT

In this dissertation, we investigate the conformations, transverse fluctuations and dynamics of two-dimensional (2D) semi-flexible polymers both in the bulk and under channel confinement. We present unified scaling relations in regard to various quantities of interest for a broad range of combinations of chain length and chain stiffness using Langevin dynamics simulation. We also present a three-dimensional (3D) heterogeneous semi-flexible chain model for a double stranded DNA (dsDNA). Our model not only confirms the established findings for homogeneous dsDNA, but also predicts new physical phenomenon for heterogeneous dsDNA. The problems studied in this dissertation are relevant to analysis of the conformations and dynamics of biopolymers (such as DNA) in living organisms, and also offer insights for developing devices which operate on the single-molecule level.

In particular, we present a unified description for the dynamics of building-blocks (monomers) of a semi-flexible chain. We consider the full range of flexibility from the case where the chain is fully flexible (no stiffness at all) to the case where the chain behaves like a rod (infinite stiffness). Our theory predicts qualitatively different sub-diffusive regimes for the monomer dynamics originating from the chain stiffness by studying the mean square displacement (MSD) of the monomers before the chain dynamics become purely diffusive.

For the conformations in the bulk, we present results confirmed and agreed by two completely different models of semi-flexible polymers, with one of which is the bead-spring model (studied by Langevin dynamics) in the continuum space, the other (studied by Monte Carlo) is a self-avoiding walk chain on the square lattice, where only discrete bond angles are possible. We point out the universal features of chain conformations and fluctuations which are independent of the models.

For the conformations under channel confinement, we discover qualitatively different conformations and dynamics of the chain as a function of the channel width and chain stiffness, and show how globule like shapes (de Gennes blobs) for more flexible chains continuously go over to shapes in the form of deflections from the wall (Odijk limit) for more stiff chains. We provide theoretical arguments how these regimes occur and interpolate among each other as one varies different parameters of the model. We also demonstrate the effect of physical dimensions (either 2D or 3D) on these regimes and argue that since in 2D the excluded volume (EV) effect is more severe compared to 3D, certain regimes do not exist in 2D.

Finally, we study a model of a dsDNA , where both base-pairing and base-stacking interactions are accounted for albeit at a low computational cost compared to the other existing models. Our model correctly recovers the stiffness for dsDNA and ssDNA at different temperatures. Under most conditions of interest, a dsDNA can locally denature and form bubbles due to thermal fluctuations. At a critical temperature, a dsDNA undergoes a phase transition, in which the two strands of dsDNA completely melt to two single strands (two

ssDNA). By considering EV interactions and calculating the bubble size distribution, recent studies have shown that this denaturation process is a first order transition. We show that for a homogeneous dsDNA made of only AT or GC pairs, our simulation results agree with the previous conclusion of first order transition, however, for sequences of periodic AT and GC regions, when the periodic size is relatively large compared to the sequence length, we show that the bubble size distribution exhibits peaks expressing the sequence pattern, and more importantly, the denaturation is no longer a first order transition.

All these studies reported in the dissertation are relevant to the physics of living systems.

To my family

ACKNOWLEDGMENTS

The time I spent at UCF on my PhD research has been a wonderful experience and a priceless asset, below I thank everyone who has contributed to this unforgettable journey.

First, I am immensely grateful to my advisor Prof. Aniket Bhattacharya for his consistent guidance from the very beginning of my research to the completion of this dissertation. Without him, my accomplishment would be nowhere close to what I have done today. Prof. Bhattacharya introduced me to the field of computational modeling in physics, he has taught me how to translate thinking into code correctly and efficiently and how to analyze problems in terms of physics. I sincerely thank Prof. Bhattacharya for his enormous support and countless ideas, advice in all aspects of my PhD life, and I have enjoyed numerous charming stories he has told about physics and physicists. I deeply believe that what I have learnt from Prof. Bhattacharya will continue to greatly benefit the rest of my life.

I thank my collaborator, a great mentor Prof. Kurt Binder. Without Prof. Binder's clear insight and broad knowledge on this research topic, this dissertation wouldn't be in its current form. Although I never had a chance to meet Prof. Binder in person, I am amazed and admire his life-long over-half-a-century unremittingly fruitful contribution to many fields of physics. I feel honored and proud to have papers coauthored with Prof. Binder.

I also thank Prof. Suren Tatulian, Prof. Viatcheslav Kokoouline and Prof. Andres Campiglia in my dissertation committee for reviewing this thesis and providing suggestions for every bit of its perfection.

I thank my colleague Dr. Ramesh Adhikari with whom I have shared most of my PhD process and worked together closely. Our discussions on many topics (not limited to research) have been very rewarding.

I also feel very fortunate that I met Xin Qiao and Anda Zhang in different parts of my PhD life, it's the company, comfort, support and encouragement they provided that help me to go through the most difficult part of this journey. Without them, I wouldn't have the patience and confidence to get to today. Each of them have taught me a lot in life, from the deepest of my heart I feel indebted and grateful to them.

In the end, I would like to reserve this last paragraph to my family. From the very beginning of my life, my parents have always had huge respect for education and been supportive of my longstanding pursuit in academics, they always put my future first and have invested and sacrificed so much in their life for me that I can never pay back. Without their uncondional love and faith put on me, I wouldn't have achieved what I have today.

TABLE OF CONTENTS

LIST OF FIGURES

LIST OF TABLES

CHAPTER 1
INTRODUCTION

Conformations and dynamics of semi-flexible polymers in bulk as well as under various applied fields, *e.g.*, confining and stretching potentials are of broad general interest in different disciplines of science [1, 2]. Important biopolymers, *e.g.*, dsDNA, F-Actin, microtubules, all have finite bending rigidity κ, often with large persistence lengths and hence the well established and matured theories for fully flexible chains often are not adequate to describe these biopolymers as flexural rigidity plays an important role in their mechanical responses [2]. Interests in these biopolymers continue to remain unabated for multiple reasons. (i) A deeper understanding of biopolymers, *e.g.*, Actin, Titin, Fibrin which offer intriguing patterns with unusual viscoelastic responses will allow to design bio-mimetic materials with improved characteristics, not seen in synthetic polymers; (ii) there is a genuine need to develop efficient separation methods of biomolecules, *e.g.*, DNA sequencing and separation of proteins for various applications pertaining to health and diseases. Finally, due to advent of sophisticated single molecule probes, *e.g.*, fluorescence correlation spectroscopy, atomic force microscope spectroscopy, scanning electron spectroscopy with which one can directly observe the dynamics of the entire chain as well as fluorescence labeled segments of these biomolecules [3]-[4] which offer new findings to be further explored. Of course, also synthetic semi-flexible polymers are of interest in many circumstances; *e.g.*, adsorbed comb

polymers [5] with densely packed side chains (so-called "bottle brush" polymers [6]) can be studied with atomic force microscopy [5, 6] and are of interest for various applications. In these systems the persistence length can be tuned by varying the side chain length.

1.1 The Gaussian chain

Before introducing semi-flexibility, in this section we first briefly review the simplest chain model formed by a random walk on a square lattice without self-avoidance, also known as the Gaussian chain, whose meaning is evinced later.

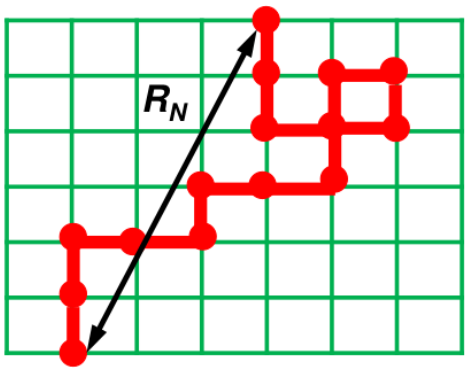

Figure 1.1: A Gussian chain formed by a random walk on a square lattice without self-avoidance. The end-to-end distance is denoted by R_N.

Consider a polymer chain made of N bonds with an identical bond length of b_l, and only 0° and $\pm 90^\circ$ are allowed for angles between neighboring bonds (see Fig. 1.1). Denote

the ith bond vector by $\vec{b}_i$, then the end-to-end vector $\vec{R}_N$ is written as

$$\vec{R}_N = \sum_{i=1}^{N} \vec{b}_i \tag{1.1}$$

It can be easily seen that for a large number of configurations of the chain, the average of the vector $\langle \vec{R}_N \rangle$ is zero, since the bond vectors in all four directions will eventually cancel out during the ensemble average. So we turn our attention to $\langle R_N^2 \rangle$, and

$$\begin{aligned} R_N^2 = \vec{R}_N \cdot \vec{R}_N &= \sum_{i=1}^{N} \vec{b}_i \cdot \sum_{j=1}^{N} \vec{b}_j \\ &= \sum_{i=1}^{N} b_i^2 + \sum_{i,j=1}^{N} \vec{b}_i \cdot \vec{b}_j, \end{aligned} \tag{1.2}$$

under average the second term in the above equation giving zero leads to

$$\langle R_N^2 \rangle = N b_l^2 \tag{1.3}$$

From Eqn. 1.3 we see that the mean square end-to-end distance for a random walk is linear to the chain size N. It should be noted that the derivation of Eqn. 1.3 is independent of the dimensionality, thus it applies for all dimensions of interest. In the simplest case, in one dimension, we can write the probability of the chain of size N having an end-to-end distance $R_N = x$ as

$$P(N, R_N = x) = \frac{1}{2^N} \frac{N!}{N_{\mathrm{L}}! N_{\mathrm{R}}!} \tag{1.4}$$

where N_{L} and N_{R} are the number of bond vectors going left and right respectively, and $R_N = x = N_{\mathrm{R}} - N_{\mathrm{L}}$, $N = N_{\mathrm{R}} + N_{\mathrm{L}}$. It can be shown [1] that for large value of N

$$P(N, R_N = x) \simeq \sqrt{\frac{2}{\pi N}} \exp\left(-\frac{x^2}{2N}\right). \tag{1.5}$$

For two dimensions, by recognizing $\langle R_{Nx}^2 \rangle = \langle R_{Ny}^2 \rangle = \frac{1}{2}\langle R_N^2 \rangle$, the probability for an end-to-end vector $\vec{R}_N$ of a 2D ideal chain is

$$P(N, \vec{R}_N) = \frac{3}{2\pi N b_l^2} \exp\left(-\frac{3R_N^2}{2N}\right), \tag{1.6}$$

which is basically a Gaussian distribution hence the name of Gaussian chain is used in most relevant contexts.

1.2 Kratky-Porod worm-like-chain (WLC) model

Historically the worm-like chain (WLC) model [7, 8] has been the paradigm for theoretical studies of semi-flexible chains. The Hamiltonian corresponding to the bending energy for the WLC model is given by

$$\mathcal{H} = \frac{\kappa}{2} \int_0^L \left(\frac{\partial^2 \mathbf{r}}{\partial s^2}\right)^2 ds, \tag{1.7}$$

where $\mathbf{r}(s)$ is the position vector of a mass point, L is the inextensible contour length, κ is the bending rigidity, and the integration is carried out along the contour s [1, 9]. Using symmetry arguments for the free energy it can be shown [10] that the chain persistence length ℓ_p for a WLC in 2D and 3D are given by

$$\ell_p = \frac{2\kappa}{k_B T} \quad \text{(2D)} \tag{1.8a}$$

$$\ell_p = \frac{\kappa}{k_B T} \quad \text{(3D)} \tag{1.8b}$$

The model has been studied quite extensively applying path integral and other techniques [11, 12, 13, 14] and exact expressions of various moments of the distribution of monomer distances

along the chain have been worked out. The end-to-end distance in the WLC model is given by [1]

$$\frac{\langle R_N^2 \rangle}{L^2} = \frac{2\ell_p}{L}\left(1 - \frac{\ell_p}{L}[1 - \exp(-L/\ell_p)]\right). \tag{1.9}$$

In the limit $\ell_p \ll L$ one gets $\langle R_N^2 \rangle = 2\ell_p L$ and the chain behaves like a Gaussian coil; for $\ell_P \gg L$, $\langle R_N^2 \rangle = L^2$ and the chain behaves like a rod. Evidently the model neglects the excluded volume (EV) (Eqn. 1.13 of the bead-spring model in Sec.-1.3) interaction and hence interpolates between rod and Gaussian limits only.

The WLC model can be viewed as a limiting case of a freely rotating chain [1], where the correlation between bond vectors $\vec{b_i}$ and $\vec{b}_{i+s}$ is assumed to follow

$$\left\langle \hat{b}_i \cdot \hat{b}_{i+s} \right\rangle = b^2 \exp(-s/\ell_p), \tag{1.10}$$

where $|\vec{b_i}| = |\vec{b}_{i+s}| = b$ and the characteristic length is defined as the persistence length ℓ_p, which can also be calculated from the bond angle

$$\ell_p = -\frac{1}{\ln(\cos\theta)}. \tag{1.11}$$

Likewise, dynamics of the WLC model have been explored using Langevin type of equation [15, 16, 17, 14, 18]. One can expect that the dynamics of a stiff chain will be dominated by transverse fluctuations (bending modes) [12] and that the short time dynamics will be governed by the chain persistence length. Indeed a relaxation dynamics using the WLC Hamiltonian (Eqn. 1.7) approach yields an expression for fluctuation

$$\langle (\Delta h)^2 \rangle \sim \ell_p^{-0.25} t^{0.75}. \tag{1.12}$$

which crosses over to simple diffusion at late time [15, 16]. As we will see later from our results that even for a Gaussian chain a more "complete theory" should have captured an intermediate regime characterized by a growth law $t^{0.5}$ for a fully flexible chain for an intermediate time when the fluctuation becomes of the order of radius of gyration of the chain. However, the Langevin theories for the WLC chain did not describe this regime.

1.3 The simulation model

We have used a bead spring model of a polymer chain with excluded volume, spring and bending potentials as follows [19]. The excluded volume interaction between any two monomers is given by a short range Lennard-Jones (LJ) potential with cut off and shifted in its minimum.

$$\begin{aligned} U_{\rm LJ}(r) &= 4\epsilon[(\frac{\sigma}{r})^{12} - (\frac{\sigma}{r})^{6}] + \epsilon \qquad \text{for} \;\; r \leq 2^{1/6}\sigma \\ &= 0 \qquad\qquad\qquad\qquad\qquad\qquad \text{for} \;\; r > 2^{1/6}\sigma \; . \end{aligned} \tag{1.13}$$

Here, σ is the effective diameter of a monomer, and ϵ is the strength of the potential. The connectivity between neighboring monomers is modeled as a Finitely Extensible Nonlinear Elastic (FENE) spring with

$$U_{\rm FENE}(r) = -\frac{1}{2} k R_0^2 \ln(1 - r^2/R_0^2) \; , \tag{1.14}$$

where r is the distance between consecutive monomers, k is the spring constant and R_0 is the maximum allowed separation between connected monomers [19]. The chain stiffness is

introduced by adding an angle dependent interaction between successive bonds as (Fig. 1.2)

$$U_{\rm bend}(\theta_i) = \kappa(1 - \cos\theta_i). \tag{1.15}$$

Here θ_i is the complementary angle between the bond vectors $\vec{b}_{i-1} = \vec{r}_i - \vec{r}_{i-1}$ and $\vec{b}_i = \vec{r}_{i+1} - \vec{r}_i$, respectively, as shown in Fig. 1.2. The strength of the interaction is characterized by the bending rigidity κ. Introducing unit tangent vector $\mathbf{t}_i = \frac{\partial \mathbf{r}_i}{\partial s}$ ($|\mathbf{t}_i| = 1$) we note that the discretized version of Eqn. 1.7 can be written as

$$\begin{aligned} \mathcal{H} \approx \frac{\kappa}{2} b_l \sum_i \left(\frac{\mathbf{t}_{i+1} - \mathbf{t}_i}{b_l} \right)^2 &= \frac{\kappa}{2b_l} \sum_i \left(\mathbf{t}_{i+1}^2 + \mathbf{t}_i^2 - 2\cos\theta_i \right) \\ &= \frac{\kappa}{b_l} \sum_i \left(1 - \cos\theta_i \right), \end{aligned} \tag{1.16}$$

where $b_l = |\vec{b}_i|$ is the bond length in our simulation. Therefore, for fixed bond length Eqn. 1.15 represents the discrete version of the WLC model of Eqn. 1.7. Thus the EV effect introduced through Eqn. 1.13 are completely absent in the WLC model.

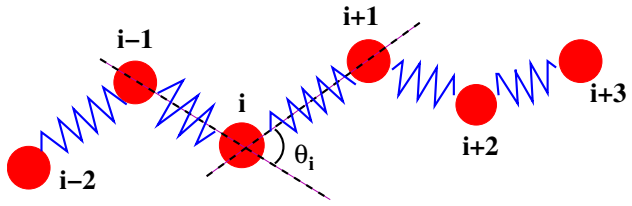

Figure 1.2: Bead-spring model of a polymer chain with bending angle θ_i subtended by the vectors $\vec{b}_{i-1} = \vec{r}_i - \vec{r}_{i-1}$ and $\vec{b}_i = \vec{r}_{i+1} - \vec{r}_i$.

We use the Langevin dynamics [20, 19] with the following equation of motion for the ith monomer

$$m\ddot{\vec{r}}_i = -\nabla(U_{\rm LJ} + U_{\rm FENE} + U_{\rm bend}) - \gamma\vec{v}_i + \vec{R}_i. \tag{1.17}$$

Here γ is the monomer friction coefficient and $\vec{R}_i(t)$, is a Gaussian white noise with zero mean at a temperature T, and satisfies the fluctuation-dissipation relation:

$$< \vec{R}_i(t) \cdot \vec{R}_j(t') >= 4k_B T\gamma\, \delta_{ij}\, \delta(t-t') \; .$$

The reduced units of length, time and temperature are chosen to be σ, $\sigma\sqrt{\frac{m}{\epsilon}}$, and ϵ/k_B respectively. For the spring potential we have chosen $k = 30$ and $R_0 = 1.5\sigma$, the friction coefficient $\gamma = 0.7$, the temperature is kept at $1.2/k_B$. The choice of the FENE potential along with the LJ interaction parameters ensures that the average bond-length in the bulk $\langle b_l \rangle = 0.971$. With the choice of these parameters the probability of chain crossing is very low. We also find that the average bond-length $\langle b_l \rangle$ is almost independent of the range of chain stiffness parameter ($\kappa = 0 - 320$) used in our simulation. Strictly speaking, the contour length L is $L = (N-1)\,\langle b_l \rangle$.

1.4 Integration algorithm of the Langevin equation

The equation of motion 1.17 is integrated with the reduced time step $\Delta t = 0.01$ following the algorithm proposed by van Gunsteren and Berendsen [20]. This algorithm is precise to the third order, and has the advantage that it is not limited by the constraint $\Delta t \ll \gamma^{-1}$ in contrast to other integration methods. Here below we outline this algorithm.

1. Given the initial configuration $\vec{r}(t_0)$, $\vec{v}(t_0)$ and $\vec{F}(t_0)$, where $\vec{F}(t_0)$ is the total force for the considered monomer at $t = t_0$, the position $\vec{r}(t_1)$ at next time step $t_1 = t_0 + \Delta t$ is

obtained as

$$\begin{aligned}\vec{r}(t_1) =&\vec{r}(t_0) + \vec{v}(t_0)\Delta t(\gamma\Delta t)^{-1}\left[1-\exp\left(-\gamma\Delta t\right)\right]\\ &+\frac{1}{m}\vec{F}(t_0)(\Delta t)^2(\gamma\Delta t)^{-2}\left[\gamma\Delta t-\left(1-\exp\left(-\gamma\Delta t\right)\right)\right]\\ &+\frac{k_BT}{m\gamma^2}C(\gamma\Delta t)z_1,\end{aligned} \tag{1.18}$$

where z_1 is a random number following the unit normal distribution $\mathcal{N}(0,1)$, and

$$C(\gamma\Delta t) = 2\gamma\Delta t - 3 + 4\exp\left(-\gamma\Delta t\right) - \exp\left(-2\gamma\Delta t\right) \tag{1.19}$$

2. At current time step $t_n = t_0 + n\Delta t$ with $n = 1, 2, ...$, calculate $\vec{F}(t_n)$ from the force field.

3. Compute the derivative of the force as following

$$\dot{\vec{F}}(t_n) = \frac{\vec{F}(t_n) - \vec{F}(t_{n-1})}{\Delta t} \tag{1.20}$$

4. Sample z_2 from the unit normal distribution $\mathcal{N}(0,1)$, and compute

$$X_n(-\Delta t) = X_{n-1}(\Delta t)G(\Delta t)/C(\Delta t) + \frac{k_BT}{m\gamma^2}\left(E(\gamma\Delta t)/C(\gamma\Delta t)\right)z_2, \tag{1.21}$$

where

$$G(\gamma\Delta t) = \exp\left(\gamma\Delta t\right) - 2\gamma\Delta t - \exp\left(-\gamma\Delta t\right) \tag{1.22a}$$

$$\begin{aligned}E(\gamma\Delta t) =&16\left[\exp\left(\gamma\Delta t\right)+\exp\left(-\gamma\Delta t\right)\right]-4\left[\exp\left(2\gamma\Delta t\right)+\exp\left(-2\gamma\Delta t\right)\right]\\ &-24-4\gamma\Delta t\left[\exp\left(\gamma\Delta t\right)-\exp\left(-\gamma\Delta t\right)\right]\\ &+2\gamma\Delta t\left[\exp\left(2\gamma\Delta t\right)-\exp\left(-2\gamma\Delta t\right)\right]\end{aligned} \tag{1.22b}$$

and resample z_1 from $\mathcal{N}(0,1)$ and calculate

$$X_n(\gamma\Delta t) = \frac{k_B T}{m\gamma^2} C(\gamma\Delta t) z_1 \tag{1.23}$$

From Eqn. 1.21 it is easy to see that $X_n(-\Delta t)$ is correlated with $X_{n-1}(\Delta t)$, and by verifying the following relation

$$G^2(\gamma\Delta t) + E(\gamma\Delta t) = -C(-\gamma\Delta t)C(\gamma\Delta t) \tag{1.24}$$

it is easy to see that $X_n(-\Delta t)$ has a variance of $-k_B T C(-\gamma\Delta t)/(m\gamma^2)$.

5. Advance the position to time step t_{n+1} according to

$$\begin{aligned}
\vec{r}(t_n + \Delta t) = {} & \vec{r}(t_n)\left[1 + \exp\left(-\gamma\Delta t\right)\right] - \vec{r}(t_n - \Delta t)\exp\left(-\gamma\Delta t\right) \\
& + m^{-1} F(t_n)(\Delta t)^2(\gamma\Delta t)^{-1}\left[1 - \exp\left(-\gamma\Delta t\right)\right] \\
& + m^{-1}\dot{F}(t_n)(\Delta t)^3(\gamma\Delta t)^{-2}\left\{\frac{1}{2}\gamma\Delta t\left[1 + \exp\left(-\gamma\Delta t\right)\right] - \left[1 - \exp\left(-\gamma\Delta t\right)\right]\right\} \\
& + X_n(\Delta t) + \exp(-\gamma\Delta t) X_n(-\Delta t) + O(\Delta t^4)
\end{aligned} \tag{1.25}$$

6. Compute the velocity $\vec{v}(t_n)$ as

$$\begin{aligned}
\vec{v}(t_n) = H(\gamma\Delta t)\{ & [\vec{r}(t_n - \Delta t) - \vec{r}(t_n - \Delta t)] \\
& + m^{-1}\vec{F}(t_n)(\Delta t)^2(\gamma\Delta t)^{-2} G(\gamma\Delta t) \\
& - m^{-1}\dot{\vec{F}}(t_n)(\Delta t)^3(\gamma\Delta t)^{-3} G(\gamma\Delta t) \\
& + [X_n(-\Delta t) - X_n(\Delta t)]\}
\end{aligned} \tag{1.26}$$

where

$$H(\gamma\Delta t) = \gamma\Delta t / \left[\exp\left(\gamma\Delta t\right) - \exp\left(-\gamma\Delta t\right)\right]. \tag{1.27}$$

7. Repeat steps from 2 to 6.

1.5 Overview of the thesis

The goal of this thesis is to explore the conformations, transverse fluctuations and monomer dynamics of semi-flexible polymers in the bulk and in the confined environment. In particular, by carrying out extensive computer simulations we show the limitations of existing scaling theories in two dimensions, clarify the boundaries across different scaling regimes, and propose and verify new scaling descriptions. Firstly, we elucidate the role of the intrinsic mechanical property of a polymer - the bending rigidity characterized by its persistence length - in determining the chain conformations and monomer dynamics in the bulk and under channel confinement; secondly, by comparing the simulation results from Langevin dynamics simulations based on the bead-spring model in the continuum space to those from Monte Carlo (MC) simulations on a discrete model, we show interesting agreement and discrepancies; thirdly, we turn to a concrete example, in which we present a coarse grained model for DNA which is one of most important biopolymers. In our model, we incorporate the thermodynamical properties of dsDNA and study their interplay with the bending rigidity. More specifically, the organization of the thesis is as follows.

In Chapter 2, with regard to the conformations we compare the main results of the WLC model to our simulation results. Specifically, we focus on the scaling dependence of end-to-end distance on the persistence length, bond vector correlations, and argue that

how the persistence length has been miscalculated in the literature and how it should be calculated correctly. We also show distributions of end-to-end distances and compare with those obtained analytically under certain approximation. For the monomer dynamics, a scaling theory is derived where we show that monomer dynamics of a semiflexible polymer exhibits *a double crossover* across the early time to the diffusion time scale, we validate the predictions of the scaling theory using Langevin dynamics simulation for chains of different length and stiffness. For the transverse fluctuations, we show novel master scaling plot for chains in broad ranges of chain size and chain stiffness and draw significance and implications of our finding to experiments. In the appendix of this chapter, we also show our scaling theory and results for one-dimensional chains.

In chapter 3 we pay our attention to semi-flexible polymers confined in a quasi-one-dimensional environment. In this chapter we study the extension of a confined polymer as a function of the chain length, the persistence length ℓ_p and the width of the channel D. Different scaling regimes in different limits of ℓ_p/D are summarized as a function of the number of dimensions, d. By carrying out Langevin dynamics simulations, we show that some scaling regimes those exist in three dimensions are missing in two dimensions, and conclude that a 2D strip is a cleaner system to study a stretched chain as the conformations interpolate between de Gennes and Odjik regimes only.

Chapter 4 discusses how the scaling theory and simulation results depend on different models of polymers. One model is the bead-spring model in the continuum space we have used in the previous two chapters, the other one is a self-avoiding model on square

lattice studied by MC simulations. These two models reflect different mechanisms by which the stiffness for different real polymers is realized, for instance, the first model is a crude description of DNA-like biopolymers, while the second model (roughly) describes synthetic polymers like alkane chains. In this chapter, we demonstrate that in the bulk the crossover from rods to self-avoiding walks for both models is very similar, when one studies average chain linear dimensions, transverse fluctuations, etc., despite their differences in local conformations. We continue to show that significant differences between both models arise in quasi-one-dimensional confinement, we compare these differences and analyze the causes. Moreover, we report a method of directly estimating for the Odijk deflection length [21, 22] and its distribution and show the results obtained accordingly.

Chapter 5 presents a heterogeneous semiflexible chain model of dsDNA. In this model, we consider both the mechanical and the thermodynamic characteristics for a dsDNA, and show that the persistence lengths for dsDNA (~ 50 nm) and ssDNA (~ 4 nm) and reasonable melting profiles for different sequences can be both obtained from our Langevin dynamics simulations. We further investigate that when the dsDNA undergoes denaturation at critical temperatures, how the bubble size distribution depends on the heterogeneity of the sequence which further determines the transition order of the DNA melting process.

In chapter 6 we draw conclusions for the thesis and provide outlooks for future work.

In the end of this section, we present a list of publications and unpublished manuscripts which have been generated from this PhD dissertation.

I. **A. Huang**, R. Adhikari, A. Bhattacharya, and K. Binder, *Universal monomer dynamics of a two-dimensional semiflexible chain*, EPL **105**, 18002 (2014).

II. **A. Huang**, A. Bhattacharya, and K. Binder, *Conformations, transverse fluctuations, and crossover dynamics of a semi-flexible chain in two dimensions*, J. Chem. Phys. **140**, 214902 (2014).

III. **A. Huang** and A. Bhattacharya, *DNA confined in a two-dimensional strip geometry*, EPL **106**, 18004 (2014).

IV. **A. Huang**, HP. Hsu, A. Bhattacharya, and K. Binder, *Semiflexible macromolecules in quasi-one-dimensional confinement: Discrete versus continuous bond angles*, J. Chem. Phys. **143**, 243102 (2015).

V. **A. Huang** and A. Bhattacharya, *A Heterogeneous Semiflexible Chain Model of dsDNA*, to be submitted to Phys. Rev. Lett.

CHAPTER 2
CONFORMATIONS, TRANSVERSE FLUCTUATIONS AND CROSSOVER DYNAMICS OF A SEMI-FLEXIBLE CHAIN IN TWO DIMENSIONS

Macromolecules adsorbed on substrate surfaces occur in many different contexts, from materials science to biophysics, *e.g.*, biomolecules interacting with cell membranes. Hence the understanding of conformations and dynamics of macromolecules in such a (quasi-) two-dimensional geometry has been of long-standing interest [23, 24, 25, 26]. Note also that many methods to characterize polymer conformations experimentally, *e.g.*, electron microscopy [27, 28, 29, 30, 31, 32, 33], atomic force microscopy (AFM) [34, 35, 36, 37, 4, 38, 39], fluorescence microscopy of suitably labelled biopolymers [40, 41], require that these macromolecules are attached to a substrate. In this context, considerations of macromolecules confined to a strictly two-dimensional geometry are of interest, at least as a limiting case. The same statement holds when one considers macromolecules confined to nanoslits with non-adsorbing walls, a topic that also has found much recent interest.

While the statistical mechanics of completely flexible polymers in $d = 2$ dimensions has been studied extensively since a long time and is well understood [42, 43], under many circumstances it should be taken into account that macromolecules are stiff and not flexible on small scales [44, 45, 1]. This is true both for simple synthetic polymers *e.g.*, polystyrene, alkane chains, *etc.*, and for various biopolymers, *e.g.*, double-stranded (ds) and

single stranded (ss) DNA, polysaccharides, proteins, *etc.* [46]. Apart from very stiff polymers (*e.g.*, Actin, Titin, microtubules, *etc.*) the "persistence length ℓ_p " [44, 45, 1, 46, 47] characterizing the stiffness typically is much less than the contour length L of a macromolecule, and the crossover from rod-like behavior to the behavior of flexible polymers needs to be considered. As is well-known, the scales of interest range from the sub-nanometer scale to the micrometer scale [48, 49], and hence in the theoretical modeling coarse-grained models must be used [48, 49, 50].

In the present work, we wish to address the problem of polymer conformation and dynamics for semi-flexible polymers in two dimensions, using Molecular Dynamics simulations of a bead-spring type model with a bond angle potential by which we can control the stiffness of the chains over a wide range. We note that the standard analytical coarse-grained description in terms of the Kratky-Porod [51, 52] model for wormlike chains in $d = 2$ dimensions is not very useful, since it neglects excluded volume effects completely, although they are known to be very important in $d = 2$ [53]. A study of semiflexible polymers in terms of a lattice model [53, 54, 55, 56] is expected to yield valid results for universal properties of semiflexible polymer, *i.e.*, on length scales much larger than the persistence length; but on smaller scales it can describe only stiffness of the type similar to that of alkane chains, where ℓ_p is of the order of the typical length of "all trans" sequences, in between monomers taking a gauche ($g\pm$) minimum in the torsional potential. For such cases *e.g.*, dsDNA we expect that the (small) flexibility of the macromolecules is due to fluctuations in bond lengths and bond angles, rather than disorder in the population of states in the torsional potential, and then

the present off-lattice model is more realistic. In addition, the lattice work [53, 54, 55, 56] applying the pruned enriched Rosenbluth method (PERM) [57, 58] could not address the dynamics of the chains at all. Previous work on the dynamics of single semiflexible chains in dilute solution [59, 60, 17, 61, 62, 63, 64, 65, 66] has focused on the case $d = 3$ almost exclusively, and most of the work [59, 60, 17, 61, 62, 63, 64, 65] has studied the effect of hydrodynamic (HD) interactions mediated by the solvent. Assuming that the substrate surface provides a stick boundary condition with respect to solvent fluid flow, one can show [67] that HD interactions are essentially screened, and hence are ignored here (as well as in our preliminary communication where a small part of our results were presented [68]) from the outset.

While the Kratky-Porod Worm-like-chain (WLC) Model has been found to be grossly inadequate to describe a semiflexible chain in 2D, vast amounts of analytical and numerical work have been accumulated using the WLC model as the starting point [11, 60, 12]. Recent experimental results of confined biopolymers on a 2D substrate are also analyzed using the well known results of WLC model [37]. The organization of the chapter is as follows. In the next section a scaling theory is derived where we show that monomer dynamics of a semiflexible polymer exhibits a double crossover as a function of time. The results of BD simulation are presented in Sec. 2.2, which is divided into two sub-sections: The equilibrium properties are presented in Sec. 2.2.1; in Sec. 2.2.2 among other results we validate the predictions of the scaling theory using (BD) simulation for chains of different length and stiffness.

2.1 Scaling description

We first develop the scaling description for the dynamics of a two dimensional semi-flexible chain in the free draining limit. The free draining limit is of particular interest in 2D because it often satisfies the experimental conditions, such as DNA confined in a 2D substrate where the effect of hydrodynamics is negligible. For a WLC several theories based on Langevin dynamics have been developed most of which indicate a $t^{0.75}$ dependence of the transverse fluctuation of the MSD $g_1(t)$ (see Eqn. 2.16a) with time t for the stiff chain. Therefore, we start with the Eqn. 2.1 below derived by Granek [15] and Farge and Maggs [16] using a Langevin dynamics framework for the WLC Hamiltonian

$$g_1(t) = b^2 \left(b/\ell_p\right)^{1/4} (Wt)^{3/4}, \tag{2.1}$$

where W is the monomer reorientation rate. Prefactors of order unity are omitted throughout [69]. For early time the monomer dynamics will be independent of the chain length N until the fluctuations in monomer position become of the order of ℓ_p. Therefore, denoting the time when the first crossover occurs as τ_1 and substituting $g_1 = \ell_p^2$ and $t = \tau_1$ in Eqn. 2.1 we immediately get

$$W\tau_1 = \left(\ell_p/b\right)^3. \tag{2.2}$$

For $0 < t \leq W^{-1}(\ell_p/b)^3$ the monomer dynamics is described by $g_1(t) \sim t^{0.75}$ according to Eqn. 2.1 until $g_1(t) = \ell_p^2$ at time $W^{-1}(\ell_p/b)^3$. The width of this region is independent of N and solely a function of ℓ_p (see Fig. 2.1).

For $\tau_1 < t < \tau_2$ the dynamics is governed by the Rouse relaxation of monomers of a fully flexible EV chain in 2D characterized by $g_1(t) \propto t^{2\nu/(1+2\nu)} = t^{0.6}$. τ_2 characterizes the onset of the purely diffusive regime when $g_1(\tau_2) = \langle R_N^2 \rangle$ [19]. Recall that the exponent ν that describes the scaling of the end-to-end distance $\vec{R}_N$ according to $\langle R_N^2 \rangle \propto N^{2\nu}$ is $\nu = \frac{3}{4}$ in 2D. Note that when we increase the stiffness of the chain at fixed chain length, the times τ_1 and τ_2 can be made to coincide; this happens for $L = Nb = \ell_p$, as expected: when the contour length and the persistence length are of the same order, the regime described by Eqn. 2.4 is no longer present. We will verify the time dependence of g_1 at various regimes from BD simulations.

We then obtain τ_2 as follows:

$$g_1(t) = \ell_p^2 \, (t/\tau_1)^{3/5} \qquad \text{for} \;\; t > \tau_1. \tag{2.3}$$

Substituting τ_1 from Eqn. 2.2 in above

$$g_1(t) = b^2 \, (\ell_p/b)^{1/5} \, (Wt)^{3/5}, \;\; \text{for} \;\; \tau_1 < t < \tau_2. \tag{2.4}$$

At $t = \tau_2$

$$g_1(t = \tau_2) = \langle R_N^2 \rangle = \ell_p^{1/2} L^{3/2}. \tag{2.5}$$

Substituting Eqn. 2.4 for $t = \tau_2$ we get

$$W\tau_2 = (\ell_p/b)^{\frac{1}{2}} \, N^{5/2}. \tag{2.6}$$

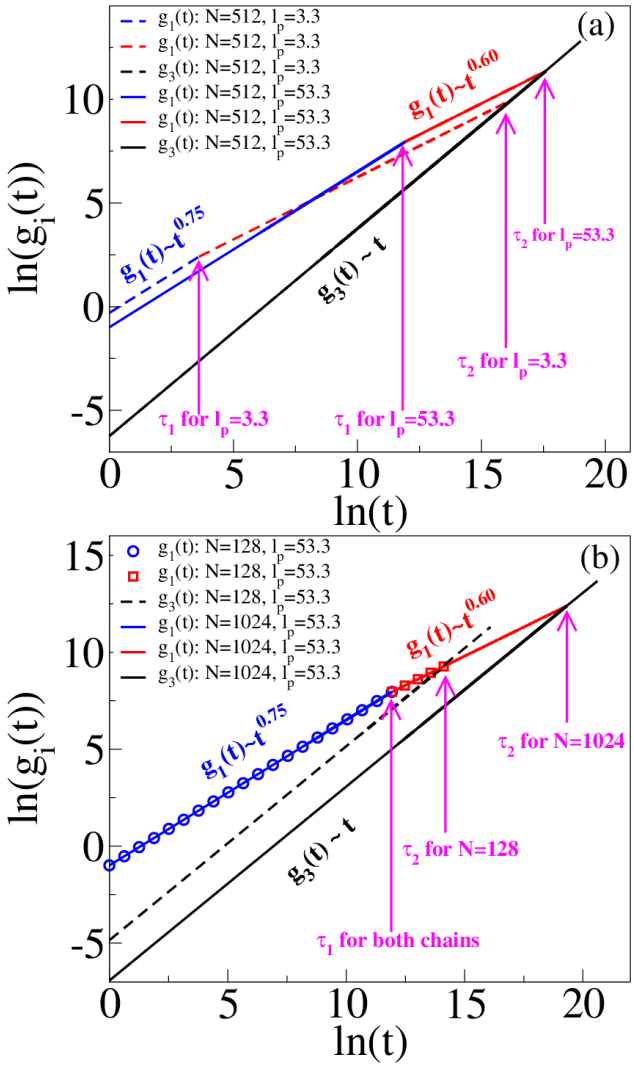

Figure 2.1: Theoretical scaling for $(N, \kappa) \equiv (512, 2)$, $(512, 32)$(a) and $(N, \kappa) \equiv (128, 32)$, $(1024, 32)$(b). Blue (red) symbols, solid and dashed lines correspond to $g_1(t) \sim t^{0.75}(g_1 \sim t^{0.60})$, black dashed, solid lines correspond to $g_3(t) \sim t$. Here the power laws Eqn. 2.1, 2.4 and 2.7 are plotted, using units of $b = 1$, $l_p = 2\kappa/k_BT$, $W = 1$. The width of each region shows how these regimes depend on ℓ_p and N. Note that in reality we expect a very gradual change of slope on the log-log plot at both crossover times, rather than sharp kinks.

We also note that the dynamics of the center of mass is given by

$$g_3(t) = b^2 W \frac{t}{N}. \tag{2.7}$$

The "phase diagram" for the crossover dynamics in terms of N, and ℓ_p are shown in Fig. 2.1. Notice that for a stiffer chain the region for $\tau_1 < t < \tau_2$ for which we predict $g_1(t) \sim t^{0.6}$ requires to study very long chains and therefore, is hard to see in simulation for a stiffer chain.

2.2 Results from Brownian dynamics simulation

We have carried out Brownian dynamics (BD) simulation for a wide range of chain length (N=16 - 2048) and bending constant (κ = 0 - 320). Because of the argument given in Sec. 2.1 very long chains were needed to clearly identify the crossover regimes. First we present the equilibrium properties of the chains in section 2.2.1 followed by the dynamical quantities presented in Sec. 2.2.2.

2.2.1 Equilibrium properties

2.2.1.1 Persistence length

From the BD simulation we have monitored the average $\langle \cos\theta \rangle$ and replacing $\cos\theta \rightarrow \langle \cos\theta \rangle$ in Eqn. 1.11 calculated the chain persistence length for various values of κ. One

expects that Eqns. 1.8a and 1.11 must give results that agree with each other when the persistence length is much larger than the range of the excluded volume interaction, but that the agreement is quite perfect for kappa = 2 already is a nontrivial result (The comparison of calculated ℓ_p by different methods is shown in Table 2.1). The two equations produce practically the same value of ℓ_p. We also observe that the ℓ_p calculated using Eqn. 1.11 practically has no dependence on chain length N. We have used Eqn. 1.11 for further analysis of our data in the subsequent sections. Note that this behavior differs from the result found by Hsu *et al.* for a lattice model [53], where a renormalization of ℓ_p by excluded volume was shown to occur. Thus on length scales of order ℓ_p there is no strict universality between different models.

Table 2.1: Comparison of three ways of calculating ℓ_p

κ	Eqn. 1.8a	Eqn. 1.11	ℓ_p from fitted slope (Fig. 2.5)
64	106.7	105.8	112.4
32	53.3	52.6	53.7
16	26.7	25.9	27.4
8	13.3	12.6	13.7
4	6.7	6.05	6.7
2	3.3	3.31	4.2

We emphasize, however, that the persistence length, when it is supposed to measure the local intrinsic stiffness of the chain (as supposed in the Kratky-Porod model), cannot be estimated from the asymptotic decay of the bond vector correlation function $\langle \vec{b}_i \cdot \vec{b}_{i+s} \rangle$ with

the "chemical distance" s along the chain, that is the conventional definition given in all the polymer physics textbooks: as will be shown below (Sec. 2.2.1.5), we verify the predicted [70] power law behavior for very long chains and large s, previously seen already for a lattice model of semi-flexible chains by Hsu *et al.* [53]. Although lattice and continuum models have different statistical properties when one considers lengths of the scale ℓ_p, for much larger scales the behavior should be universal, and hence this power law decay is expected. We also note that a definition of the persistence length dating back to Flory, where one considers the correlation of the first bond vector $\vec{b}_1$ with the end-to-end vector $\vec{R}_N$,

$$\ell_p^{\text{Flory}} = \langle \vec{b}_1 \cdot \vec{R}_N \rangle / \langle b \rangle \ , \tag{2.8}$$

which has been advocated by Cifra [71] as an "exact expression", must similarly be refuted: in 2D, Redner and Privman [72] have shown that ℓ_p^{Flory} for large N is logarithmically divergent with N already for a simple self-avoiding walk (SAW). For completeness, we mention that an analogous definition for inner bond vectors

$$\ell_p' = \langle \vec{b}_i \cdot \vec{R}_N \rangle / \langle b \rangle \quad , \quad 1 \ll i \ll N \tag{2.9}$$

even shows a power-law divergence, $\ell_p' \propto N^{(2\nu-1)}$, both in 2D and 3D (see Hsu et al. [47] and [73]). Thus we urge that the results and discussion presented in this section need to be taken seriously in writing future review articles and newer edition of the existing textbooks.

2.2.1.2 Scaling of semi-flexible chain: comparison with theory

The extension of Flory theory for a semi-flexible chain has been done by Schaefer, Joanny, and Pincus [59] and Nakanishi [74] which states that the RMS of the end-to-end distance $\langle R_N^2 \rangle$ in d spatial dimensions exhibits the following scaling relation

$$\sqrt{\langle R_N^2 \rangle} \sim N^{\frac{3}{d+2}} \ell_p^{\frac{1}{d+2}} b^{\frac{d-2}{d+2}}, \tag{2.10}$$

where b is the bond length ($\langle b_l \rangle$ in our simulation). For $d = 2$ this reduces to $\sqrt{\langle R_N^2 \rangle} \sim N^{0.75} \ell_p^{0.25}$. In other words if the end-to-end distance is scaled by the appropriate power of the persistence length ℓ_p, then this renormalized end-to-end distances $\langle \tilde{R}_N \rangle = \sqrt{\langle R_N^2 \rangle}/\ell_p^{0.25}$ for different values of the chain stiffness parameter κ will fall onto the same master plot. For a large combination of chain length N and stiffness parameter κ we observe excellent fit to our equilibrium data for $\langle \tilde{R}_N \rangle$ to Eqn. 2.10 as shown in Fig. 2.2. It is worth noting that the persistence length calculated from Eqn. 1.11 using the formula from WLC model uses the local correlation, namely the angle between the subsequent bond vectors and hence is expected to provide a decent value of the persistence length when EV is also included. The excellent collapse of the data for $\tilde{R}_N \sim N^{0.75}$ for various values of the stiffness parameter ($\kappa = 1 - 192$) on the same master curve indicates that Eqn. 1.11 *can be used as the standard definition of persistence length even in presence of the EV effect.*

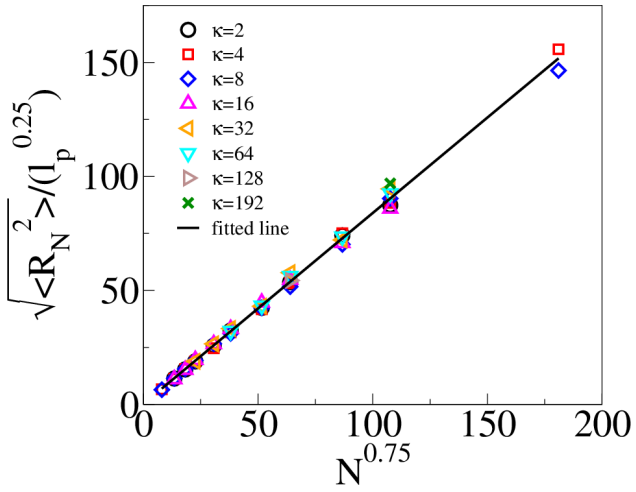

Figure 2.2: Plot of $\sqrt{\langle R_N^2 \rangle}/\ell_p^{0.25}$ versus $N^{0.75}$ for various values of the chain stiffness parameter. All the data for different stiffness parameter collapse on the same master plot. The solid line is a fit to a straight line. Only data points for which the contour length exceeds the persistence length were included in this plot.

2.2.1.3 Comparison with WLC in 2D

Having established the definition of persistence length which validated Eqn. 2.10, we now use Eqn. 1.9 presented in section 1.2 to analyze the BD simulation results for the end-to-end distance. Please note that limiting cases of Eqn. 1.9 are either a Gaussian coil ($\langle R_N^2 \rangle = 2\ell_p L$ for $L \gg \ell_p$) or a rod ($\langle R_N^2 \rangle = L^2$ for $L \ll \ell_p$). We have used simulation results to plot $\frac{\langle R_N^2 \rangle}{2\ell_p L} \sim L/\ell_p$ for a large number of values(~ 100) of L/ℓ_p ($0.05 \leq L/\ell_p \leq 170$). We have also taken additional care that a given value of L/ℓ_p is generated for different combinations of L and ℓ_p. These results are shown in Fig. 2.3. For $L/\ell_p \ll 1$ we observe that $\frac{\langle R_N^2 \rangle}{2\ell_p L} \sim (L/\ell_p)^{0.95}$ while for $L/\ell_p \gg 1$ the data very nicely fit with $\frac{\langle R_N^2 \rangle}{2\ell_p L} \sim (L/\ell_p)^{0.50}$.

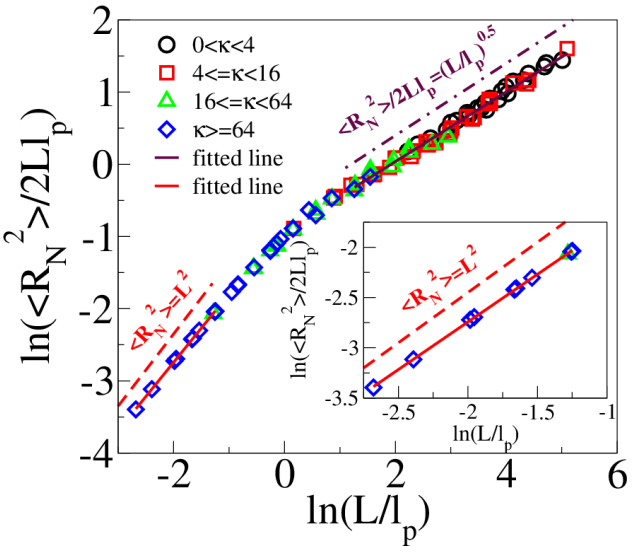

Figure 2.3: $\langle\langle R_N^2\rangle\rangle/(2L\ell_p)$ as a function of L/ℓ_p obtained from different combinations of chain length N and stiffness parameter κ (log-log scale). The solid (maroon) line is a fit to the formula $\langle R_N^2\rangle/2L\ell_p \sim (L/\ell_p)^{0.5}$ for $4 < L/\ell_p < 170$. The inset shows the same for small values of $0 < L/\ell_p < 1$ which clearly indicates that limiting slope of unity ($\langle R_N^2\rangle = L^2$) for $L/\ell_p \to 0$.

This is consistent with prior MC results using a lattice model by Hsu *et al.* [53]. However, since our studies are done in continuum we are able to get data that is for much shorter length scales. The fact that in the rod-like regime ($L < \ell_p$) the "best fit" exponent is 0.95 rather than the asymptotic value 1.0 is due to the fact that for κ=32 and 64 the "rods" still exhibit nonnegligible transverse fluctuation unlike truly stiff rods. The Gaussian behavior that Eqn. 1.9 implies $\langle R_N^2\rangle/2L\ell_p = 1$ for large L would mean a horizontal straight line in Fig. 2.3, but no indication of such a behavior is seen. The simulation data then implies the strict absence of a Gaussian limit for 2D swollen semi-flexible chains due to severe dominance of the EV interaction. This result should be contrasted with the simulation results in 3D,

where one sees a gradual crossover from rod limit to the EV limit (in 3D) passing through a Gaussian regime [75, 76].

2.2.1.4 Transverse fluctuations

It is reasonable to define an average axis for a polymer chain in the rod limit ($\ell_p \gg L$). In this limit using WLC chain Hamiltonian the transverse fluctuation with respect to this average axis has been shown [77, 78, 79] to obey the following equation

$$\langle l_\perp^2 \rangle \sim L^3/\ell_p, . \tag{2.11}$$

The above equation implies that the roughness exponent [80] $\zeta = 3/2$ ($\sqrt{\langle l_\perp^2 \rangle} \sim L^\zeta$) for a weakly bending rod. Starting from an extremely stiff chain where the transverse fluctuations are expected to be governed by the roughening exponent $\zeta = 3/2$, if we approach the limit of fully flexible chain, then the fluctuations become isotropic and in this limit one can expect that $\langle l_\perp^2 \rangle \sim L^\nu$, so that in 2D $\langle l_\perp^2 \rangle \sim L^{0.75}$. In order to calculate the transverse fluctuation, in our simulation, for each configuration of the polymer chain, we choose $\hat{x} = \vec{R}_N/R_N$ as the longitudinal axis and calculate transverse fluctuations as follows:

$$\langle l_\perp^2 \rangle = \frac{1}{N} \sum_{i=1}^{N} y_i^2, \tag{2.12}$$

where y_i is the perpendicular distance of the i^{th} monomer with respect to the instantaneous direction $\vec{R}_N$. We have repeated this calculation for several chain lengths from extremely stiff chains to fully flexible chains. This is shown in Fig. 2.4(a).

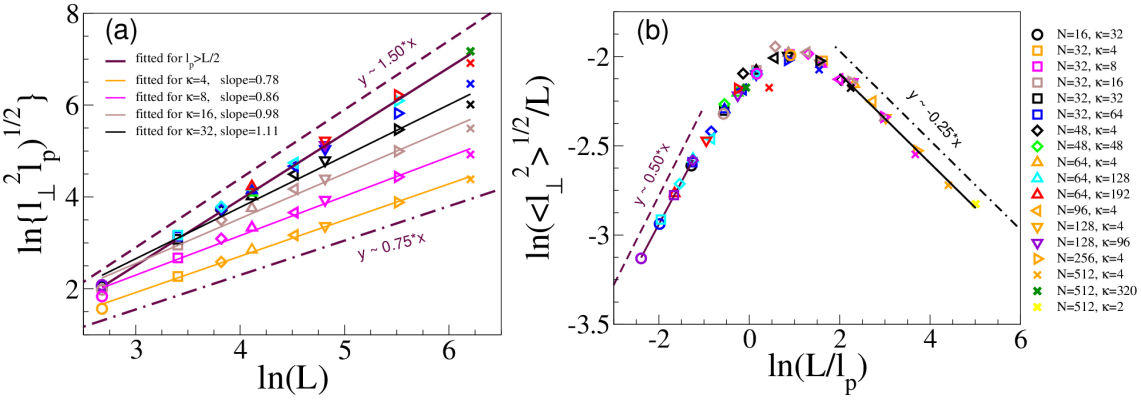

Figure 2.4: (a) Plot of $\langle l_\perp^2 \rangle \sim L^3/\ell_p$ for chains of chain length $N = 16$(circle), 32(square), 48(diamond), 64(up triangle), 96(left triangle), 128(down triangle), 256(right triangle), 512(×) with various bending stiffness $\kappa = 2$(yellow), 4(orange), 8(magenta), 16(brown), 32(black), 48(green), 64(blue), 96(indigo), 128(cyan), 192(red), 320(dark green). The orange, magenta, brown, black solid lines are fitted to chains with $\kappa = 4, 8, 16, 32$, respectively. The maroon solid line is fitted for chains with $\ell_p > L/2$. (b) Log-log plot of $\sqrt{\langle l_\perp^2 \rangle}/L$ as a function of L/ℓ_p showing that from the rod limit to the fully flexible limit, the transverse fluctuation first increases then decreases.

If one does not analyze the data carefully, one might be misled to conclude that the exponent ζ increases gradually with the chain stiffness κ. However, as we will see that the proper interpretation requires a scaling description in terms of L/ℓ_p as scaling variable. The interesting aspect of this rescaled dimensionless transverse fluctuation is shown in Fig. 2.4(b) as a function of rescaled length L/ℓ_p where the rescaled fluctuations collapse on the same master curve. This plot exhibits a maximum and then decreases gradually for large value of L/ℓ_p. It is worth noting that analytical results do not exist for chains with intermediate stiffness. The physical origin of this maximum can be interpreted as follows. Starting from the stiff chain limit when $L/\ell_p \ll 1$ it increases for a more flexible chain when the chain undergoes shape changes from rod to ellipsoid-like blob, and finally to isotropic spherical blobs. Naturally, when chain flexibility is defined in units of the persistence length for some value of L/ℓ_p ($L/\ell_p \sim 3$ from Fig. 2.4(b)) the fluctuation becomes maximum before it becomes isotropic. To the best of our knowledge this result is new and in principle can be used to measure the persistence length of a semiflexible polymer by measuring the transverse fluctuations using fluorescence probes. This would require to numerically analyze a large number of images of semiflexible chains (of a given kind of polymer) with varying contour length. For each image of a chain one can extract L as well as the end-to-end vector $\vec{R}_N$ and then use Eqn. 2.12 to extract $\langle l_\perp^2 \rangle$. Plotting then $\sqrt{\langle l_\perp^2 \rangle}/L$ versus L one would find l_p from the position of the maximum of this plot.

2.2.1.5 Bond vector correlation

The orientational correlation between successive bonds decays exponentially in a WLC model according to Eqn. 1.10. However, recent Monte Carlo (MC) studies by Hsu, Paul, and Binder have verified that a swollen semiflexible chain in 2D exhibits a power law decay as a function of the separation s between the beads [53] given by

$$\left\langle \hat{b}_i \cdot \hat{b}_{i+s} \right\rangle \propto s^{-\beta},\ \beta = 2 - 2\nu \ \text{ for } s \ll N. \tag{2.13}$$

For a fully flexible chain $\nu = 0.75$ in 2D so that $\beta = 0.5$. It is then expected that a semiflexible chain will exhibit the same behavior when $L/\ell_p \gg 1$. While for very stiff chain one needs to have extremely long chain to see this asymptotic regime for large $L/\ell_p \gg 1$, yet satisfying the condition $s \ll N$, from our simulation we clearly see this trend for moderate values of κ.

We calculated the bond correlation function from its definition and tested both Eqn. 1.10 and 2.13. First in Fig. 2.5 we show the semi-log plot of Eqn. 1.10. The straight lines are fitted only with the first several data points in order to get values of ℓ_p which are close to those calculated from $\ell_p = -1/\ln\langle\cos(\theta)\rangle$. The deviation from the initial slope (only after few points) clearly shows that Eqn. 1.10 predicted by the WLC model does not hold good for a 2D swollen chain as expected from the result of Fig. 2.3.

Fig. 2.6 shows the log-log plot of Eqn. 2.13 where we have also included the graph for a fully flexible chain for reference. Please note that even for a fully flexible chain it requires a rather long chain length ($N = 1024$) to clearly see the regime with slope with $\beta = 0.5$ over

an appreciably broad range of abscissa values.

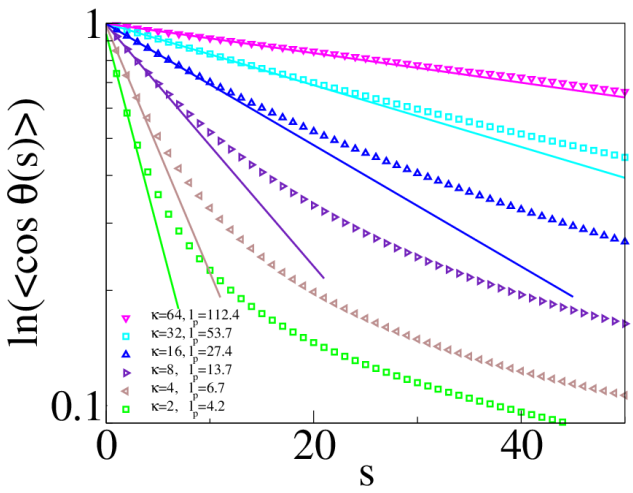

Figure 2.5: Semi-log plot. ℓ_p is calculated from the slope of the fitted line, which is very close to the values (correspondingly 105.8, 52.6, 25.9, 12.6, 6.05, 3.31) from $\ell_p = -1/\ln\langle\cos(\theta)\rangle$ (see Table 2.1).

For comparison we put the graph for a shorter fully flexible chain of $N = 512$. Here the curve starts to decrease faster before it reaches the slope corresponding to $\beta = 0.5$. Naturally for stiffer chains (which could be thought of a flexible chain of length L/ℓ_p for this purpose) for the maximum chain length $N = 2048$ considered in this chapter we only see the regime characterized by $\beta = 0.5$ only for $\kappa = 2.0$ and 4.0.

It is expected that the bond vector correlation also exhibits a scaling behavior when studied as a function of s/ℓ_p, as even for moderate values of $\ell_p \sim 5$ (see Fig. 2.5), this length rescaling $L \to L/\ell_p$ overrides the exponential decay for small s/ℓ_p. With a choice of distance between monomers in units of ℓ_p all chains are expected to behave as fully flexible chains. Therefore, if we use the renormalized distance s/ℓ_p to replot Fig 2.6(a) then one expects that

the power law correlation for chains with different stiffness will collapse on the same master plot. This is shown in Fig. 2.6(b).

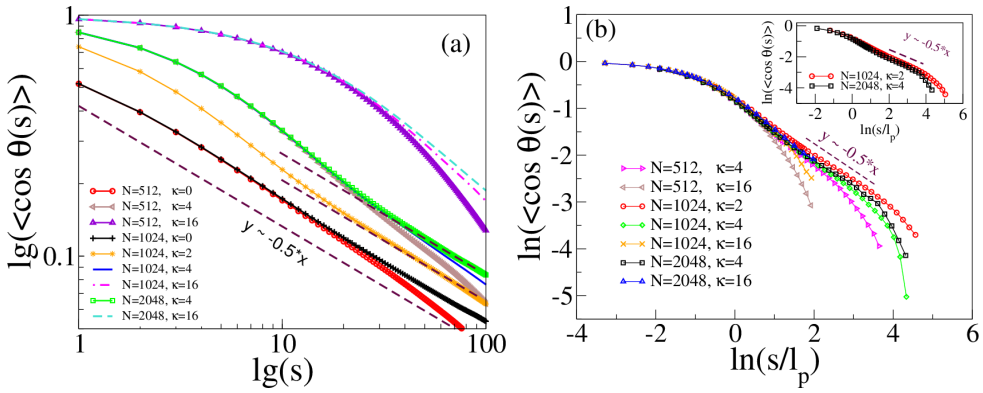

Figure 2.6: (a) Log-log plot of $\langle \cos\theta(s) \rangle$ as a function of s for various combinations of N and κ. While for large κ the asymptotic slope of $s^{-0.5}$ is preempted by finite size effect, for $(N, \kappa) \equiv (1024, 2)$ and $(N, \kappa) \equiv (2024, 4)$ the slope of -0.5 is clearly visible; (b) Same as in (a) but using rescaled variable s/ℓ_p which shows excellent data collapse for $s/\ell_p \leq 1$. The inset shows the same but only for the cases to emphasize that in the limit $L/\ell_p \gg 1.0$ there is a perfect data collapse for the power law scaling.

We observe excellent data collapse for $s/\ell_p \leq 1$. Deviations from this collapse occur at a progressively larger value of s/ℓ_p as the ratio L/ℓ_p increases either by increasing the contour length L for a fixed ℓ_p or for the same contour length L and lowering the value of ℓ_p. This is expected, since Eqn. 2.13 can hold only for $s \ll N$. Of course, a numerical study of the regime $\ell_p/\langle b \rangle \ll s \ll N$ for large ℓ_p is prohibitively difficult. However, the inset shows both the data collapse and the $\beta = 0.5$ regimes for two chain lengths ($N = 1024$ and 2048) and

for two values of κ ($\kappa = 2$ and $\kappa = 4$) which proves beyond doubt that for $1 \ll s/\ell_p \ll L/\ell_p$ the bond autocorrelation exhibits a power law decay of a fully flexible chain.

2.2.1.6 Radial distribution function for end-to-end distance

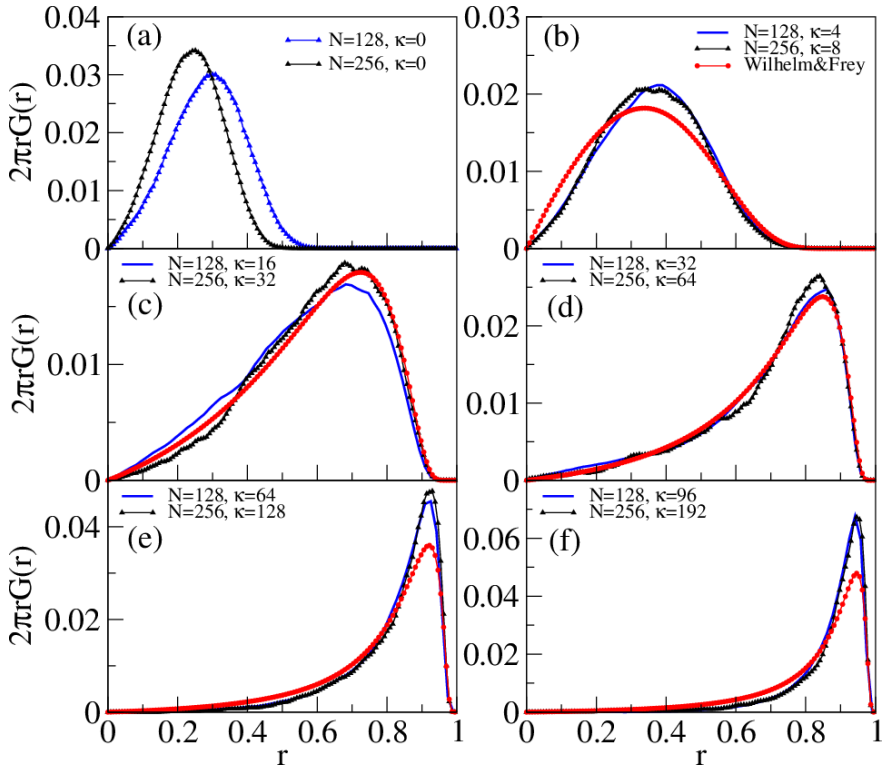

Figure 2.7: Comparison of the radial distribution for Eqn. 2.15 and the simulation for N=128 and 256 with various values of κ.

The Hamiltonian for the WLC chain model has been studied by many analytic technics assuming that for moderate chain lengths and stiff enough chains the EV effect will not dominate. Since we already established the severe dominance of the EV effect, Gaussian

regime is absent for a 2D swollen chain. Here we compare the radial distribution functions for chains with different stiffness. In particular we compare the results from our simulation with analytic results of Wilhelm and Frey [14]. For the WLC model Wilhelm and Frey [14] have derived the radial distribution function in terms of an infinite series (Eqn. 2.14) as given below,

$$\begin{aligned} G(r) =& \text{const} \times t \sum_{l=0}^{\infty} \frac{(2l-1)\,!!}{2^l l\,!} \left[\frac{1}{2t(1-r)}\right]^{5/4} \\ & \times \exp\left[-\frac{(l+1/4)^2}{2t(1-r)}\right] D_{3/2}\left[\frac{2l+1/2}{\sqrt{2t(1-r)}}\right], \end{aligned} \tag{2.14}$$

where $t = \ell_p/L$, $r = R_N/L$ and $D_{3/2}(x)$ is a parabolic cylinder function. For the whole range of values of κ in our simulation, when we plot the analytic result of Eqn. 2.14 we find that this series is fully dominated by the first term and we didn't see visual differences from the plot that includes the first four terms. Therefore, in Fig. 2.7 we plot only the first term of this series ($l = 0$) term given by

$$G_{l=0}(r) = \text{const} \times t \times \left[\frac{1}{2t(1-r)}\right]^{5/4} \times \exp\left[-\frac{(1/4)^2}{2t(1-r)}\right] D_{3/2}\left[\frac{1/2}{\sqrt{2t(1-r)}}\right] \tag{2.15}$$

Please note that for the radial distribution function Wilhelm and Frey does not take into account excluded volume effects. In Fig. 2.7 we have also included the distribution for a completely flexible chain ($\kappa = 0$) for comparison purposes. For $\kappa = 4$ and 8 (*i.e.*, $L/\ell_p \approx 16$) the simulated distribution still is intermediate between the behavior of fully flexible chains (which we expect to result for $N \to \infty$ for all κ!) and the distribution of the Kratky-Porod model. For $\kappa = 8 - 64$ the radial distribution functions $G(r)$ of Wilhelm and Frey [14] are closer to the data.

2.2.2 Dynamics

We now look at the dynamics of a swollen semi-flexible chain. We are using a Brownian dynamics (BD) scheme and therefore, HD effects are not included in our studies. However, for polymers adsorbed on a flat surface simulation studies have shown that the HD effects are negligible for no-slip boundary conditions [67]. Thus we expect the results are relevant for a fair comparison of experimental studies. Also we would like to point out that unlike equilibrium properties, computational time increases dramatically to study time dependent properties for the same chain length. Thus the diffusion and relaxation studies for the longest chain length reported in this chapter took significant time for well converged runs. We have also verified that the diffusion constant D being independent of the persistence length ℓ_p only depends on chain length N and scales as $D \sim k_B T/N$ with very good accuracy, as expected in a BD formalism.

2.2.2.1 Diffusion of the center of mass

We first start with the very basic question if the diffusion of the center of mass of chains of same contour length depends on the persistence length. If the motions of the monomers are uncorrelated with the center of mass motion then one would expect that the diffusion constant in the BD formalism will depend on the chain length N only, and should not depend on the persistence length ℓ_p.

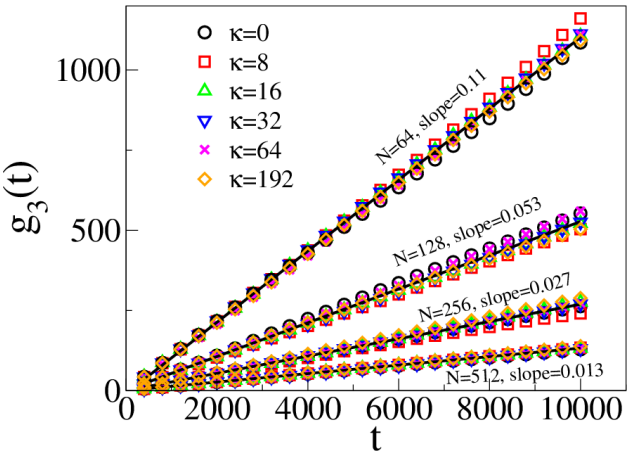

Figure 2.8: Plot of MSD of the center of mass of the chain of length $N = 64$, 128, 256, 512, respectively for chain stiffness parameter $\kappa = 0.0$ (black circles), $\kappa = 8.0$ (red squares), $\kappa = 16.0$ (green triangles up), $\kappa = 32.0$ (blue triangles down), $\kappa = 64.0$ (magenta cross), and $\kappa = 192.0$ (orange diamonds) respectively. The diffusion constant is independent of the chain stiffness parameter and scales as $1/N$.

In other words, a fully flexible chain and a rod of same length will diffuse with the same translational diffusion constant $D \sim k_B T/N$ in the BD scheme. This turns out to be true for the all the semiflexible chains studied here. The results are shown in Fig. 2.8 where we show the MSD of the center of mass of the chain for four different chain lengths as well as for several values of κ. The slope of these lines correspond to the diffusion constant. From this figure we observe that the $D(N) \sim 1/N$ and $D(N)$ does not depend on the chain persistence length. Thus if hydrodynamics are unimportant for chains constrained on a 2D surface it will be worthwhile to study the diffusion constant of same length but of different stiffness to check if this prediction is true.

2.2.2.2 Monomer Dynamics

Next we consider monomer relaxation dynamics of the chain. Following previous work for the relaxation of a fully flexible chain [19, 81, 82, 83] we have monitored various quantities pertaining to a single monomer relaxation. These quantities have been studied in the past using BD algorithm [19], and dynamical Monte Carlo algorithms (DMC) [81, 82], including the bond-fluctuation model (BFM) [83]. The dynamics of the individual monomers and the collective dynamics for the whole chain have been characterized by the functions $g_1(t)$, $g_2(t)$, $g_3(t)$, $g_4(t)$, and $g_5(t)$. They are defined as follows:

$$g_1(t) = \langle \big[\mathbf{r}_{N/2}(t) - \mathbf{r}_{N/2}(0)\big]^2 \rangle, \tag{2.16a}$$

$$g_2(t) = \langle \big[\big(\mathbf{r}_{N/2}(t) - \mathbf{r}_{CM}(t)\big) - \big(\mathbf{r}_{N/2}(0) - \mathbf{r}_{CM}(0)\big)\big]^2 \rangle, \tag{2.16b}$$

$$g_3(t) = \langle [\mathbf{r}_{CM}(t) - \mathbf{r}_{CM}(0)]^2 \rangle, \tag{2.16c}$$

$$g_4(t) = \langle [\mathbf{r}_{end}(t) - \mathbf{r}_{end}(0)]^2 \rangle, \tag{2.16d}$$

$$g_5(t) = \langle [(\mathbf{r}_{end}(t) - \mathbf{r}_{CM}(t)) - (\mathbf{r}_{end}(0) - \mathbf{r}_{CM}(0))]^2 \rangle. \tag{2.16e}$$

The quantities $g_1(t)$, $g_3(t)$, and $g_4(t)$ reflect the time dependence of the position of the middle monomer, the center of mass, and the end monomer of the chain respectively. At late times for distances greater than the gyration radius the functions $g_1(t)$, $g_3(t)$ and $g_4(t)$ will describe the motion of the entire chain. Consequently,

$$g_1(\tau(N, \ell_p)) \sim g_3(\tau(N, \ell_p) \sim g_4(\tau(N, \ell_p) \sim t, \tag{2.17}$$

for $t \geq \tau_2(N, \ell_p)$ where τ_2 is given by Eqn. 2.6. The quantities $g_2(t)$ and $g_5(t)$ on the contrary measure the relative displacement of the middle and the end monomer with respect to the center of mass of the chain. The functions $g_2(t)$ and $g_5(t)$ saturate at finite static values $2\langle(\vec{r}_{N/2} - \vec{r}_{CM})^2\rangle$ and $2\langle(\vec{r}_{end} - \vec{r}_{CM})^2\rangle$ respectively, since for $t \to \infty$ the orientations of the vectors $\vec{r}_{N/2}(t) - \vec{r}_{CM}(t)$, $\vec{r}_{end}(t) - \vec{r}_{CM}(t)$ are uncorrelated with their counterparts at $t = 0$.

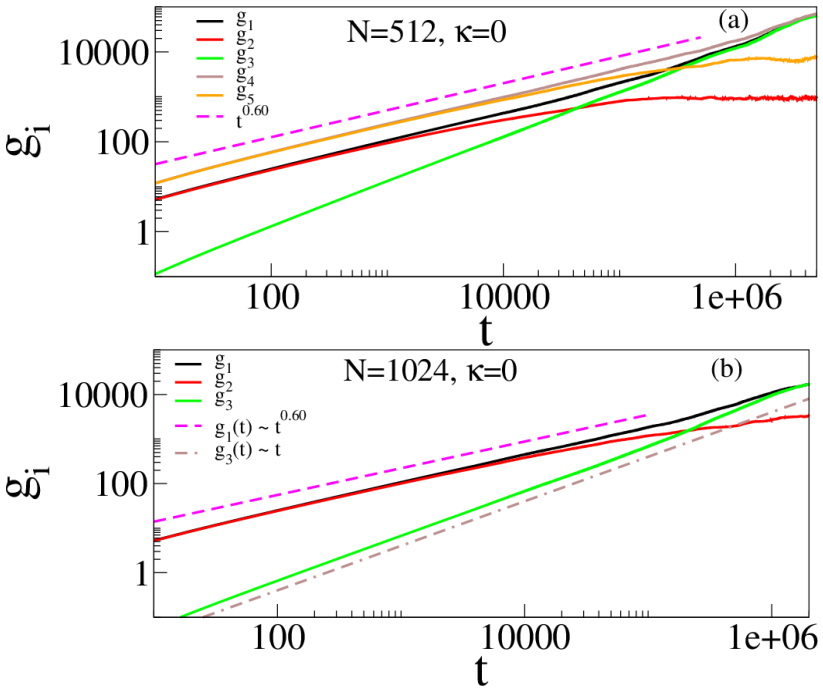

Figure 2.9: (a) $g_i(t) \sim t$ $(i = 1 - 5)$ for a fully flexible chain $(\kappa = 0.0)$ of length $N = 512$. (b) $g_i(t) \sim t$ $(i = 1 - 3)$ for a fully flexible chain of length $N = 1024$.

To study monomer dynamics, we have carried out BD simulation for various chain lengths $N = 64 - 1024$ and for chain stiffness $\kappa = 0 - 64$. We only show a limited set of data. As a reference and for comparison with the data for chains with $\kappa \neq 0$, we first show data for a fully flexible chain where we expect to see a single crossover dynamics from

$g_1(t) \sim t^{0.6}$ at an early time for $0 < t < \tau_2$ to a purely diffusive dynamics for the entire chain ($g_1(t) \sim t$). This is shown in Fig. 2.9 for chain length $N = 512$ and 1024 respectively. We have checked that the graphs for other chain length are similar and have the $t^{0.6}$ dependence for the fully flexible chain. At late times the functions g_2 and g_5 saturates and the functions g_1, g_3 and g_4 grow linearly as a function of time, becoming practically indistinguishable from each other. Similar studies have been reported earlier by Grest and Kremer [19] and by Gerroff, Milchev, Paul, and Binder [81, 82, 83]. However, our studies are much more exhaustive and quantitatively captures the crossover from $t^{0.6}$ to the purely diffusive regime which were only qualitative in previous studies and for shorter chains.

We now show data for the double crossover to support our scaling analysis for $\kappa \neq 0$. In particular we show data for chain length $N = 512$ with κ =2.0 and $N = 1024$ with κ =2.0, 4.0 respectively. Unlike Fig. 2.9 for $\kappa = 0$, plots for $g_1(t)$, $g_2(t)$ shown in Fig. 2.10 are characterized by a $t^{0.75}$ slope which then crosses over to the regime characterized by $g_1(t) \sim g_2(t) \sim t^{0.6}$ and that $g_1(t)$ eventually merges with $g_3(t)$. When we compare Fig. 2.10(a) and Fig. 2.10(b) consistent with the prediction of scaling theory we observe that the extent of the $t^{0.75}$ region in both the graphs are the same as they have the same value of $\kappa = 2$, although the chain lengths are different. Likewise, comparing Fig. 2.10(b) and Fig. 2.10(c) we note that since both plots have the same chain length the beginning of the second crossover occur almost at the same time ($\tau_2 \propto N^{2.5}$) but since the latter chain is twice as stiff it has a wider $t^{0.75}$ regime resulting in a narrower span of $t^{0.6}$ regime. Thus Fig. 2.10 unambiguously confirms predictions from the scaling theory. We observe that at early time $g_1(t) = g_2(t)$;

however the width of the region $g_2(t) \sim t^{0.6}$ is narrower than that of $g_1(t) \sim t^{0.6}$ and it exhibits a slightly lower value of slope before saturation. Considering that the crossovers are broad, we believe that this is due to finite size effect as it is evident if we compare Fig. 2.10(a) and Fig. 2.10(b). In the latter case, which is for a larger chain length, the difference between $g_1(t)$ and $g_2(t)$ are much smaller and we notice that the difference begins at a later time. Ideally for very large system the point when $g_1(t)$ would change its slope towards $g_1(t) \sim t$, $g_2(t)$ also tend to saturate. The sharpness of this feature would require a much larger system. We also note the same feature in Fig. 2.9. But the plots for $g_1(t)$ quite clearly show three distinct scaling regimes of $g_1(t) \sim t^{0.75}$ crossing over to $g_1(t) \sim t^{0.6}$ and then merging with $g_3(t) \sim t$ at late times. We have further confirmed the existence of this double crossover by plotting $g_1(t)/t^{0.75} \sim t$ as shown in Fig. 2.11. The existence of an initial plateau ($t < \tau_1$), followed by a decay ($\propto t^{-0.15}$), and of a minimum (near τ_2) before the diffusion ($\propto t^{0.25}$) starts further demonstrates quite conclusively that the exponent changes from $t^{0.75} \rightarrow t^{0.6} \rightarrow t$. We would like to mention that because of the width of the $t^{0.6}$ regime becomes narrower for stiffer chains we were unable to see this regime unambiguously in simulation of shorter chains and/or larger κ (*e.g.*, for $N = 512$ and $\kappa \geq 4$). While for $N = 512$ the double crossover is clear for $\kappa = 2.0$, but becomes ambiguous for $\kappa \geq 4.0$ which required an increased chain length of $N = 1024$. As expected, the crossovers are rather gradual, spread out over a decade in time t each, and hence for chains that are not long enough the existence of these regimes is missed in previous work.

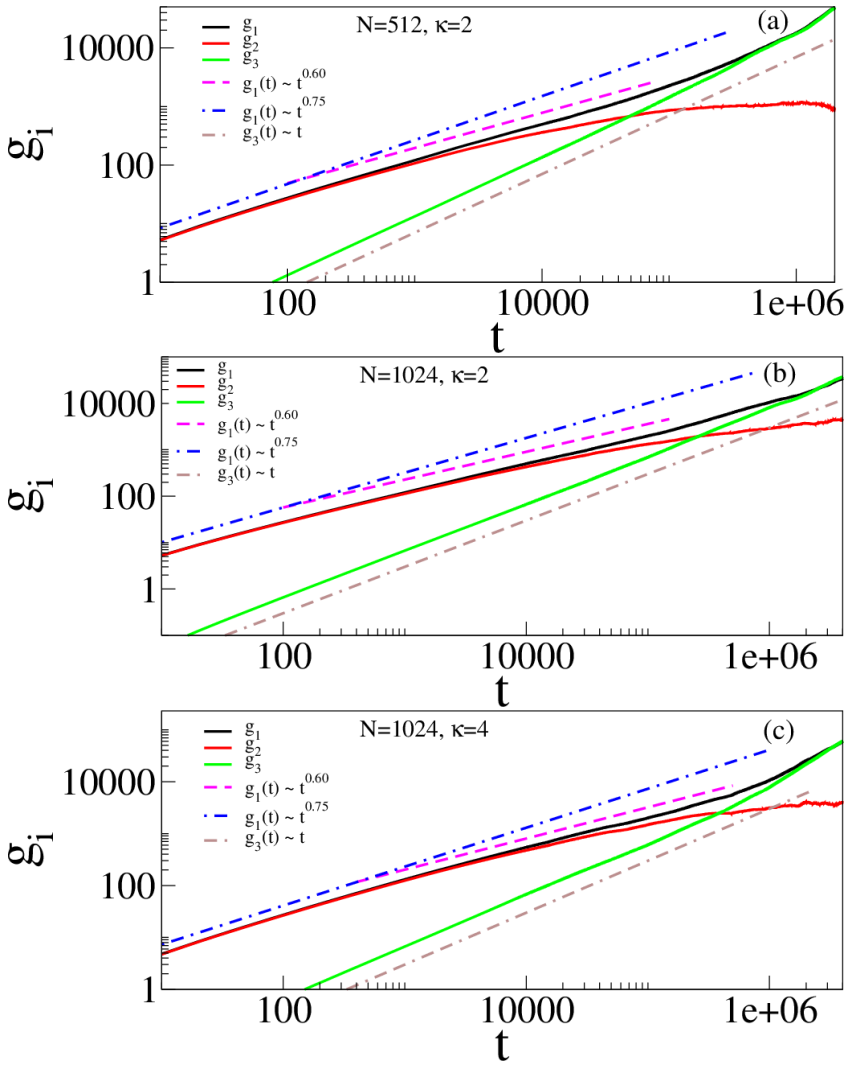

Figure 2.10: (a) Plot for $g_1(t)$ (black), $g_2(t)$ (red) and $g_3(t)$ (green) as a function of time on a log-log scale for chain length $N = 512$ and $\kappa = 2.0$. The blue and magenta dashed lines correspond to straight lines $g_1(t) = At^{0.75}$, and $g_1(t) = Bt^{0.60}$, respectively, where A and B are constants. (b) same but for $N = 1024$ and $\kappa = 2.0$. (c) same but for $N = 1024$ and $\kappa = 4.0$. Note that for a fully flexible chain the slope of the curve $\log(g_i)$ versus $\log(t)$ would monotonously increase with time, unlike the present case.

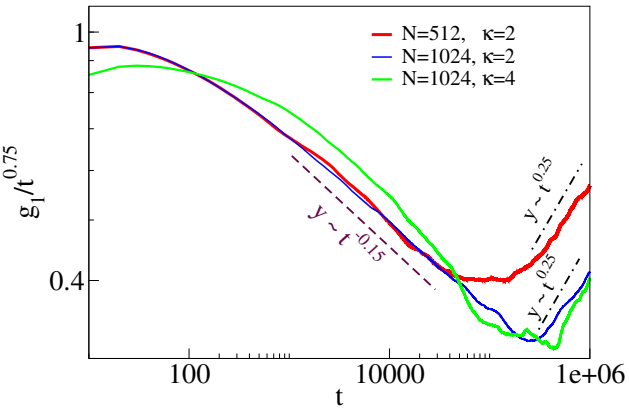

Figure 2.11: Log-log plot of $g_1(t)/t^{0.75}$ as a function of t corresponding to the plots of Fig. 2.10(a) (red), (b) (blue) and (c) (green) respectively. In each graph the minimum occurs in the intermediate regime characterized by $t^{0.6}$.

The interplay of Rouse modes and the bending modes with respect to the monomer dynamics of semiflexible chains was considered in early work by Harnau *et al.* [11], in the framework of a Rouse model generalized by higher order terms to account for chain stiffness. They ignored excluded volume, and considered a single chain length, attempting to model C100 alkanes in a melt. They found that their results were neither consistent with the Rouse behavior ($g_1(t) \sim t^{1/2}$) nor with the power law due to bending modes ($g_1(t) \sim t^{3/4}$). In our view, the chain length studied in this work was too small to observe both power laws separately, rather all their data fall in a regime of smooth crossover. Having established the double-crossover we now further investigate the consequence of scaling prediction that the first crossover occurs at time $\tau_1 \propto \ell_p^3$ when $g_1(\tau_1) \propto \ell_p^2$. Fig. 2.12 shows a plot of $g_1(t)/\ell_p^2$ as a function of rescaled time t/ℓ_p^3 which shows data collapse for $g_1(t)/\ell_p^2 \leq 1.0$ and $t/\ell_p^3 \leq 1.0$ for various combinations of chain length N and κ confirming the length and the time scales

for these crossovers.

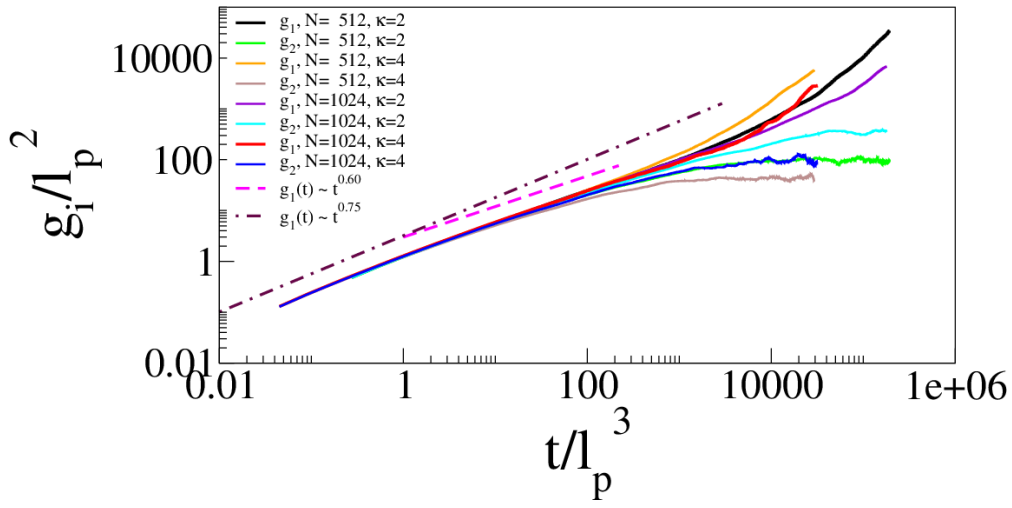

Figure 2.12: Plot for $g_1(t)/\ell_p^2$ and $g_2(t)/\ell_p^2$ as a function of t/ℓ_p^3 on a log-log scale for chain lengths $N = 512,\ 1024$ with $\kappa = 2.0,\ 4.0$ respectively. The dot-dashed and dashed lines correspond to slopes 0.75 (maroon) and 0.6 (magenta) respectively.

Note that the scaling theory of section 2.1 implies

$$g_i(t)/\ell_p^2 = \tilde{g}(t/\tau_1, t/\tau_2), \tag{2.18}$$

where τ_1, τ_2 are the times defined in Eqn. 2.2 and 2.6. If the first argument of the scaling function $\tilde{g}$, t/τ_1 is small in comparison to unity, we can approximate Eqn. 2.18 as $g_1(t)/\ell_p^2 \approx \tilde{g}(t/\tau_1, 0) \propto (t/\tau_1)^{3/4}$, which reduces to Eqn. 2.1. For $t/\tau_1 > 1$ we can rewrite the scaling function as

$$g_i(t)/\ell_p^2 = \tilde{\tilde{g}}(t/\tau_1, \tau_2/\tau_1) = \tilde{\tilde{g}}(t/\tau_1, (Nb/\ell_p)^{5/2}). \tag{2.19}$$

Note that τ_2/τ_1 remains constant when we increase N and ℓ_p by the same factor: this observation explains that the scaling of the data in Fig. 2.12 encompasses the full range of times.

2.3 Summary and discussion

In conclusion, we have studied conformations, fluctuations, and crossover dynamics of a swollen semiflexible chain in 2D. We first developed a scaling theory which generalizes early time monomer dynamics of a fully flexible chain for a semiflexible chain characterized by its contour length and the persistence length. We predict a double crossover which arises due to the presence of an additional length scale introduced through the chain persistence length. Monomer dynamics up to a length scale ℓ_p is independent of chain length and is characterized by the $t^{0.75}$ power law. At a later time $t > \tau_1$ when the size of the fluctuations becomes bigger than ℓ_p the dynamics begin to look like that of a fully flexible chain and characterized by the well known $t^{2\nu/1+2\nu}$ growth. Both of these exponents have been discussed in the literature separately but have not been emphasized that before the entire chain reaches purely diffusive regime, there ought to be two and not one crossover, the first crossover differentiates chains of different stiffness. Previously the dynamics of monomer MSD of semiflexible polymers has also been studied by Harnau *et al.* [11], using a Rouse-type model generalized to include chain stiffness. They saw a gradual crossover, in between bending modes and Rouse modes,

but did not consider the scaling description of the crossover. Note that excluded volume effects were absent in their model, and hence it is not appllcable in d=2 dimensions.

Motivated by recent lattice MC results for a swollen chain in 2D predicting the absence of a Gaussian regime we undertook similar studies in 2D continuum using BD simulation. While checking our data for the RMS end-to-end distance for chain of different contour length and persistence length we discovered that we regain the well known results for the end-to-end distance due to Schaefer, Joanny, and Pincus [59] and Nakanishi [74] provided we use the definition of the persistence length given by either the lattice or continuum version of the Kratky-Porod WLC model. We explain this by noting that the persistence length being a local property of a chain does not depend on the EV interaction. This is further reassured when we note that the persistence length calculated this way does not depend on the chain length unlike well used textbook definition of persistence length where the projection of the end-to-end vector on the first bond is used as the definition and does depend on the chain length. Therefore, we emphasize that the latter definition needs to be discarded.

We also confirm the absence of the Gaussian regime in the continuum bead-spring model where the swollen chain for $L/\ell_p \ll 1$ behaves like a rod and thereafter always behaves like a swollen chain. Considering that there are increased number of activities to explore the properties of biomolecules on a surface, our result (Fig. 2.3) will be extremely valuable to analyze the experimental data correctly for stiff molecules on flat surfaces. It has not escaped our attention that many such reported analyses are still done using the WLC model and/or calculating the chain persistence length from projected end-to-end to the first bond.

Transverse fluctuations in a stiff chain has been addressed analytically in the literature only in the extremely stiff chain limit where one finds that it is described by the roughening exponent. Analytic calculations for moderately stiff chains are hard to carry out, and to date there are no results for transverse fluctuations spanning the entire regime from a stiff to a fully flexible chain. We have numerically obtained this result and pointed out that the appropriate length variable to analyze the data is to use the persistence length as the unit of length. When we use L/ℓ_p as the length scale to plot transverse fluctuation we discover the non-monotonic behavior of this fluctuation reaching a maximum for some $L \gtrapprox \ell_p$. We point out that this universal scaling of the transverse fluctuation can be used to measure the persistence length of the chain. Another accompanying consequence of the absence of Gaussian regime for a swollen chain in 2D is the decay of the bond correlation function which exhibits a power law decay. Again, by choosing the normalized contour segment s/ℓ_p as the appropriate variable we regain the exponent $\beta = 0.5$ which describes the decay of bond autocorrelation for a fully flexible chain. We must point out that many of these results and analyses on chain conformations and equilibrium fluctuations point to a common theme. In the limit $L/\ell_p \gg 1$ we recover the expected behavior of a fully flexible chain and chains with different stiffness exhibit universal scaling behavior when persistence length is chosen as the unit of length.

This general idea extends to our study of monomer dynamics as well. We have provided a new scaling theory of monomer dynamics for semiflexible polymers in 2D. Our theory predicts novel crossover dynamics at an intermediate time when the fluctuations of

the monomers $g_1(\tau_1) \sim \ell_p^2$. Around this time the monomer dynamics become the same as that of a fully flexible swollen chain characterized by $g_1(t) \sim t^{2\nu/(1+2\nu)} = t^{0.6}$ in 2D . The theory expands the existing scaling theory for monomer dynamics for a WLC and that of a fully flexible chain to include the effect of the chain persistence length. Fully flexible swollen chains are self-similar objects, while a polymer segment up to its own persistence length is not. Therefore, it is expected that for length scales up to ℓ_p the dynamics will have different characteristics due to bending modes arising out of the chain stiffness. The EV effect is almost negligible for the $t^{0.75}$ regime and therefore, our result is the same as that of previous studies using WLC Hamiltonian [15, 16]. For the $t^{0.6}$ regime originating from the EV effect, where the monomer dynamics are governed by Rouse relaxation of a fully flexible chain, our theory elucidates the exact role of chain persistence length neither contained in WLC model nor studied before. We also validate our new scaling theory by extensive BD simulation results.

A subtle issue concerns the limit κ towards infinity while keeping the contour length L fixed. Then transverse motions of the monomers relative to each other, in a coordinate system where the x-axis is fixed along the rod-like polymer, are completely suppressed. In the "laboratory coordinate system", however, the rod still can make random transverse motions, namely rigid body rotations and translations. However, in addition to those motions still motions of the monomers reative to each other along the axis of the rod are possible. These motions may give rise to a transient $t^{1/2}$ behavior, as a model calculation for a one-dimensional harmonic chain shows 2.4. However, our data for $g_i(t)$ for large κ due to the

smoothness of crossovers did not allow to clearly separate this mode of motions from the displacements due to transverse fluctuations.

In the present manuscript we have ignored HD interactions as they are not significant for 2D swollen chains on a substrate. However we now present simple estimates of generalization of our results in 3D and/or in presence of HD interactions which will be relevant for a 3D swollen chain. In the free draining limit, the results $t^{0.75}$ will remain the same in 3D [15, 16], but the intermediate Rouse relaxation regime will be characterized by $t^{2\nu/(1+2\nu)} = t^{0.54}$ ($\nu = 0.59$ in 3D), for the case where the EV is relevant (*i.e.*, MSDs exceeding $R^{*2} = \ell_p^2/b^2$). For MSD in between ℓ_p^2 and R^{*2} Gaussian behavior prevails, $\nu = 1/2$, and hence $g_1(t) \propto t^{1/2}$ in that regime. The crossover between flexible and stiff chain dynamics in 3D in the free draining limit was studied by Steinhauser *et al.* [66], but no scaling analysis is done.

Replacing Rouse relaxation by Zimm relaxation one immediately sees that in presence of HD interaction the intermediate regime is characterized by $t^{2\nu/3\nu} = t^{2/3}$ [64, 63, 65]. Notice that in this case ν cancels out and this relaxation should be the same in 2D and 3D. However, as shown by Hinczewski and Netz [63, 65], very complicated crossovers occur in this case.

We now make some comments about some recent experiments to study monomer dynamics. This is typically done using FCS where a tagged monomer can be directly watched in real time. However, as has been mentioned by Petrov *et al.* [62] that since the $t^{0.75}$ regime or the intermediate regimes (either $t^{0.5}$ or $t^{2/3}$) occur at much shorter time scales compared to the longest relaxation time, unless extreme caution is taken for the measurement

of MSD of a labeled particle, the interpretation can be misleading, especially for shorter DNA fragments [61]. For dsDNA of length $10^2 - 2 \times 10^4$ base pairs (which is equivalent to $L/\ell_p \sim 0.7 - 140$) FCS studies of Petrov *et al.* observed the Zimm regime characterized by a $t^{2/3}$ power law. However, a clear demonstration of the double crossover is lacking in recent experiments with biopolymers [3, 84, 79, 61, 62]. This is partly due to lack of resolution of the experiments and partly due to the fact that lacking any theoretical predictions for this phenomenon, researchers did not specifically investigate the precise behavior of MSD before the onset of overall chain diffusion very carefully. We will provide some physical arguments why the experimental detection can be hard: a simple calculation for Fig. 2.1 shows that in order for the width of the $t^{0.75}$ and $t^{0.60}$ to be equal (in logarithmic scale) one needs $N = \ell_p^{2.2}$ in 2D. In other words for a stiffer chain one needs a very long chain to see the $t^{0.60}$ regime. Indeed in our simulation we found (not shown here) that for $\kappa = 16$, 32, and 64, the results with chain length up to $N = 512$ are largely dominated by the $t^{0.75}$ regime and we did not clearly see the $t^{0.60}$ regime. It is only after we lowered the value of κ and used longer chain ($N = 1024$), we identified these two regimes quite conclusively (Fig. 2.10). We suspect that the same might happen in experiments [3]. For extremely stiff chains the $t^{0.6}$ (or $t^{0.54}$ in 3D) region can be extremely narrow and could either be missed or the rather smooth double crossover might be mistakenly interpreted as a single crossover (with $t^{2/3}$ in 2D). Therefore, we believe that these results will not only promote new experiments but will be extremely valuable in identifying and interpreting different scaling regimes for the monomer dynamics of semiflexible polymers.

he research has been partially supported (AH) by the UCF Office of Research & Commercialization and the UCF College of Science SEED grant. AB acknowledges travel support from Deutsche Forschungsgemeinschaft at the Institut für Physik, Johannes Gutenberg-Universität, Mainz.

2.4 Appendix

In this section following density relaxation in reptation theory [1], we provide physically motivating argument about the double crossover. For pedagogical reason we consider a simpler system consisting of a bead-spring model of length N in one dimension as shown in Fig. 2.13 which we call a compressible rod (Fig. 2.13). This can be thought of as the

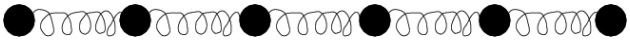

Figure 2.13: Bead-spring model for a compressible rod in one dimension.

$\kappa \to \infty$ of the 2D bead-spring model without rotational degrees of freedom so that all N monomers perform one dimensional random walk along a line. In this case the mean square displacement of the center of mass of the rod is given by

$$\begin{aligned} \langle [X_{CM}(t) - X_{CM}(0)]^2 \rangle &= 2d_N t, \\ \langle [Y_{CM}(t) - Y_{CM}(0)]^2 \rangle &= 0, \end{aligned} \tag{2.20}$$

and the mean square end-to-end distance is

$$\langle R^2 \rangle = (N-1)^2 l_b^2 \approx N^2 l_b^2, \tag{2.21}$$

where l_b is the average distance between the neighboring monomers along the rod. The time needed for the center of mass to diffuse over the distance $\sqrt{\langle R^2 \rangle}$ is

$$2d_N\tau = N^2 l_b^2, \;\; \tau = \frac{N^2 l_b^2}{2d_N} = \frac{2N^3 l_b^2}{(\delta^2 W)}. \tag{2.22}$$

In above W is the rate of random displacement per unit time and δ is the average step length for such random motion. If we assume, that monomer MSD in the compressible rod limit satisfies a power law

$$\langle [x_i(t) - x_i(0)]^2 \rangle = \delta^2 (Wt)^x \tag{2.23}$$

and assume that for $t = \tau$ the same MSD as for the center of mass, $\langle R^2 \rangle$, is reached

$$\langle [x_i(t) - x_i(0)]^2 \rangle = \delta^2 (W\tau)^x = \langle R^2 \rangle = N^2 l_b^2, \tag{2.24}$$

we obtain

$$\delta^2 \left(\frac{2N^3 l_b^2}{\delta^2} \right)^x = N^2 l_b^2, \;\; x = 2/3 \tag{2.25}$$

This would mean one simple crossover for the compressible rod. This is shown in Fig. 2.14(a).

However, it is not obvious that this simple scaling description must be correct. Recall that a law $\tau \propto N^3$ is reminiscent of reptation! The reptation idea can be recognized in Fig. 2.13, if we reinterpret the x-coordinate as a coordinate along the TUBE axis of reptation theory. Then the picture due to de Gennes is that density excess diffuses along chain contour, until all the density excesses are equilibrated (in view of Fig. 2.13, this picture is really plausible when we introduce an intermediate length scale l_{cg} on which we estimate a coarse grained density by counting the number of bonds on this length scale, n_{cg}, we will see that the coarse grained density $\rho_{cg} = n_{cg}/l_{cg}$ for every instantaneous configuration is inhomogeneous,

but these inhomogeneities decay by diffusion of excess density). In this case we conclude that the diffusion time is just the standard Rouse time

$$\tau_R \propto L^2/(\delta^2 W) \qquad (L = Nl_b). \tag{2.26}$$

and we have for the monomer MSD

$$\langle [x_i(t) - x_i(0)]^2 \rangle = \delta^2 (Wt)^{1/2}, \qquad for\ t < \tau_R \tag{2.7}$$

$$\langle [x_i(t) - x_i(0)]^2 \rangle = W\delta^2 t/N, \qquad for\ t > \tau_R \tag{2.8}$$

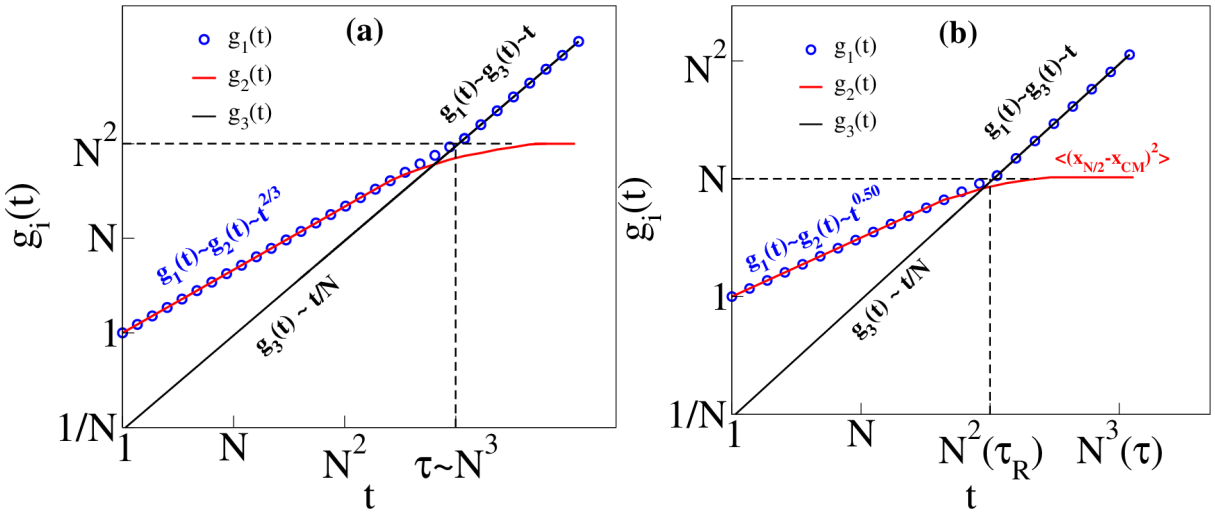

Figure 2.14: (a) Scaling description of compressible rods. Different regimes of monomer relaxation and crossover. (b) True scaling description of compressible rod dynamics.

One obtains the "ordinary" reptation picture of deGennes by transferring from the coordinate of the tube axis (which is what Figs. 2.13 and 2.14(b) describe) to the coordinates in real space, assuming that the tube is a random walk. This transformation has the effect

that

$$\begin{aligned} \langle[\Delta x_i(t)]^2\rangle \propto t^{1/2} \quad &\rightarrow \quad \langle[\Delta \vec{r}_i(t)]^2\rangle \propto t^{1/4} \quad for \;\; t < \tau_R \\ \langle[\Delta x_i(t)]^2\rangle \propto t \quad &\rightarrow \quad \langle[\Delta \vec{r}_i(t)]^2\rangle \propto t^{1/2} \quad for \;\; t < \tau \end{aligned} \tag{2.9}$$

and only then at $t = \tau$ a crossover shows up.

Thus our conclusion is that Fig. 2.14(a) is wrong and Fig. 2.14(b) represents the right scenario. In order to verify this theory we have carried out Brownian dynamics simulation of a compressible rod using the same algorithm as outlined in Sec. 1.3. In order to observe the density relaxation of the monomers we had to choose the FENE spring constant to a smaller value. The results are shown in Fig. 2.15 where we clearly see the double cross over with $g_1(t) \sim t^{0.25}$ (early time) and $g_1(t) \sim t^{0.50}$ respectively. Moreover since the first cross over occurs for $g(\tau_1) \propto N$ at $\tau_1 \propto N^2$ the rescaled plots for three different chain lengths fall on the same master curve. Unlike, the 2D system of semiflexible chain while we only see some evidence of this cross over for chain length up to N=256, in this idealized system this double crossover with two distinct powers is seen very clearly for much smaller chain length. Now the crucial effect is in 2D semiflexible (rather than infinitely stiff!) polymers is due to bond bending collective modes. Therefore, the natural second length scale that comes in to the early time dynamics of this system is the chain persistence length. The corresponding scaling theory is developed in Sec. 2.1.

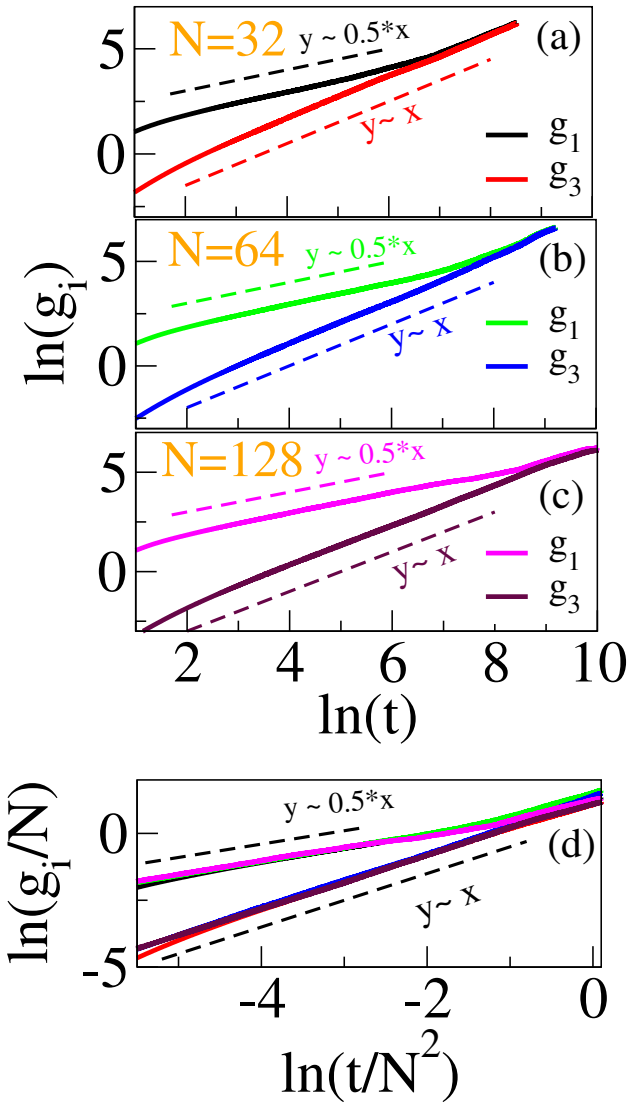

Figure 2.15: $g_1(t)$ and $g_3(t)$ for a one dimensional compressible chain as a function of time t for chain lengths (a) $N = 32$, (b) $N = 64$, and (c) $N = 128$ respectively which show the crossover dynamics from $t^{0.5}$ to $t^{1.0}$; (d) rescaled $\bar{g}_1(t) = g_1(t)/N$ and $\bar{g}_3(t)(t) = g_3(t)/N$ as a function of rescaled time t/N^2 where both the regimes collapse on the same master curve.

CHAPTER 3
DNA CONFINED IN A TWO-DIMENSIONAL STRIP GEOMETRY

Conformations and dynamics of DNA inside a nanochannel have attracted considerable attention among various disciplines of science and engineering [85]. Important biomolecules, such as, chromosomal DNAs, or proteins whose functionalities are crucially dependent on the exact sequence of the nucleotides or amino acids usually exist in highly compact conformations. By straightening these molecules on a two dimensional sheet [86, 87, 88] or inside a nanochannel [89, 90, 91, 92, 93, 94] it is possible to obtain the structural details of these molecules. It is believed that a complete characterization of the DNA sequence for each individual and a proper understanding the role of genetic variations will lead to personalized medicine for diseases, such as, cancer [95]. DNA confined and stretched inside a nanochannel offers significant promise towards this goal. Unlike, traditional sequencing using Sangers method [96, 97] which requires fragmentation and replication, analysis of a single DNA will be free from statistical errors and sequence gaps while reconstruction [95]. Naturally quests for efficient but low cost techniques have attracted considerable attention. Along with optical maps [86, 91], recently DNA melting characteristics inside a nanochannel have been studied showing further promises [93]. These recent experiments have generated renewed interests in theoretical and computational studies of confined polymers [98]-[99].

Confined DNAs inside nanochannels often studied in high salt concentrations [85] where the charges of the individual nucleotides are heavily screened [100, 90]. Besides, the resolution of optical studies set by the diffraction limit is typically of the order of 100 base pairs. Under these conditions a double-stranded DNA is often described as a worm-like chain (WLC) [1] whose end-to-end distance $\langle R^2_{bulk}\rangle = 2\ell_p L\left(1 - \frac{\ell_P}{L}\left[1 - \exp\left(-L/\ell_P\right)\right]\right)$ interpolates from a rod ($\langle R^2_{bulk}\rangle \sim L^2$ for $L \ll \ell_p$) to a Gaussian coil ($\langle R^2_{bulk}\rangle \sim 2L\ell_p$ for $L \gg \ell_p$). However, for a very long chain eventually the excluded volume (EV) effect becomes important [76, 75], and for $L \gg \ell_p$ the end-to-end distance in d dimensions should be characterized by the bulk conformation of a swollen semi-flexible chain [59, 74]

$$\sqrt{\langle R^2_{bulk}\rangle} = a\left(\frac{L}{a}\right)^{\frac{3}{d+2}}\left(\frac{\ell_p}{a}\right)^{\frac{1}{d+2}}, \tag{3.1}$$

where a is the effective width of the chain. It is noteworthy that while in 3D there is a broad Gaussian regime for $L \gtrapprox \ell_p$ [76, 75] before EV effects become important, in two dimensions (2D) the intermediate Gaussian regime is absent due to severe dominance of the EV effect [53, 101].

Recently confined polymers in rectangular, cylindrical and triangular channels have been studied by several groups [98]-[99]. One first sees the effect of the confinement (described by the length of the cross section of the channel D) for $D < R_g$, where R_g is the radius of gyration of the chain. This limit has been identified as the Flory-de Gennes regime where chain conformations can be described as a series of spherical blobs of size D [102, 42]. Further decrease of the ratio D/R_g first leads to an extended de Gennes regime with anisotropic blobs followed by a Gaussian regime analogous to the 3D bulk case, which has been referred

as the Gauss-de Gennes regime [103]; for extreme confinement when $\ell_p \gg D$, the blob picture breaks down and the chain enters into the Odjik regime [21, 22] where the chain conformations are described as a series of straight segments deflected from the confining wall [104]. While both de Gennes and Odjik regimes are well established, characteristics of the transition regions (the extended de Gennes and the Gaussian) have been the main goal of several recent studies [104, 100, 103, 105]. However, the extension of the confined DNA in the extended de Gennes regime has been determined to be the same as in the de Gennes regime by minimizing the free energy [85, 100, 105], so making a difference of these two regimes has been either difficult or not evident [100, 103].

3.1 Scaling regimes

Confined chains inside 3D nano-channels exhibit analogous regimes as found in their respective bulk counterparts [103]. In this letter we study confined DNA in a 2D strip geometry. As mentioned before, that unlike in 3D, the bulk Gaussian regime does not exist for semi-flexible chains in 2D [53, 101]. Therefore, one wonders, if regimes of confined DNA in 2D will follow their corresponding bulk counterpart. The second motivation comes from the observation that the Flory exponent in 2D (0.75) is significantly larger than the corresponding exponent in 3D (0.588) which implies that a chain is more elongated in a 2D strip rather than in a tube of the same width D. Therefore, the elongation would be more profitable by further reducing the physical dimension of the region. Finally, in the Odjik

limit, prior theoretical and numerical results [98] have indicated that the prefactor A in the expression for the chain elongation (see Eqn. 3.9) is nearly independent of the shape of the nanochannel. By studying elongation along a 2D strip, we further observe that this constant is almost the same as the values in 3D indicating that this constant is independent of the spatial dimension. While in 3D the extended de Gennes limit is somewhat controversial, we provide scaling arguments for a 2D strip and validate by carrying out BD simulation that the extended de Gennes regime is vanishingly small. This result along with the absence of a Gaussian regime in a 2D strip geometry implies that a 2D strip is a cleaner system to study a stretched chain as the conformations interpolate between de Gennes and Odjik regimes only, and therefore, is another reason to think about designing DNA elongation experiments inside a 2D strip.

3.1.1 de Gennes regime

The starting point of our theoretical analysis is the ansatz for the normalized free energy $\mathcal{F}/k_BT$ of confinement along a tube axis first proposed by Jun, Thirumalai, and Ha [106], later used for a square channel [100] and a slit [105], and is given by

$$\mathcal{F}/k_BT = \frac{X^2}{(L/L_{\text{blob}})\,D^2} + D\frac{(L/L_{\text{blob}})^2}{X}, \tag{3.2}$$

and the expression for the end-to-end distance of a swollen semi-flexible chain as given by Eqn. 3.1. Here X is the extension along the tube/strip axis, and L_{blob} the contour length of the chain in a blob [102, 42], k_B is the Boltzmann constant, and T is the temperature.

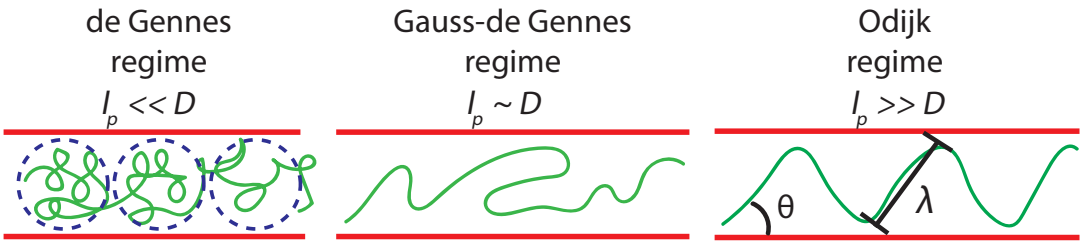

Figure 3.1: Three established regimes for a semi-flexible polymer under a three-dimensional channel confinement. In the de Gennes regime($\ell_p \ll D$), the chain configuration can be viewed as a series of blobs of size D, in Gauss-de Gennes regime($\ell_p \sim D$), the chain behaves like an ideal chain, and in Odijk regime($\ell_p \gg D$), the chain deflects back and off the wall. Note that the controversial extended de Gennes regime is not present here, and one of the main results in this chapter is that the Gauss-de Gennes regime is also absent under a quasi-one-dimensional confinement.

The dimension dependence comes from the chain statistics for $L_{\rm blob}$ (Eqn. 3.1). In order to contrast the results for polymers confined in a 2D strip with those for cylindrical, square, and rectangular channels, in the following we derive expressions in terms of d spatial dimensions ($d = 2$ for a strip and $d = 3$ for a tube). By differentiating Eqn. 3.2 with respect to X, one can easily check (i) $X = Dn_{\rm blob}$, where $n_{\rm blob} = L/L_{\rm blob}$ is the number of blobs, (ii) $\mathcal{F}/k_BT \sim n_{\rm blob}$, and (iii) $\mathcal{F}/k_BT \sim L$. For the de Gennes regime monomers inside the blob are described by the conformation of a swollen chain either in $d = 2$ (strip) or d =3 (tube), so that $D = {L_{\rm blob}}^{3/d+2} {\ell_p}^{1/d+2} a^{d-2/d+2}$ (Eqn. 3.1). It is then easy to check that the elongation is given by

$$\langle X \rangle_{\rm de\,Gennes} = Dn_{\rm blob} = L \left(\frac{D}{a}\right)^{\frac{1-d}{3}} \left(\frac{\ell_p}{a}\right)^{\frac{1}{3}}. \tag{3.3}$$

Likewise, the second derivative of Eqn. 3.2 gives the effective stiffness constant k_{eff} for the DNA polymer [85, 89] under confinement, so that the longitudinal fluctuation of the extension $\langle \sigma^2 \rangle$ can be obtained as

$$\langle \sigma^2 \rangle = \frac{k_B T}{k_{\text{eff}}} = La \left(\frac{\ell_p}{a} \right)^{\frac{1}{3}} \left(\frac{D}{a} \right)^{\frac{4-d}{3}} . \tag{3.4}$$

3.1.2 Extended de Gennes regime

It was argued [85, 104, 100] that the scaling relation Eqn. 3.1 for each spherical blob in de Gennes regime only holds true when the channel size D and chain length L both are above certain critical values D_{**} and L_{**} respectively to be determined in the following manner. When $D < D_{**}$ the EV repulsion becomes less significant resulting in a local ideal chain behavior in each blob, while strong enough to sustain the global picture of linearly ordered blobs, each turning into an ellipsoid characterized by its major axis H (and of volume $\sim D^{d-1}H$) along the long axis of the nanochannel [107]. The critical length L_{**} and the critical channel width D_{**} can be obtained by equating the size of an ideal chain and a Flory coil in the bulk: $D_{**} \simeq (L_{**}\ell_p)^{1/2} \simeq \ell_p{}^{\frac{1}{d+2}} L_{**}{}^{\frac{3}{d+2}}$, from which we get

$$L_{**} \simeq a \left(\frac{\ell_p}{a} \right)^{\frac{d}{4-d}} \text{and} D_{**} \simeq a \left(\frac{\ell_p}{a} \right)^{\frac{2}{4-d}} . \tag{3.5}$$

Notice that $L_{**} \simeq l_p^3 a^{-2}$, $D_{**} \simeq l_p^2 a^{-1}$ in 3D while $L_{**} \simeq D_{**} \simeq l_p$ in 2D. Both ideal and EV effects coexist in this regime [104]. This balance of ideal and EV behavior is obtained by

setting $a^{d-2}L_{\rm blob}^2/HD^{d-1}=1$ from which the length H can be obtained as follows:

$$H=\sqrt{L_{\rm blob}\ell_p}=a^{d-2}\frac{L_{\rm blob}^2}{D^{d-1}} \tag{3.6}$$

Denoting $L_{\rm blob}$ as $L_{\rm ellip}$, from Eqn. 3.6 we get

$$L_{\rm ellip}={\ell_p}^{\frac{1}{3}}\left(\frac{D^{d-1}}{a^{d-2}}\right)^{\frac{2}{3}}\text{and}H=\ell_p^{\frac{2}{3}}\left(\frac{D^{d-1}}{a^{d-2}}\right)^{\frac{1}{3}}. \tag{3.7}$$

Replacing $D\rightarrow H$, $L_{\rm blob}\rightarrow L_{\rm ellip}$ in Eqn. 3.2 and minimizing with respect to X, we get $X=H(L/L_{\rm ellip})$, and substituting $L_{\rm ellip}$ and H by Eqn. 3.7 we obtain Eqn. 3.3. This completes the proof that the de Gennes regime and the extended de Gennes regime can not be differentiated from the elongation of the chain.

However, by repeating the same procedure we note, unlike Eqn. 3.4 in the extended de Gennes regime the fluctuation is different and is given by $\langle\sigma^2\rangle=L\ell_p$. Therefore, the de Gennes regime and the extended de Gennes regime can be differentiated by measuring the characteristic fluctuations in their respective chain extensions [100]. The lower bound D_* of the extended de Gennes regime where it merges with the Gauss-de Gennes regime, following Odijk's scaling analysis [104] (which is also valid in 2D) is given by $D_*\simeq c\ell_p$, where the prefactor $c\gtrapprox 1$ (in [100] it was found to be ≈ 2). Using Eqn. 3.5 we note that while the range for the extended de Gennes regime being $[D_*, D_{**}]=[c\ell_p,\ \ell_p^2]$ is broad in 3D, it would be either very narrow or vanishingly small to be observed in $[c\ell_p,\ D_{**}\simeq\ell_p]$ in 2D.

3.1.3 Gauss-de Gennes regime

Upon further decrease of the confining region, for $D < D_*$ the EV effect plays no role, and the DNA behaves as a Gaussian chain [104, 103], so that $D = (L_{\rm blob}\ell_p)^{1/2}$ [103]. Then according to Eqn. 3.2, we have the extension

$$\langle X\rangle_{\rm Gauss-deGennes} = L\frac{\ell_p}{D}, \tag{3.8}$$

which holds both in 2D and 3D. It is easy to check that in this regime the fluctuation $\langle\sigma^2\rangle = L\ell_p$, the same as in the extended de Gennes regime.

While Eqn. 3.8 has been recently tested to be true for 3D [103] channels, similar studies have not been done for confined polymers in 2D strips. Considering the absence of Gaussian regime for a bulk 2D swollen chain [53, 101] one wonders if this new Gauss-de Gennes phase will be observed in a 2D strip. The universal fluctuations from our BD simulation studies (Fig. 3.5) will provide conclusive evidence for the absence of a Gaussian regime inside a 2D strip.

3.1.4 Odjik regime

For $\ell_p \gg D$ Odijk [21, 22] argued that the chain deflects back and forth off the wall with a deflection length of $\lambda \simeq (\ell_p D^2)^{1/3}$, and the extension of the confined polymer can be written as [108]

$$\langle X\rangle_{\rm Odijk} = L\left[1 - A\left(\frac{\ell_p}{D}\right)^{-\frac{2}{3}}\right], \tag{3.9}$$

where A is a "universal"[109] prefactor [98, 110]. In this limit it is easy to check that the the free energy and fluctuations in chain length both in 2D and 3D are given by

$$F/k_BT = B\frac{L}{(\ell_p D^2)^{1/3}} \text{and} \langle\sigma^2\rangle = \frac{LD^2}{\ell_p}. \tag{3.10}$$

3.2 Brownian dynamics simulation results

To provide further support to our scaling analyses we have performed Brownian dynamics (BD) simulation with a bead-spring model for a swollen chain having pairwise repulsive Lennard-Jones (LJ) interaction between any two monomers (excluded volume), a finitely extensible nonlinear elastic (FENE) potential between the successive beads (elastic bond energy), and a three-body potential $U_{\text{bend}} = \kappa(1 - \cos\theta_i)$, where θ_i (Fig. 3.2) is the angle between two consecutive bonds, and the parameter $\kappa = \frac{1}{2}k_BT\ell_p$ is a measure of the chain stiffness proportional to the chain persistence length ℓ_p. The DNA-wall interaction is also modeled as LJ. We observed that during simulation the average bond length stays at 0.97 with a fluctuation less than 0.2%, and the bending potential hardly affects the bond length. By monitoring $\langle\cos\theta\rangle$ we also find that $\ell_p = -1/\ln(\langle\cos\theta\rangle) \equiv 2\kappa/k_BT$ to be the same as in a WLC [101]. Numerical integration of the equation of motion with respect to time in the canonical ensemble was done according to the algorithm developed by Gunsteren and Berendsen [20]. In our simulation we have used reduced units of length, time, and temperature to be a, $a\sqrt{\frac{m}{\epsilon}}$, ϵ/k_B, respectively. We have chosen a large number of combinations of $256 \leq N \leq 1024$, the chain persistence length $2 \leq \ell_p \leq 270$ (by varying κ from 1 to

160), and the strip width $D = 18$, 36, and 80 such that the ratio l_p/D is in the window $0.025 \leq l_p/D \leq 15$ and $1 \leq L/\ell_p \leq 400$.

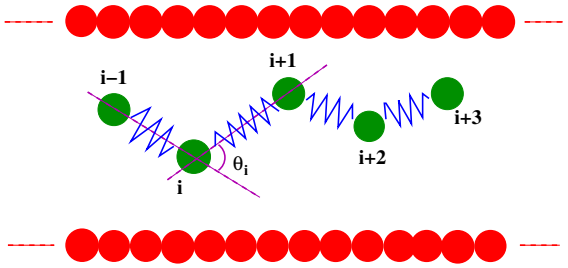

Figure 3.2: Bead-spring model of a 2D polymer confined in a 2D channel.

With these choices we cover experimental study scales (the commonly used λ DNA in experiments has a contour length $L = 16.5\mu$m with a persistence length $\ell_p \simeq 50$ nm, and the channel diameter ranges between 10 nm -200 nm [85]) and fully interpolate from the de Gennes limit to the Odijk limit. The confined chains were equilibrated for several Rouse relaxation time before data were collected over a span of 10 - 25 Rouse relaxation time to ensure convergence.

Fig. 3.3 shows the normalized chain extension. All the data for many combinations of L, ℓ_p, and D collapse onto one master curve and shows a smooth transition from de Gennes regime to Odijk regime, which also indicates the absence of Gauss-de Gennes regime predicted by Eqn. 3.8. For $\ell_p \leq D$ excellent linear fit of $\langle X \rangle / L \sim (\ell_p/D)^{1/3}$ validates theoretical prediction of de Gennes regime (Eqn. 3.3). For $\ell_p > D$ we used Eqn. 3.9 to fit the data and the prefactor is determined to be $A_{strip} = 0.171$. With prior reported values for this prefactor $A_{square} = 0.183$ and $A_{cylin} = 0.170$ [98, 110]) it indicates that the constant A has little dependence on the physical spatial dimension and nearly universal, being consistent

with the fact that one can show the validity of Eqn. 3.9 in both 3D and 2D.

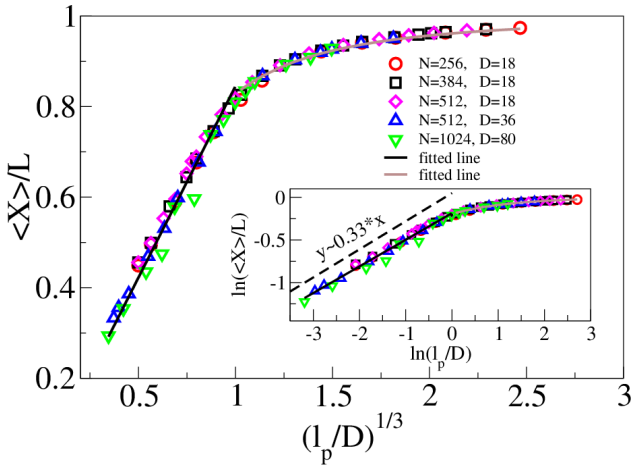

Figure 3.3: Dimensionless chain extension $\langle X\rangle/L$ as a function of $(\ell_p/D)^{1/3}$ for various combination of chain length N, persistence length ℓ_p, and width D of the confining strip. The inset is the log-log plot $\langle X\rangle/L$ as a function of ℓ_p/D showing excellent data collapse with initial slope of 1/3 for $\ell_p \leq D$ verifying Eqn. 3.3.

In the log-log plot shown in the inset of Fig. 3.3, the 1/3 power law dependence in the de Gennes regime expands to $l_p/D \simeq 1$ and the scaling relation Eqn. 3.8 in Gauss-de Gennes regime is not seen at all. Furthermore, around $\ell_p/D \simeq 1$ we find that both Eqn. 3.3 as well as Eqn. 3.9 give *almost the same value for the extension, which shows that a description by Eqn. 3.8 is not necessary indicating that there is no Gauss-de Gennes regime between them.*

We also observe another interesting feature by plotting chain extensions $\langle X\rangle$ normalized by the corresponding bulk end-to-end distance R_{bulk} as a function of ℓ_p/D which exhibits a peak for each curve as shown in Fig. 3.4. This peak can be reconciled by noting

that the normalized extensions in the de Gennes and Odijk limits can be expressed as

$$\frac{\langle X\rangle_{\text{de Gennes}}}{R_{\text{bulk}}} = \left(\frac{L}{\ell_p}\right)^{1/4}\left(\frac{\ell_p}{D}\right)^{1/3} = \tilde{L}\tilde{\ell_p}^{\,1/12}, \tag{3.11a}$$

$$\frac{\langle X\rangle_{\text{Odijk}}}{R_{\text{bulk}}} = \left(1 - A\tilde{\ell_p}^{\,-2/3}\right)\tilde{L}^{1/4}\tilde{l_p}^{\,-1/4}, \tag{3.11b}$$

where we have used D as the unit of length (data points in each curve in Fig. 3.4 have the same D) so that $\tilde{L} = L/D$ and $\tilde{\ell_p} = \ell_p/D$ respectively.

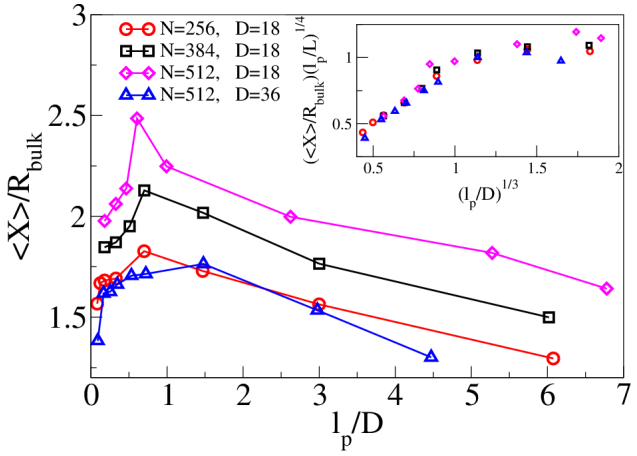

Figure 3.4: Plot of the normalized extension by the end-to-end distance R_{bulk} in the bulk. The inset shows plot of Eqn. 3.11a.

Eqns. 3.11a and 3.11b readily follow from Eqns. 3.1, 3.3, and 3.9 respectively. One notices as ℓ_p/D increases, *i.e.* $\tilde{\ell_p}$ increases, and the extreme left and right side of the peak correspond to de Gennes and Odijk limits respectively. But from Eqn. 3.11a and 3.11b we note that for small values of $\tilde{\ell_p}$ the normalized extension increases as $\sim \tilde{l_p}^{\,1/12}$ (de Gennes limit) whereas, for large values of $\tilde{\ell_p}$ the normalized extension decreases as $\sim \tilde{l_p}^{\,-1/4}$ (Odijk limit), which implies that for finite extension of a chain, the normalized extension will exhibit a maximum as a function of ℓ_p/D. It is also noteworthy that this maximum occurs for $\ell_p/D \sim 1$ at the

confluence of de Gennes and Odijk limit. This description is also consistent with the critical channel width $D_* \simeq 2\ell_p$ which marks the onset of Odijk regime. We also plotted Eqn. 3.11a which is only valid in de Gennes regime (i.e., for $\ell_p < D$) at the inset of Fig. 3.4 showing data collapse similar to Fig. 3.3.

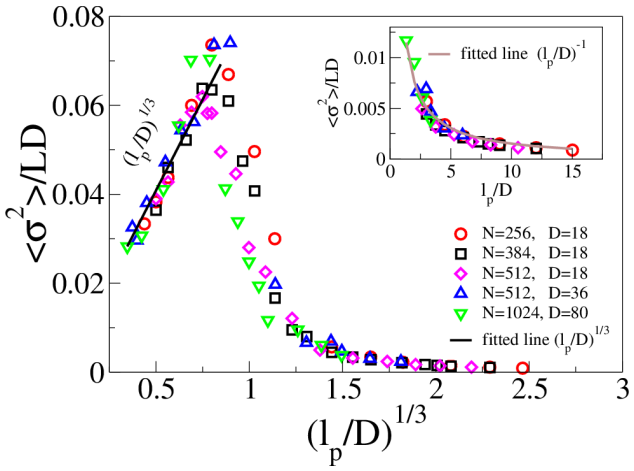

Figure 3.5: Normalized fluctuation $\langle\sigma^2\rangle/LD$ as a function of $(\ell_p/D)^{1/3}$ for the same combinations of N, ℓ_p, and D as in Fig. 3.3. The inset shows $(\ell_p/D)^{-1}$ dependence in the Odijk limit.

We now show simulation results for the fluctuation in the chain extensions and compare these results with the theoretical predictions. According to Eqn. 3.4 and Eqn. 3.10 the normalized fluctuation $\langle\sigma^2\rangle/LD$ scales as $(\ell_p/D)^{1/3}$ and $(\ell_p/D)^{-1}$ in the de Gennes and Odjik limits respectively. Indeed we find in Fig. 3.5 that the fluctuation grows as $(\ell_p/D)^{1/3}$ in the de Gennes regime until $\ell_p \simeq 0.5D$ when it enters the Odijk limit and decays as $(\ell_p/D)^{-1}$ (inset). It is reassuring to note that since both the extended de Gennes and the Gauss-de Gennes regimes do not occur inside a 2D strip, in Fig. 3.5 we do not see any intermediate regime where $\langle\sigma^2\rangle/LD \sim \ell_p/D$, the characteristic fluctuations of both the extended de Gennes as

well as the Gauss-de Gennes regimes. The excellent data collapse for same combinations of N, ℓ_p, and D as in Fig. 3.3 and the sharp peak signifies the onset of a transition from the de Gennes regime to the Odijk regime.

To summarize, in this letter we have provided a generalized scaling theory of confined DNA in d-dimensions and compared/contrasted the behavior in 2D with those in 3D reported recently in the literature. We validate the scaling analyses by BD simulation where we identify each regime from excellent data collapse for the characteristic universal dimensionless extensions and fluctuations in terms of the dimensionless parameter ℓ_p/D. From the scaling analysis and results from BD simulation reported in this letter, and prior work for 3D cylindrical and square channels, we concur that the different regimes of confined polymers follow their corresponding regimes in the bulk. We find that for a 2D strip, the Gaussian regime is absent and the extended de Gennes regime is vanishingly small, so that the chain conformations inside the channel are described either by the de Gennes or by the Odjik regime. Thus the chain conformations for a straightened DNA inside a 2D strip are cleaner than for those of the 3D cylindrical and square geometries. Therefore, we believe that this work will motivate further experimental and theoretical work to study confined DNA inside nano-strips.

CHAPTER 4
SEMI-FLEXIBLE MACROMOLECULES IN QUASI-ONE-DIMENSIONAL CONFINEMENT: DISCRETE VERSUS CONTINUOUS BOND ANGLES

Semiflexible polymers confined in narrow channels have found abiding interests recently, both in experiments [85, 91, 89, 111, 112, 88, 113, 114, 115, 93, 90, 94, 116, 117], analytical theory [78, 118, 119, 120, 121, 122, 106, 104, 123, 124, 125], and in computer simulations [126, 127, 128, 100, 129, 103, 130, 131, 56, 132, 133, 134, 135, 136].From the application side, this problem is of great interest for the detection of single DNA molecules, separating them by size, and to develop tools for their sequence analysis. On the theoretical front, confined semiflexible polymers pose a variety of challenging questions: what aspects of the behavior are specific to a particular polymer, and what aspects of the behavior are generic? For fully flexible polymers confined into cylinders with non-attractive walls under good solvent conditions, one expects a fairly universal picture as soon as the cylinder diameter D is much bigger than the size ℓ of an effective segment. Then scaling theory predicts [102, 42] that a chain takes a cigar-like conformation of length $L_{\|} \approx Dn_b$ where n_b is the number of blobs of diameter D forming a one-dimensional string. Inside each blob self-avoiding walk (SAW) statistics prevails, and hence the number of monomers n per blob satisfies the relation $D \approx \ell n^{\nu}$, where ν is the Flory exponent [42], and prefactors of order unity in such scaling arguments are omitted, as usual. Noting that the total number of monomers per chain is $N =$

$n_b n$, one readily concludes $L_\parallel \approx \ell(D/\ell)^{1-1/\nu}N$. This result has been verified by simulations of various coarse-grained models (e.g., Refs. [137, 138, 139, 98, 140, 141, 142, 143, 144, 145] and [146]).

However, when we deal with semiflexible chains, the persistence length l_p introduces already additional length scales for chains in bulk solution. Indeed, for contour lengths $L = (N-1)\ell$, the chain conformation in a coarse-grained view may resemble a flexible rod of diameter ℓ for $L < \ell_p$, while for $L \geq \ell_p$ in d = 3 dimensions, the polymers resemble Gaussian coils, with a mean-square end-to-end distance R2 = 2pL, as long as excluded volume effects can be neglected. If one models a semiflexible polymer as a freely jointed chain of rods that have length ℓ_p and diameter w (Fig. 4.1(a)), one concludes (that in d = 3 dimensions) excluded volume effects become relevant [59, 74, 75] if L exceeds $L^* \approx \ell_p^3/w^2$ and hence the associated chain radius $R^* \approx \ell_p^2/w$. For $\ell_p < L < L^*$, the conformation of a semiflexible polymer in d = 3 dimensions under good solvent conditions resembles a Gaussian coil, and only for $L > L^*$ does one find swollen coils, $\langle R^2 \rangle = \ell_p^{2/5} w^{2/5} L^{6/5}$ (if one uses the Flory estimate [42, 45] $\nu = 3/5$ instead of the more accurate estimate [147] $\nu \approx 0.5877$). In $d = 2$, however, this intermediate Gaussian regime is absent [74, 53], and for $L \approx \ell_p$, one immediately crosses over to two-dimensional self-avoiding walk like conformations, with $\langle R^2 \rangle \approx \ell_p^{1/2} L^{3/2}$ (remember $\nu = 3/4$ in $d = 2$) [42, 45]. We now draw attention to the length scales of confined semiflexible polymers. For semiflexible chains confined in a cylinder or in a planar slit of diameter (or width) D, the Odijk deflection length [78] (Fig. 4.2(a))

$$\lambda \approx D^{2/3} \ell_p^{1/3}, \tag{4.1}$$

which describes the typical length scale over which a chain maintains its orientation in a very narrow channel ($D \ll \ell_p$), gives rise to additional length scales due to hairpin formation [104, 148],such as the typical distance g between neighboring hairpins (Fig. 4.2(a)), when D is of the same order as ℓ_p. While one expects that semiflexible chains in wide channels ($D \gg \ell_p$) also are compatible with the Daoud-De Gennes [102] picture of a string of blobs, the crossover from the Odijk regime ($D \ll \ell_p$) where $L_\parallel$ differs from L only by a small correction (of order [78, 98] $(D/\ell_p)^{2/3}$) to this regime is still a matter of debate [85, 127, 128, 100, 129, 103, 133]. However, we note that Eqn. 4.1 is based on the use of the Kratky-Porod model of wormlike chains [8, 7] which describes the polymer in terms of a contour $\vec{r}(s)$ in space, s being a coordinate along this contour, and the Hamiltonian involves a single parameter, the bending rigidity κ_{KP},

$$\mathcal{H} = \frac{\kappa_{KP}}{2} \int_0^L ds \left(\frac{d^2\vec{r}}{ds^2} \right)^2 . \tag{4.2}$$

The persistence length ℓ_p is related to κ_{KP} via $\ell_p = \kappa_{KP}/k_B T$ (in d = 3) or $\ell_p = 2\kappa_{KP}/k_B T$ (in $d = 2$, respectively).

Of course, linear macromolecules are chain molecules where discrete monomers are linked together with covalent chemical bonds along the backbone of a chain; a continuum model such as Eqn. 4.2 can make sense only if the number n_m of such monomers on the length scale ℓ_p is very large. This is the case for double-stranded (ds) DNA, where in typical cases, $\ell_p \approx 50$nm [149] and $\ell \approx 0.260.5$ nm [46]; however, when we consider a situation where D is significantly smaller than ℓ_p and two hairpins have to fit into the scale D (Fig. 4.2(a)), the accuracy of such continuum descriptions seems to us somewhat doubtful.

Moreover, it also is of interest to consider also polymers with smaller persistence length, even almost flexible polymers like polyethylene (PE), Fig. 4.1(b), and polystyrene (PS) exhibit already some local stiffness that needs to be accounted for, and many other rather stiff synthetic polymers exist. Thus, while for PE at $T = 400$ K, $\ell_p \approx 0.75$ nm (and the length ℓ of the CC bond is 0.15 nm) [150] and for PS corresponding literature estimates [151, 152] are $\ell = 0.25$ nm, $\ell_p \approx 1.01.15$ nm, a comparative study of various synthetic polymers [153] has yielded estimates for ell_p in the range from 1 nm to 42 nm, giving also evidence for the double crossover (from rods to Gaussian coils and then to swollen coils) with increasing contour length, in bulk solution under good solvent conditions. For biopolymers one can find examples where $\ell_p \approx 25$ nm (acetan) or $\ell_p = 120$ nm (xanthan) [154], and thus, we prefer not to constrain ℓ_p in our study to a particular value, but rather find it useful to vary it from the fully flexible limit to very stiff chains.

We focus on the fact that for semiflexible polymers, different coarse-grained models are useful (see Fig. 4.1), depending on the underlying chemistry of the macromolecules that are studied which may differ in their mechanism of flexibility [155]. For dsDNA (under many conditions of interest), there is no conformational disorder on length scales much less than ℓ_p, and flexibility only arises due to the gradual accumulation of the effect of small deviations of valence angles, bond lengths, etc., from their energetically preferred average values. Such deviations inevitably are present due to thermal vibrations [155].In polymers such as PE and PS, however, the dominating mechanism of flexibility is of the type of the rotational isomeric states (RIS) model [44], where the chain can be viewed as a succession of all-trans sequences

(n CC bonds where the torsion angle φ), separated by gauche ($g^{\pm}$) states where the torsional angle is $\pm 120°$(Fig. 4.1(b)). The typical length of all-trans sequences is controlled by the depth of the trans-minimum in the torsional potential relative to the gauche minima, and thus strongly temperature-dependent.

In the context of computer simulations, a much simpler model of this type is defined on the square (Fig. 4.1(c)) or simple cubic lattice, where one models macromolecules simply as self-avoiding walks on these lattices, modeling local chain stiffness via introduction of an energy penalty ϵ_b whenever the walk makes a $\pm 90°$ turn. While this model clearly is only a crude caricature of any real polymer, it shares the property of the alkane-type chains that the local chain contour does not resemble the smooth wormlike chain picture implied by Eqn. 4.2. We feel that different coarse-grained models of semiflexible polymers may be needed for different circumstances: models of the type of Figs. 4.1(b) and 1(c) may be appropriate for the description of an alkane chain in a carbon nanotube, while the wormlike chain model may be more appropriate for DNA in channels that are 150 nm wide [85].

Of course, it is well-known particularly for biomolecules that one has to deal there with a multitude of energy scales and length scales, and the optimum choice of a coarse-grained model does depend on the phenomena under study [49, 156]. As a disclaimer, we emphasize that the models shown in Figs. 4.1 and 4.2 are not meant as an exhaustive list: there are many other interesting models in the literature that we do not discuss here (e.g., Refs. [157] and [158]). In our paper we shall also not discuss further the model of Fig. 4.1(a), although it was used in related studies [131, 135]. Here, we shall only focus on a comparison

of the two models of Figs. 4.2(b) and 2(c), both in the bulk and under confinement, to clarify to what extent their properties are universal and to find out what the consequences of different assumptions (such as discrete versus continuous bond angle distributions) are. Also the question to what extent the wormlike chain model (Fig. 4.2(a)), which ignores the fact that there are individual monomers along a chain rather than a continuous mass distribution, describes the properties of these models accurately will be addressed. Thus, it is the aim of this study to elucidate some general questions on the concept of coarse-graining of macromolecules and study the question which properties of (confined) semiflexible polymers are universal and which are model-dependent.

In Sec. II, the models studied and the simulation methodologies will be briefly summarized. In Sec. III, a comparison of the properties of single chains in bulk (two-dimensional) solution for both models will be given. Sec. IV describes our findings for confined chains, focusing on the case of confinement by repulsive boundaries only. We shall address also the problem of the extent of depletion of monomers near these repulsive walls, since the density profiles of flexible and semiflexible polymers near hard walls are predicted to have characteristic differences [159].Throughout this work, we pay attention to the fact that the persistence length is a meaningful concept for the local chain stiffness only [47, 76], it must not be associated with the decay of long range orientation correlations along the chain contour. Sec. V finally summarizes our conclusion.

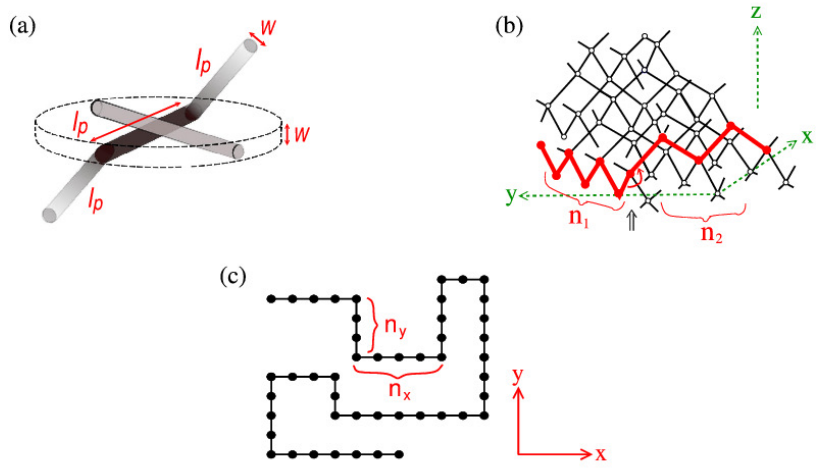

Figure 4.1: Some coarse-grained models for semiflexible polymers (schematic). Case (a) shows a model where rigid cylinders of length ℓ_p and diameter w are freely jointed at their links. The excluded volume for a link of another chain (displayed in lighter gray) is a disk of height w and diameter ℓ_p, as indicated by broken lines. This type of model is used as an input for the Flory-theory treatment. Case (b) shows a model for alkane chains with rigid bond lengths and perfect tetrahedral bond angles, so that the chain fits on an ideal diamond lattice (the sites of the lattice are shown by open circles, connected by thin bonds). The monomers (CH_2-groups) are shown as black dots, connected by C-C bonds (thick lines). An all-trans sequence of n_1 bonds (torsion angles = 0 in the all-trans sequence) terminates by a gauche $\pm$ state (torsional angle $\varphi = \pm 120°$, highlighted by an arrow) where a differently oriented all-trans sequence of n_2 bonds follows. Case (c) shows a two-dimensional generalized self-avoiding walk model on the square lattice. Due to an energy penalty for $\pm 90°$ kinks along the chain, the numbers of straight sequences of bonds along the x-axis (nx) and along the y-axis (ny) typically are much larger than unity. A possible definition of the persistence length then is $\ell_p = \langle n_x \rangle a = \langle n_y \rangle a$, where a is the lattice spacing.

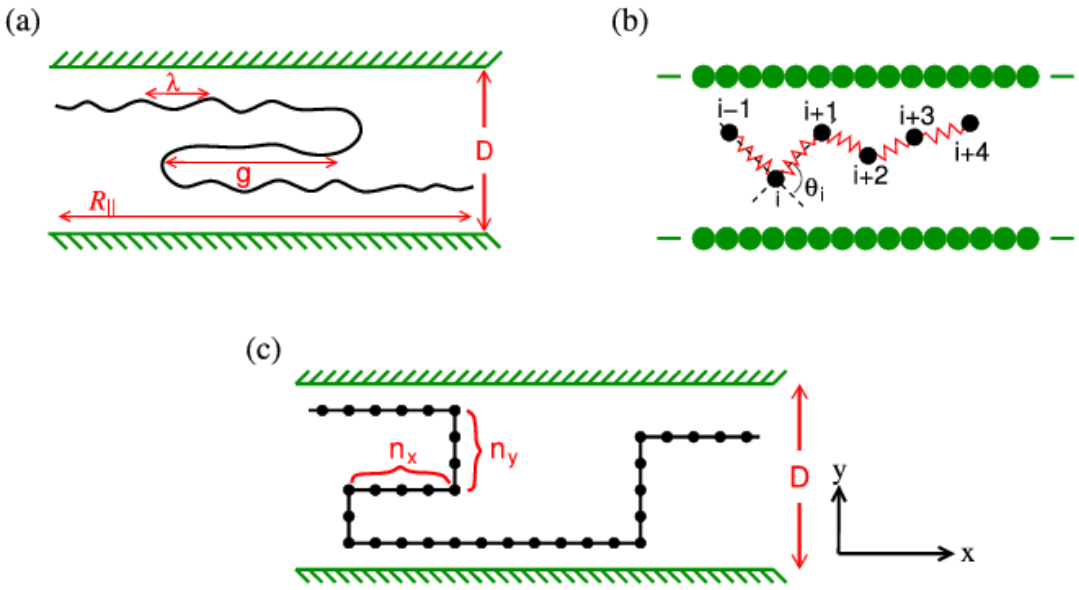

Figure 4.2: Some models for confined semiflexible chains: Case (a) shows the Kratky-Porod worm-like chain in a strip of width D, illustrating the definition of the deflection length λ and the typical distance g between neighboring hairpins. Also the component of the end-to-end distance parallel to the boundaries $R_{||}$ is indicated. Case (b) shows a bead-spring model, where flexibility is controlled by a potential $U_b(\theta_i)$ for the bond angles θ_i. Walls are indicated by particles touching each other. Case (c) shows the model of case (Fig. 4.1(c)) assuming confinement in a strip of width D, displaying also a lattice analog of a double hairpin configuration.

4.1 Models and simulation methodology

In this paper, we consider models in $d = 2$ space dimensions only. Although this restriction precludes a direct comparison of our results with most experimental work, there is the major simplifying feature, that unconfined semiflexible polymers exhibit a single crossover, from rods to self-avoiding walk like chains [74, 75, 54, 160, 68].The intermediate region of Gaussian random walk-like chains does not occur, and there is evidence to believe that this intermediate regime complicates the crossover behavior of confined semiflexible polymers considerably (see, e.g., Refs. [100]and [129]). Also the complication that knots may form (which is relevant for dsDNA in various circumstances [161, 162]) cannot occur in $d = 2$. Our preliminary work [56, 133] on confinement effects on chains in $d = 2$ already has indicated a rather complex behavior, and hence in the present work, we shall address this problem in more detail, with an emphasis on the question to what extent the phenomena are universal and which aspects are model-dependent. Hence, we shall contrast results for the lattice model of Figs. 4.1(c) and 4.2(c) with results for the bead-spring model of Fig. 4.2(b) and shall explore to what extent the predictions of the Kratky-Porod wormlike chain model in the continuum (Fig. 4.2(a)) can be verified.

In our lattice model, each effective monomer occupies a lattice site of the square lattice, and the bond length ℓ between nearest neighbors along the chain is just the lattice spacing, taken as a unit of length for this lattice, so the contour length L, related to the number of beads N as $L = (N - 1)\ell$ also is an integer. Both for this model and the

continuum bead-spring model we assume that the standard bond bending potential (θ is the angle between subsequent bonds along the chain)

$$U_b(\theta) = \epsilon_b(1 - \cos\theta) \tag{4.3}$$

On the lattice, however, only angles $\theta = 0°$ and $\pm 90°$ are permitted ($\theta = 180°$, i.e., immediate reversals are forbidden by excluded volume, of course) and so $U_b(\theta) = 0$ if the SAW continues straight on, while $U_b(\theta) = \epsilon_b$ if it makes a kink. The partition sum of the semiflexible SAW hence can be written as a polynomial in the Boltzmann factor $q_b = \exp(-\epsilon_b/k_BT)$,

$$Z_N(q_b, D) = \sum_{\text{config.}} C_{N,N_{\text{bend}}}(D) q_b^{N_{\text{bend}}} \tag{4.4}$$

Here, the sum over configurations includes all SAWs with y coordinates of the monomers in the range $1 \leq y \leq D$, to realize the confinement by repulsive (one-dimensional walls) placed at $y = 0$ and $y = D + 1$ (so the geometric distance between the walls is $D + 1$). Of course, the limit $D \to \infty$ means we consider an unconfined polymer. This problem can be studied very efficiently with Monte Carlo (MC) simulations applying the pruned-enriched Rosenbluth method (PERM) [54, 57, 58].This chain growth algorithm with population control and depth-first implementation has been thoroughly reviewed in Ref. [58], where the reader can find more details. We could study chain lengths up to $N \sim 10^5$, for a wide variety of chain stiffness, varying $q_b = 1.0$(fully flexible chains) to $q_b = 0.005$ (rather stiff chains, with a persistence length [56, 54] $\ell_p \approx 118\ell$). Note that both for the lattice model and the continuum model the persistence length is extracted from $\langle\cos\theta\rangle$ via

$$\ell/\ell_p \equiv -\ln(\cos\theta) \tag{4.5}$$

We recall that the persistence length has a physical meaning (for real polymer chains) only as a characteristic for the local angular correlation between neighboring bonds but cannot be interpreted in terms of orientational correlations for large chemical distances along the chain [54, 47, 76]:the textbook formula [45] $\langle \cos\theta \rangle \propto \exp(-\ell s/\ell_p)$ for the angular correlation of bonds a chemical distance ℓs apart along the contour holds only for Gaussian phantom chains, while in reality $\langle \cos\theta \rangle$ decays with a power law in s. We emphasize this simple point again, because the misleading textbook formula still is widely used in the literature, without being aware of its limitations (it makes sense only for $\ell s < \ell_p$, of course). The persistence length as defined in Eqn. 4.5, however, can be related to the stiffness parameter κ_{KP} of the Kratky-Porod model, since for stiff chains $\langle \cos\theta \rangle$is close to unity and hence $\ell/\ell_p \approx \langle \theta^2 \rangle/2$.

If excluded volume could be neglected on the local scale, we would have $\langle \cos\theta \rangle = 1/(1+2q_b)$in $d = 2$ and hence $\ell_p/\ell \approx 1/(2q_b)$ for small q_b. The data (Table 4.1 [54]) rather imply $\ell_p/\ell \approx 0.61/q_b = 0.61 \exp \epsilon_b/k_BT$. This exponential dependence between ℓ_p and ϵ_b is a characteristic of the lattice model (since thermal activation is required to make a bend), but a similar variation can also be expected for the alkane-type chains (Fig. 4.1(b)), where the energy difference between the gauche $\pm$ and trans-minima of the torsional potential would correspond to ϵ_b.

The bead-spring model used by us describes excluded volume interactions between the monomers by the standard short range Lennard-Jones (LJ) potential $U_{LJ}(r)$ as Eqn. 1.13. The connectivity between neighboring monomers along the chain is ensured by using the Finitely Extensible Nonlinear Elastic (FENE) potential [19] as Eqn. 1.14.

Table 4.1: Estimates of the persistence length ℓ_p/ℓ (Eqn. 4.5) of polymer chains in the bulk for the lattice model and the continuum model.

Lattice			Continuum			
q_b	ϵ_b	ℓ_p/ℓ	κ	ℓ_p/ℓ	κ	ℓ_p/ℓ
1.0	0	1.06	1.5	2.74	48.0	79.04
0.4	0.92	2.00	2.0	3.30	64.0	105.60
0.2	1.61	3.50	3.0	4.58	96.0	159.10
0.1	2.30	6.46	4.0	6.05	128.0	212.40
0.05	3.00	12.35	6.0	9.25	192.0	319.10
0.03	3.51	20.21	8.0	12.56	320.0	532.50
0.02	3.91	30.02	12.0	19.27		
0.01	4.61	59.22	16.0	25.91		
0.005	5.30	118.22	32.0	52.62		

We choose σ as the unit of length for this off-lattice model and ϵ/k_B as the unit of temperature T. Choosing $T = 1.2$ throughout and $k = 30$, the average bond length $\ell = 0.971$ and we find that this length does not depend on the choice of the parameter ϵ_b in Eqn. 4.3, which we use here as a bond bending potential as well. However, unlike the case of the lattice model, a continuous range of bond angles θ from $\theta = 0$ to (almost) $\theta = 180°$ is possible, and the parameter ϵ_b now can be related to the rigidity parameter k_{KP} of the Kratky-Porod wormlike chain model, as is well-known (see, e.g., Ref. [160, 68] where it is shown that $k_{KP}/\ell = \epsilon_b$). In order to easily distinguish in the present paper the data of the continuum model from those of the lattice model, we shall define $\kappa \equiv \epsilon_b$ for the data of the continuum model, to remind the reader that this parameter (apart from the factor l which is very close to unity anyway) essentially measures the chain rigidity in the usual way. Likewise, the chain length N for long chains in our units is numerically very close to the contour length L(strictly speaking, $L = (N-1)\ell$, of course). The potential for the monomer-wall interaction is chosen in full analogy to Eqn. 1.13, namely, when we orient the walls along the x-axis, we have

$$U_{\text{wall}}(y') = 4\epsilon \left[\left(\frac{\sigma}{y'} \right)^1 2 - \left(\frac{\sigma}{y'} \right)^6 \right] + \epsilon, \quad \text{for} \quad y' \leq 2^{1/6}\sigma,$$
$$U_{\text{wall}}(y') = 0, \quad \text{for} \quad y' > 2^{1/6}\sigma, \tag{4.6}$$

and $y' = y$ at the lower wall while $y' = Dy$ at the upper wall. When we compare the continuum model to the lattice model, the correspondence of what a particular strip thickness means is somewhat subtle. On the lattice, the geometric distance between the two walls is $D+1$ lattice spacings, but only a region of extent D (lattice rows $n = 1, 2, ..., D$) is accessible

for occupation by the monomers of the chain. In the continuum, the full range $0 < y < D$ is in principle accessible for the monomers, but due to the repulsive potential, the regions $0< y < \sigma/2$ and $D - \sigma/2 < y < D$ are practically almost excluded for the monomers. Thus, one could argue that the parameter D of the continuum model should be compared to the parameter $D + 1$ of the lattice model. Such ambiguities in the comparison will not matter if D is very large, of course. To be better able to compare data of both models directly, we shall introduce the notation of an effective strip thickness D_{eff}, with $D_{\text{eff}} = D + 1$ in the lattice case and $D_{\text{eff}} = D$ for the continuum model.

For the off-lattice model, chain configurations are equilibrated by using standard Molecular Dynamics (MD) methods applying the Langevin thermostat as usual [19] (See Eqn. 1.17). The reduced unit of time then is $(m\sigma^2/\epsilon)^{1/2}$, and this set of equations of motion then is integrated with the reduced time step $\Delta t = 0.01$, applying the algorithm of van Gunsteren and Berendsen [20] Typically the length of the runs was 10^9 time steps.

We note that slightly more complicated models of this type can serve as coarse-grained models for chemically specific macromolecules exhibiting some angular rigidity, e.g., polyvinyl alcohol [163],but this is not our focus here.

4.2 Single chains in bulk dilute solution: a comparison between the lattice and the continuum model

In this section, we demonstrate that the scaled mean square end-to-end distance and the scaled mean square transverse fluctuation of two-dimensional semiflexible chains of contour length L exhibit an almost universal behavior, when one studies these quantities as a function of the dimensionless parameter L/ℓ_p, i.e., measuring the contour length in units of the persistence length.

Of course, such a type of scaling is already suggested by the Kratky-Porod model [8, 7], which would yield for the mean-square end-to-end distance $\langle R_N^2 \rangle$ for a wormlike chain,

$$\langle R_N^2 \rangle / (2\ell_p L) = 1 - \frac{\ell_p}{L} \left[1 - \exp\left(-L/\ell_p \right) \right] \tag{4.7}$$

Evidently for $L \ll \ell_p$ the chain behaves like a rigid rod, $\langle R_N^2 \rangle = L^2$, while the limiting behavior for $L \gg \ell_p$ is that of a Gaussian coil, $\langle R_N^2 \rangle = 2\ell_p L$. Thus, it is natural to provide a plot of our simulation results in the normalization suggested by Eqn. 4.7, studying $\langle R_N^2 \rangle / (2\ell_p L)$ as a function of L/ℓ_p (Fig. 4.3(a)). It is seen that on the log-log plot there are essentially two regimes of straight lines, with slopes of unity and one half, respectively. The regime with slope unity is the rod-like regime expected from Eqn. 4.7, and there the lattice and continuum results precisely superimpose, which is no surprise at all, of course. As expected, the rod regime stops near $L/\ell_p \approx 1$. While Eqn. 4.7 would predict for $L/\ell_p \gg 1$ a horizontal plateau, i.e., slope = zero on the log-log plot, this regime of Gaussian behavior is completely absent.

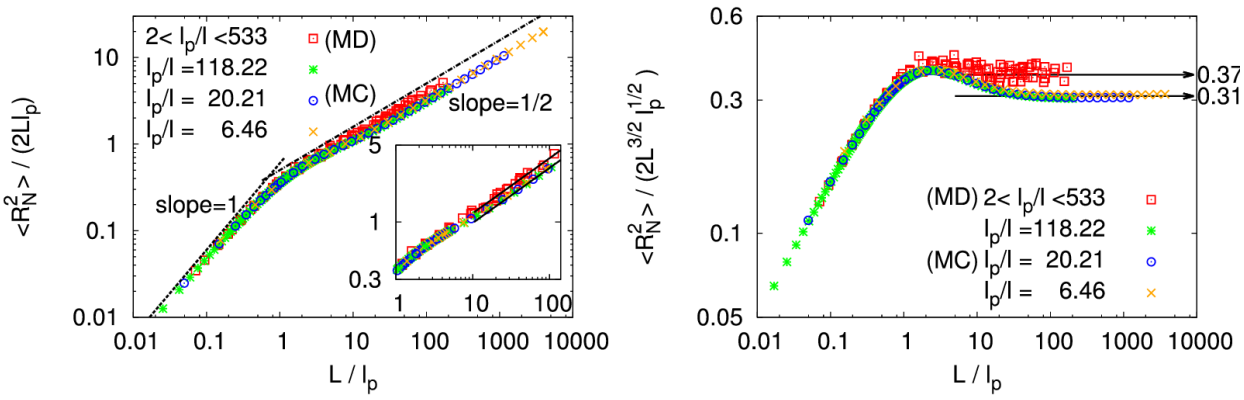

Figure 4.3: (a) Log-log plot of $\langle R_N^2/(2L\ell_p)\rangle$ as a function of L/ℓ_p, combining the result of both MC and MD simulations, for the models of Sec. II. MC data include many chain lengths up to $N = 25600$, for three choices of the stiffness: $\ell_p/\ell = 6.46(q_b = 0.1), 20.21(q_b = 0.03)$, and 118.22 ($q_b = 0.005$), respectively. MD data [160, 68] (indicated as squares) are for $16 \leq N \leq 2048$, with $0 \leq \kappa \leq 320$ ($\ell_p/\ell \approx 1.66\kappa$). The dashed and dotted-dashed lines indicate the rod regime and the excluded volume power law, respectively. No adjustable parameters whatsoever have been used in this plot. The inset shows the same data in the range from $1 < L/\ell_p < 140$, and separate straight lines were fitted to the data from MD and MC for $L/\ell_p > 10$, respectively. (b) Log-log plot of the dimensionless ratio $\langle R_N^2\rangle/(2L^{3/2}\ell_p^{1/2})$ versus L/ℓ_p, using the same (non-universal!) amplitude factors $A/2 = 0.31$ for the lattice model and $A/2 = 0.37$ for the continuum model, respectively. Note that statistical errors of the MC data are smaller than the size of the symbols throughout. In (b), statistical errors of the MD data are almost twice the size of the squares, for $L > \ell_p$, but not shown for the sake of clarity.

This breakdown of the Kratky-Porod model in $d = 2$ dimensions due to excluded volume forces has been studied in earlier work [74, 75, 54, 53, 160, 68], but the new feature of Fig. 4.3(a) is that the behavior is almost universal. Only on magnified scales (inset of Fig. 4.3(a)) can one distinguish that the continuum model data and the lattice model data settle down on two distinct parallel straight lines for $L/\ell_p > 10$. In fact, for $L \gg \ell_p$ we expect a behavior typical for SAWs in $d = 2$, namely,

$$\langle R_N^2 \rangle = A \ell_p^{1/2} L^{3/2}, L \gg \ell_p \tag{4.8}$$

where the dimensionless amplitude factor A is a nonuniversal constant. Fig. 4.3(b) hence presents a plot of $\langle R_N^2 \rangle / \left(2L\ell_p(L/\ell_p)^{1/2}\right)$ which shows in more detail how the limiting behavior of Eqn. 4.8 is approached. One can see that in the crossover region between rods and SAWs, namely, for $1 \leq L/\ell_p \leq 10$, there occurs some overshoot, and this overshoot is more pronounced for the lattice model than for the continuum model. Of course, this behavior in the crossover region is quite nontrivial, and there is no simple interpretation by scaling arguments known.

Next we consider transverse fluctuations of the semiflexible chains. For this purpose we introduce an instantaneous coordinate system (ξ, η) for each configuration of the chain such that the ξ-axis is oriented along the end-to-end vector of the chain, so $\hat{\xi} = \vec{R}_N/|\vec{R}_N|$ is a unit vector along the ξ direction. We then define the transverse fluctuations as

$$\ell_\perp^2 = \frac{1}{N} \sum_{i=1}^{N} \eta_i^2 \tag{4.9}$$

with (ξ_i, η_i) being the coordinates of the ith monomer in this (ξ, η) coordinate system. Fig. 4.4 then presents a plot of $\langle \ell_\perp^2 \rangle^{1/2}/L$ versus L/ℓ_p.

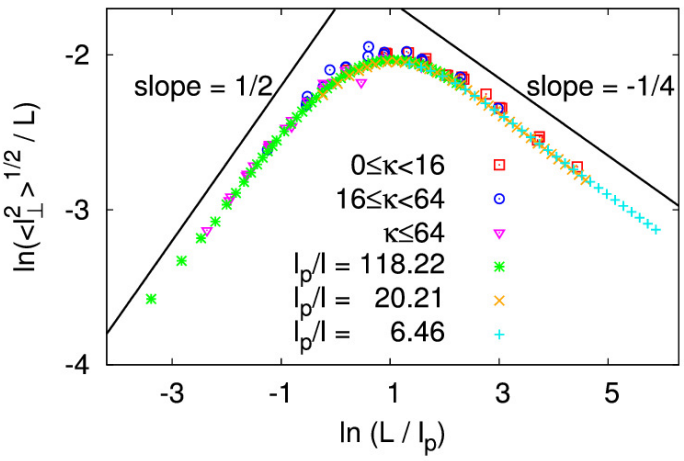

Figure 4.4: Logarithm of the scaled transverse fluctuation $\langle \ell_\perp^2 \rangle^{1/2}/L$ as a function of $\ln(L/\ell_p)$ with data of both MC and MD for various choices of the persistence length listed in Table 4.1, as indicated. The asymptotic power laws $\langle \ell_\perp^2 \rangle^{1/2}/L \propto (L/\ell_p)^{1/2}$ for $L < \ell_p$ and $\langle \ell_\perp^2 \rangle^{1/2}/L \propto (L/\ell_p)^{-1/4}$ for $L > \ell_p$ are indicated by solid straight lines.

In the rod regime, it is well-known [78, 77, 79] that

$$\langle \ell_\perp^2 \rangle \propto L^3/\ell_p, L \ll \ell_p \tag{4.10}$$

while for $L \gg \ell_p$ the configuration of the chain simply is a swollen coil, and the direction of $\hat{\xi}$ does no longer play a special role: so we expect $\langle \ell_\perp^2 \rangle = A' \ell_p^{1/2} L^{3/2}$, compare with Eqn. 4.8, where A' is another amplitude factor. Hence, $\langle \ell_\perp^2 \rangle^{1/2}/L = (A')^{1/2}(\ell_p/L)^{1/4}$ in this limit, and this is what we see in Fig. 4.4. The result that Eqn. 4.10 also applies to the lattice chains is rather unexpected, of course, since on the lattice for $L \ll \ell_p$ typical configurations have either no kink at all on the length L or exhibit a single kink (the walk goes straight along a lattice direction for L' steps and then L'' steps in the direction perpendicular to the direction

of the first L' steps with $L = L' + L''$, while walks with two or more kinks make negligible contributions). Figs. 4.3 and 4.4 hence reveal that the average geometrical properties of semiflexible polymers depend only very little on the model used to describe them, lattice and continuum models exhibit almost no difference, although the actual conformations are very different.

We also suggest that a plot of experimental data of $\langle \ell_\perp^2 \rangle^{1/2}/L$ versus $\ln(L/\ell_p)$ would be a good way to obtain an estimate for the persistence length ℓ_p, since the maximum of this curve (Fig. 4.4) seems to occur for $\ln(L/\ell_p) = 1$, i.e., $\ln(L/\ell) = 1 + \ln(\ell_p/\ell)$. This analysis, applied to atomic force microscope (AFM) images of DNA chains (as are available in the literature [37, 39]), may be an interesting alternative to the traditional fitting of the Kratky-Porod results, Eqn. 4.7, to the chain linear dimensions of such semiflexible polymers adsorbed to substrates. Since Eqn. 4.7 breaks down in $d = 2$, for $L \gg \ell_p$ use of Eqn. 4.7 may lead to significant systematic errors.

4.3 Semi-flexible polymers confined in a slit with repulsive boundaries

We now study semiflexible polymers in quasi-one-dimensional confinement, extending the discussions that were already given in our preliminary work [56, 133]. The considered lattice model is defined in Fig. 4.2(c), and the continuum model (sketched in Fig. 4.2(b)) is defined precisely by Eqns. 1.13 and 4.6.

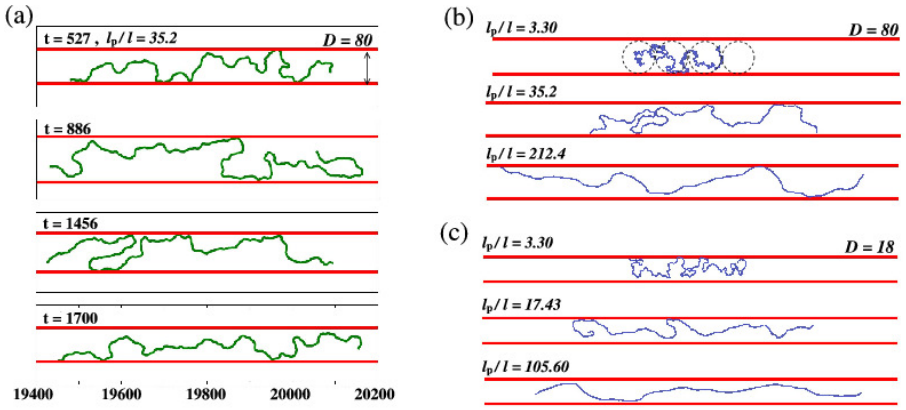

Figure 4.5: (a) Selected snapshots from the MD simulation for $N = 1024, D = 80, \ell_p = 35.2\ell$ (i.e., the choice $\kappa = 21.6$) at various times (the time of the snapshots is the number in the left upper corner of the snapshot, given in units of 5000 MD time units, times $t = 527, 886, 1456,$ and 1700 being shown). Note that the resolution of the snapshot is not high enough to display the individual effective monomers of the simulated model (at high resolution, the snapshots would resemble Fig. 4.2(b)). Note that the x and y axes are plotted with equal length scale, avoiding any distortion between the length in x and y directions. The solid straight lines represent the two boundaries of the strip. (b) Snapshots for chains with $N = 1024$ for $D = 80$ and three choices of persistence length, $\ell_p = 3.30\ell, 35.2\ell,$ and 212.4ℓ, as indicated. (c) Snapshots for chains with $N = 256$ for $D = 18$ and three choices of persistence length, $\ell_p = 3.30\ell, 17.43\ell,$ and 105.60ℓ, as indicated. Movies shown online are made with visual molecular dynamics (VMD). [164]

In computer simulations of very long polymer chains in confinement, a crucial question is whether the statistical effort invested is large enough so that the configuration space of the model is sampled sufficiently well. This problem is a serious concern both for the PERM Monte Carlo algorithm (when the coarse-grained free energy function of the model splits into distinct valleys separated by entropic barriers, one must make sure that all valleys are properly sampled [144]) and for MD. In MD, we expect very long relaxation time to form hairpins [Fig. 4.2(a)] and to equilibrate them; it might occur that hairpins form primarily at the free chain ends and then diffuse along the contour of the chain towards its center.

To clarify such problems, we have recorded time sequences of snapshot pictures of the chain configurations for representative choices of parameters. Fig. 4.5(a) (Multimedia view) gives a few typical examples. One can see that at the first time ($t = 527$), there is no hairpin, at the second time ($t = 886$), there is a hairpin at the rightmost part of the chain and another one in the central part of the chain, and at the third picture ($t = 1456$), all these structures are gone, and a double hairpin configuration (similar to the qualitative sketch in Fig. 4.2(a)) near the left end of the chain has formed. At a still later time ($t = 1700$), a state with no hairpin is found again. Thus, one can see that (for the chosen parameters) hairpins are quickly formed and relax again, the lifetime of hairpins being small in comparison to the length of the MD run. For the chosen parameters the polymer neither resembles a string of blobs nor a flexible rod, but takes intermediate types of states. For $D \ll ell_p$ (Figs. 4.5(b) and 4.5(c) (Multimedia view)), one finds in practice never any configurations with hairpins, the latter occur typically when $\ell_p \leq D \leq 3\ell_p$, while for still wider strips, the string of blobs

picture starts to apply. However, for the choice $D = 80$, $\ell_p = 3.30\ell$ shown in Fig. 4.5(b) (Multimedia view), the chain of length $N = 1024$ is merely long enough to form 2-3 blobs only. From the snapshots, it also is evident that monomers occur near the walls occasionally, but much more frequently they are near the center of the strip.

Fig. 4.5 (Multimedia view) does display some qualitative similarity to the description proposed by Odijk [78] who introduced for the case $D < \ell_p$ the concept of the deflection length, Eqn. 4.1, see also Fig. 4.2(a), using the Kratky-Porod model, Eqn. 4.2. It is an interesting issue to examine to what extent our simulations confirm this description quantitatively.

A naive analysis of the configurations can be based on a study of the local angle ϕ_i of the bond between monomers i and $i+1$ and the x-axis, and search for the locations of local maxima of $\cos\phi_i$ along the chain contour: in the (x, y)-plane these local maxima correspond to extrema of the curve that is generated by connecting the discrete points (x_i, y_i) making the monomer positions along the chain (Fig. 4.6(a)). The distance between subsequent extrema could be taken as a first estimate of the deflection length λ.

However, little thoughts reveal that such a procedure would be quite misleading: the bond angles θ_i between subsequent bonds due to thermal fluctuations have random values of order $\pm\sqrt{k_B T/\kappa}$ (equipartition theorem). Adding up such random increments gives rise to wiggles in the chain configurations on many length scales. Of course, the discreteness of the chain provides a small scale cutoff, and we need to average of the order of 10 subsequent monomers to obtain this random walk-like behavior of the angular increments, but such

small scale wiggles create a displacement Δy in y-direction which is of order unity only, not of order D. The deflection length, however, is intended to rather measure the length scale of wiggles in the chain configurations, with displacement of order D.

In order to measure this large scale, we have to construct a coarse-grained configuration. A practically useful prescription is to apply a coordinate smoothing procedure

$$\bar{x}_i = (2m+1)^{-1} \sum_{j=i-m}^{i+m} x_j, \bar{y}_i = (2m+1)^{-1} \sum_{j=i-m}^{i+m} y_j \tag{4.11}$$

We have found that for persistence lengths of the order of 100, a value of $m = 31$ yielded satisfactory results, smoothing out the small scale wiggles but leaving the large scale configuration of the chain intact (Figs. 4.6(b) and 4.6(c)). Of course, there is still the problem that near an extremum of the coarse-grained curve, ϕ_i changes its sign many times, leading to several close by extrema of cosi. For automatic detection of local maxima for cosi, only sites i that satisfy $\cos\theta_i > c$ were considered (with a threshold value $c = 0.998$ if the persistence length is of order 100, i.e., $|\phi_i| \approx 4^\circ$), and among the deflection sites thus found only those are kept, which are more distant from each other than a distance $d = \lambda/3$ where λ is the Odijk result, Eqn. 4.1. These remaining extrema are indeed the desired deflection points of the coarse-grained configuration where the distance y in y-direction from one deflection point to the next one is much larger than unity (Figs. 4.6(b) and 4.6(c)). From this coarse-graining procedure, we obtain estimates for both the average deflection length $\bar{\lambda}$ and the width $\Delta\lambda$ of the distribution function $P(\lambda)$, see Table 4.2. It is seen that the results are of the same order as Eqn. 4.1; of course, in Eqn. 4.1, a prefactor of order unity is suppressed, as always in scaling arguments, and hence perfect agreement cannot be expected.

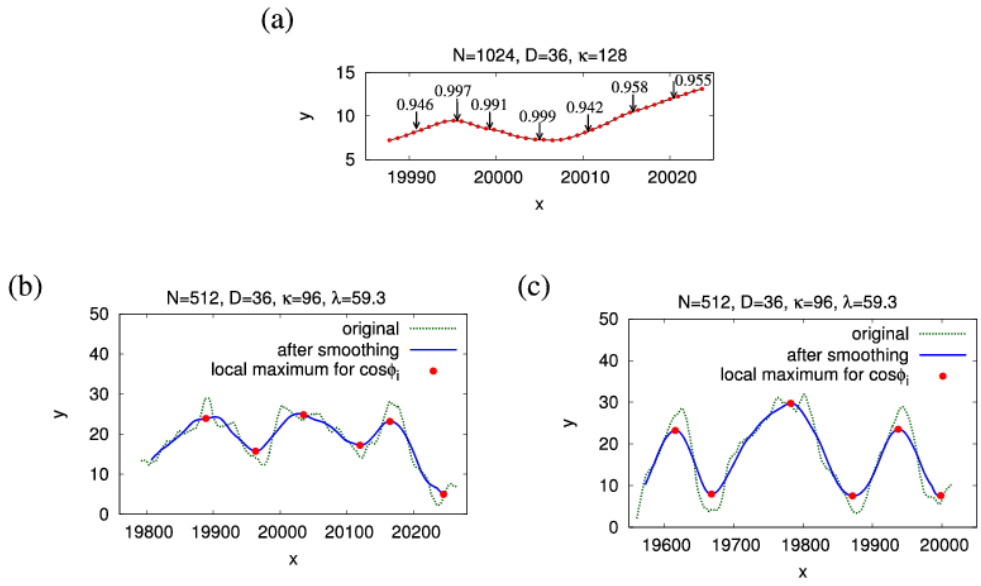

Figure 4.6: (a) Plot of a small part of a typical configuration of a chain with $N = 1024$ monomers for the case $D = 36, \kappa = 128$. Each solid dot indicates the (x, y) coordinates of a monomer: note that the lengths in x and y directions are plotted with equal scale. The arrows show selected values of $\cos\phi_i$: for the shown wiggle from the maximum with $\cos\phi_i = 0.997$ to the next minimum of the contour with $\cos\phi_i = 0.999$, only 10 monomers occur, but $\Delta y \approx 2$ (see text). (b) and (c) Comparison of two configurations after smoothing (full curves) to their corresponding original unsmoothed configurations (broken curves) for the case $N = 512, D = 36$, and $\kappa = 96$. Note that here the scale for the x-axis is compressed in comparison to the scale for the y-axis by a factor of 6. The dots show the deflection points that are kept for the measurement of $P(\lambda)$, λ being the distance between neighboring deflection points.

The fact that $\Delta\lambda$ and $\bar{\lambda}$ are of the same order reflects the irregularity of the chain configurations, expected from entropic reasons.

Table 4.2: Selected estimates for the deflection length.

N	D	κ	$\lambda(Eqn.\ 4.1)$	$\bar{\lambda}$	$\Delta\lambda$
512	36	96	59.3	76.2	28.5
1024	36	128	65.2	85.0	30.9
1024	80	128	111.0	102.4	43.9

The first question to ask is whether or not confinement leads to a change of the local persistence length (which we always define from Eqn. 4.5). Fig. 4.7 shows the unexpected result that the persistence length $\ell_p(D)$ does depend strongly on the strip width D for the lattice model when D is less than the persistence length of the unconfined chain in the bulk ($\ell_p^{\mathrm{bulk}} = \ell_p(D \to \infty)$), while for the off-lattice model, ℓ_p remains completely unaffected by the confinement. When we henceforth use ℓ_p without any further specification, always the bulk value will be meant. This finding implies for the continuum model that the average orientational correlation between subsequent bonds (as measured by $\langle \cos\theta \rangle$) is the same for the confined chains as it is in the bulk, although for small D (and in the absence of hairpins), all bond vectors of the confined chains are oriented almost parallel to the x-axis, while for semiflexible polymers in the bulk, this dominance of one orientation does not occur. For off-lattice semiflexible chains, we have $\langle \theta^2 \rangle \approx \ell/\ell_p$ and if $D \ll \ell_p$ we can expect that after $n_\lambda = \lambda/\ell$ steps along the chain, the angle $\theta(n_\lambda)$ has added up in a random walk-like fashion [78], i.e., $\langle [\theta(n_\lambda)]^2 \rangle = n_\lambda \ell/\ell_p = \lambda/\ell_p$.

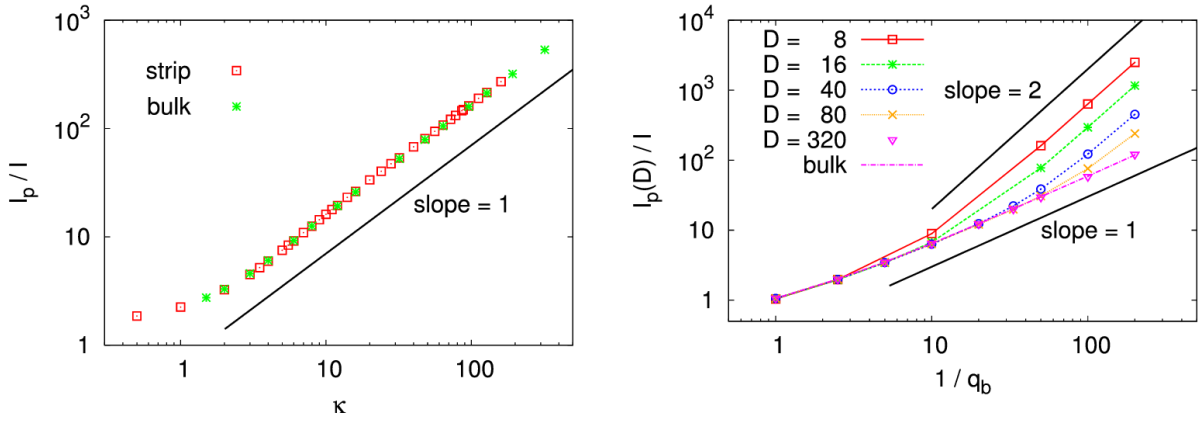

Figure 4.7: Comparison of the persistence length ℓ_p/ℓ under confinement in a strip and in the bulk for the continuum model (a) and for the lattice model, using strip widths from $D = 8$ to $D = 320$ (b). Note that the estimates of persistence length under confinement in (a) were obtained by taking the average of $\ell_p(D)$ for several choices of D at fixed κ. Note that error bars in this plot are smaller than the size of the symbols throughout.

However, this growth of $\langle[\theta(n_\lambda)]^2\rangle$ must stop when $\langle[\theta(n_\lambda)]^2\rangle = (D/\lambda)^2$, and equating both expressions readily yields the deflection length [78], Eqn. 4.1. The different behavior of the lattice model can be interpreted by the fact that the typical configuration of the chain (Fig. 4.1(c)) consists of a sequence of kinks, where at each kink point a sequence of n_x bonds in x-direction is followed by n_y bonds in y-direction. The numbers of n_x, n_y follow an exponential distribution [54]

$$P(n_x, n_y) = \left(\frac{\ell}{\ell_p}\right)^2 \exp\left(-n_x \ell/\ell_p\right) \exp\left(-n_y \ell/\ell_p\right) \tag{4.12}$$

In a bulk square lattice, both n_x and n_y can vary from 1 to infinity. For large ℓ_p/ℓ, the average length of a sequence can be computed simply as

$$\langle n_x \rangle = \int_0^\infty dn_x \int_0^\infty dn_y P(n_x, n_y) = \ell_p/\ell, \text{unconfined case,} \tag{4.13}$$

and the same result would be obtained for $\langle n_y \rangle$, since in the bulk both lattice directions are equivalent. However, for the confined system, n_y must be in the range $1, ..., n_y, ..., D$ (Fig. 4.2(c)). While Eqn. 4.12 implies that a kink with some choice of (n_x, n_y) occurs with probability unity, for the confined system Eqn. 4.12 allows for the occurrence of a kink only with the reduced probability $P_{\text{kink}} = 1 - \exp(-D/\ell_p)$. This reduction in the number of kinks must show up in the distance between subsequent kinks along the x-direction, and hence, we tentatively suggest

$$\langle n_x \rangle = (\ell_p/\ell) P_{\text{kink}} = (\ell_p/\ell) / [1 - \exp(-D/\ell_p)]. \tag{4.14}$$

The data of Fig. 4.7(b) are indeed compatible with this simple argument, implying that for $D < \ell_p$, the effective persistence length [56] $\ell_p(D) \equiv \langle n_x \rangle \ell \approx \ell_p^2/D$.Hence for $D < \ell_p$ in the case of the lattice model, it will matter whether we study the behavior of the chain linear dimensions as a function of ℓ_p/D or $\ell_p(D)/D$, respectively. For simplicity, in this discussion we have ignored the possible effect of hairpins completely (note that when hairpins occur and the end-to-end vector is oriented from left to right, numbers n_x of sequences parallel and antiparallel to the x-component of the end-to-end vector are not equivalent).

We first demonstrate that the possible renormalization of the persistence length does not matter when we study the regime where the Daoud-De Gennes [102] prediction applies

(Fig. 4.8),

$$\langle R_{\|}^2 \rangle^{1/2} \propto (\ell_p/D)^{1/3}\, L. \tag{4.15}$$

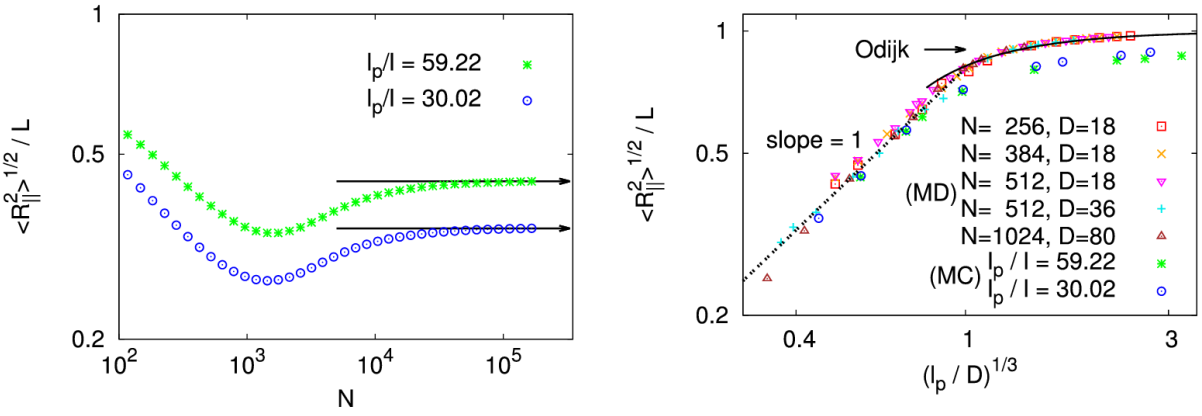

Figure 4.8: (a) MC data for $\langle R_{\|}^2 \rangle^{1/2}/L$ plotted vs. chain length N, for $D = 320$, and two choices of the persistence length, $\ell_p/\ell = 59.22 (q_b = 0.01)$ and $\ell_p/\ell = 30.02 (q_b = 0.02)$, respectively. The solid horizontal lines indicate the extrapolation towards $N \to \infty$. (b) Log-log plot of the dimensionless chain extension $\langle R_{\|}^2 \rangle^{1/2}/L$ versus the ratio $(\ell_p/D)^{1/3}$ for data from both MD and MC. The dashed straight line indicates the De Gennes regime for $D > \ell_p$, $\langle R_{\|}^2 \rangle^{1/2} \propto L(\ell_p/D)^{1/3}$. The solid line shows a fit of the MD data to the Odijk prediction. Note that the MC data were all extrapolated towards $N \to \infty$, as shown in part (a), while the MD data refer to specific values of N in the range $256 \leq N \leq 1024$ for $D = 18$, 36, and 80, as indicated. Statistical errors are at most of the size of the symbols.

From the MC calculation, data for a very wide range of N are available, and hence for each choice of D and ℓ_p, one can perform an extrapolation to $N \to \infty$. Since the variation of

$\langle R_{\|}^2\rangle^{1/2}/L$ with N is non-monotonic (Fig. 4.8(a)), such a procedure would be completely misleading if only data for rather short chains (on the left side of minimum) were available. Thus, no such extrapolation was attempted for the MD data, but nevertheless a reasonable scaling could be obtained (Fig. 4.8(b)). We note that the nonmonotonic variation of Fig. 4.8(a) is not specific for the lattice model; a similar behavior was also found for a chain of tangent hard spheres [134]. The location of this minimum of the ratio $\langle R_{\|}^2\rangle^{1/2}/L$ depends on both D and ℓ_p, as demonstrated in our earlier work [56]. It is seen that the lattice and off-lattice models yield a qualitatively similar behavior, the constant of proportionality in Eqn. 4.15 is somewhat smaller for the lattice model, and also the approach to saturation in the limit of strong confinement ($\ell_p/D \gg 1$) is much slower. In view of the fact that for the lattice model in the regime $\ell_p > D$, the persistence length gets renormalized to much larger values, it may seem paradoxical that nevertheless the scaled chain extension $\langle R_{\|}^2\rangle^{1/2}/L$ is smaller than in the continuum case. However, the explanation of this behavior is that those parts of the chain that are oriented along the y-axis (Fig. 4.2(c)) do not contribute to the extension in x-direction at all, while in the continuum case the angles ϕ_i due to the weak deflections all are rather small and hence all bonds contribute predominantly to the chain extension along the x-axis. In fact, as we shall see later, in the lattice model monomers are less repelled by the confining boundaries than in the continuum case (compare the density profiles across the slit in Figs. 4.12(a) and 4.13(a)).

In the lattice model, both the mean square radius $\langle R_{\|}^2\rangle$ and the mean square gyration radius $\langle R_{g\|}^2\rangle$ in x-direction have been obtained for a wide range of choices of both D and

the persistence length ℓ_p, and display the expected scaling as a function of ℓ_p/D very well (Fig. 4.9), in the limit of very long chains.

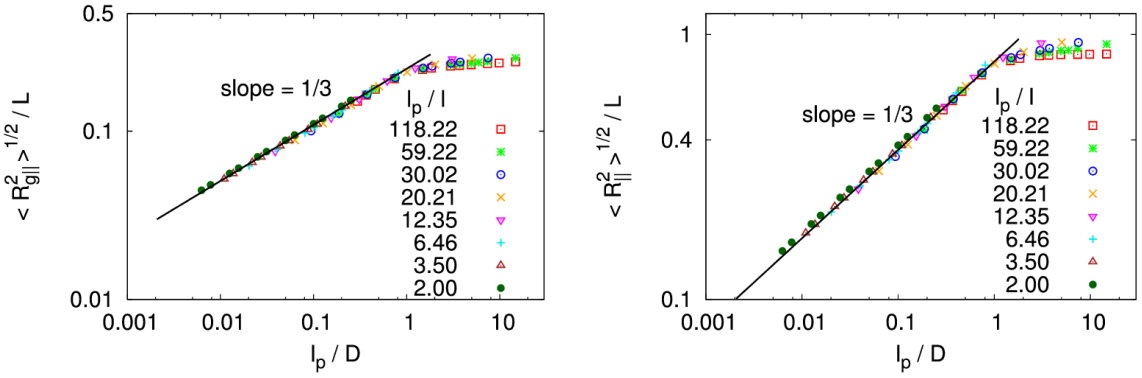

Figure 4.9: Log-log plot of $\langle R_{g\|}^2\rangle^{1/2}/L$ (a) and $\langle R_{\|}^2\rangle^{1/2}/L$(b) versus ℓ_p/D. Various values of q_b are shown, as indicated. Note that all these data were obtained by first extrapolating the data for finite L (see Fig. 4.8(a)) at fixed q_b and fixed D towards $L \to \infty$.

We stress that for the MC data in Figs. 4.8(b) and 4.9, the unrenormalized values of ℓ_p (i.e., the persistence length of the unconfined chains in the bulk) were used in the variables $(\ell_p/D)^{1/3}$ or ℓ_p/D, respectively. However, if we use $\ell_p(D)/D$ rather than ℓ_p/D for such plots, they look very similar: this happens because $\ell_p(D)/D$ differs from ℓ_p/D only for $\ell_p/D > 1$ and in this region the scaling functions in Figs. 4.8(b) and 4.9 are almost flat.

Next we discuss the variation of the linear dimension with chain length, normalizing $\langle R_{\|}^2\rangle$ by the Kratky-Porod prediction $2\ell_p L$, and measure the contour length L in units of $2\ell_p L$(Fig. 4.10). There are three regimes: for $L/(2\ell_p L) < 1$, the chains behave like rods, $\langle R_{\|}^2\rangle = L^2$ and hence $\langle R_{\|}^2\rangle/(2\ell_p L) = (L/\ell_p)/2$, the first linear regime in the log-log plot.

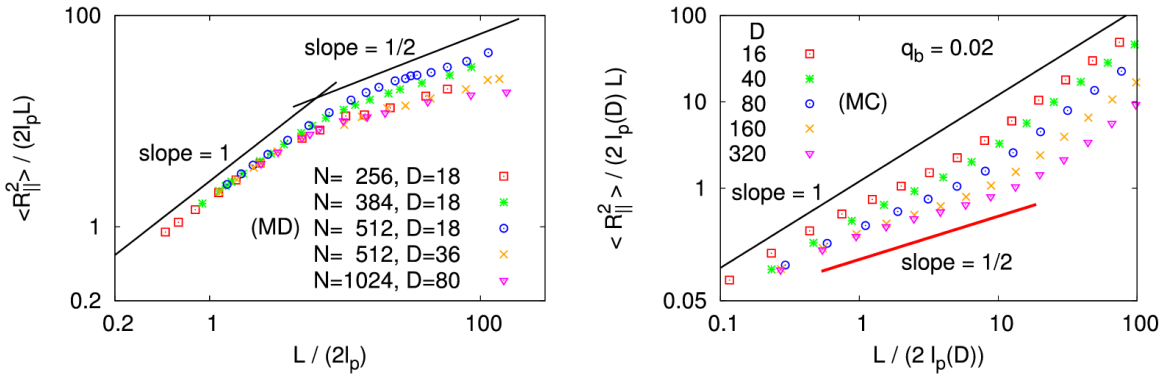

Figure 4.10: Log-log plot of $\langle R_{\|}^2\rangle/(2\ell_p L)$ (a) or $\langle R_{\|}^2\rangle/(2\ell_p(D)L)$ (b), versus $L/(2\ell_p)$ or $L/(2\ell_p(D))$, respectively. For the MD data, both L, D, and ℓ_p were varied, as indicated in the key to the figure. For the MC data, the choice $q_b = 0.02$ (i.e., $\ell_p = 30.02\ell$) was fixed and L was varied, showing five different choices of D, as indicated.

For wide strips ($D \gg \ell_p$), there is an intermediate regime, where the chain behaves like a weakly constrained free chain [Eqn. 4.8], and hence $\langle R_{\|}^2\rangle/(2\ell_p L)$ varies like $(L/\ell_p)^{1/2}$. For narrow strips (such as the case $D = 16, \ell_p = 30.02\ell$ in Fig. 4.10(b)), this regime is absent, of course. For the MD data in Fig. 4.10(a), this regime is realized by choosing not so large values of ℓ_p, since extremely large values of N are not accessible. The MC data show a third regime where $\langle R_{\|}^2\rangle/(2\ell_p(D)L)$ again varies linearly with $L/(2\ell_p(D))$, which simply is the Daoud-De Gennes regime again (where the chain is a string of blobs). For the rather wide strip used for the MD data, this regime cannot be recognized yet in Fig. 4.10(a). When we study the regime $D < \ell_p$ for the lattice model and consider the crossovers with increasing L, it is the renormalized persistence length $\ell_p(D)$ which matters for the crossover to the final regime $\langle R_{\|}^2\rangle \propto L^2$ for large L. Therefore, we used $\ell_p(D)$ in Fig. 4.10(b).

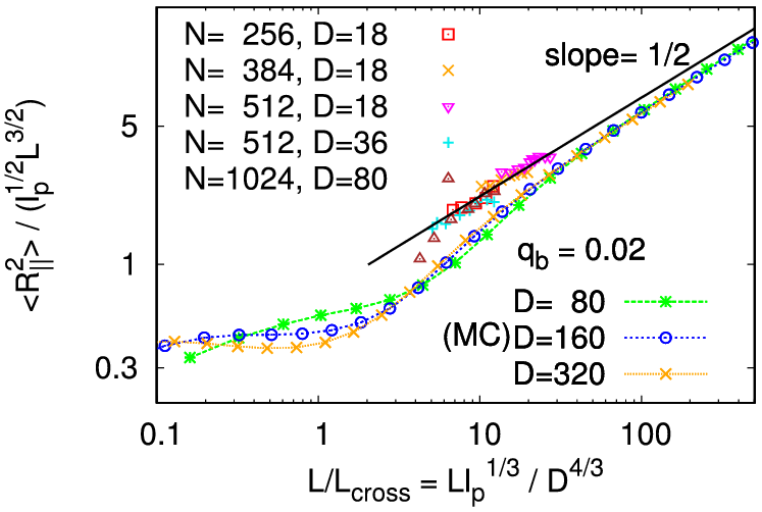

Figure 4.11: Log-log plot of $\langle R_\parallel^2 \rangle / (\ell_p^{1/2} L^{3/2})$ versus $L/L_{\rm cross} = L\ell_p^{1/3}/D^{4/3}$ including both the MD and MC data. Note that $L_{\rm cross}$ denotes the contour length where the crossover from the unconfined SAW to the string of Daoud-De Gennes blobs occurs (so $L/L_{\rm cross}$ is essentially the number of blobs). The straight line illustrates Eqn. 4.16.

At the first glance, Fig. 4.10 seems at variance with Fig. 4.10, since from the MD data plotted there no evidence for the string of blobs-picture of Daoud and De Gennes [102] was seen. However, this is not the case: when we plot $\langle R_\parallel^2 \rangle / (\ell_p^{1/2} L^{3/2})$ versus the effective number $L/L_{\rm cross}$ of blobs in the string (Fig. 4.11), we find that a significant part of the MD data falls in the range $4 < L/L_{\rm cross} < 30$ and roughly is consistent with Eqn. 4.15, which in this representation can be rewritten as

$$\langle R_\parallel^2 \rangle / (\ell_p^{1/2} L^{3/2}) \propto (L/\ell_p)^{1/2} \, (\ell_p/D)^{2/3} = \left(L\ell_p^{1/3}/D^{4/3} \right)^{1/2} \tag{4.16}$$

Of course, the MC data include a much wider range of $L/L_{\rm cross}$, including the chains that are almost unperturbed by the confinement ($L/L_{\rm cross} < 1$, then $\langle R_{\|}^2 \rangle / (\ell_p^{1/2} L^{3/2})$ is essentially constant), as well as very long chains (where $L/L_{\rm cross} > 100$).

A very interesting aspect is the monomer density profile near the wall. For flexible chains, it was shown [140] that for the lattice model this profile can be very accurately described by

$$D_{\rm eff}\rho(y) = C\left[\xi(1-\xi)\right]^{4/3}, \xi = y/D_{\rm eff} \tag{4.17}$$

where $D_{\rm eff} = D + 1$. This form is compatible with the density profile expected for a semi-infinite solution (with density ρ_b in the bulk) of flexible chains near a hard wall [165, 25],

$$\rho(y) = \rho_b \bar{\rho}(y/R), R \approx \ell(L/\ell)^{\nu} \tag{4.18}$$

with $\nu = 3/4$ in $d = 2$ dimensions, and $\bar{\rho}(\xi) \propto \xi^{1/\nu}$ for $\xi \ll 1$. However, Semenov [159] predicted on the basis of the Kratky-Porod model that

$$\rho(y)/\rho_b \propto y^{2/3} \text{for} \ell \ll y \ll \ell_p \tag{4.19}$$

irrespective of dimensionality. However, the data for the lattice model do not yield any evidence in favor of this prediction (Fig. 4.12).

For the off-lattice case the conclusion is different; however, the monomer density near the walls does not extrapolate to a nonzero value when $\xi = y/D_{\rm eff} \to 0$ or $\to 1$, Fig. 4.13(a), and when ℓ_p is large, Eqn. 4.17 then no longer provides a good fit of the data. Thus, it is tempting to try a log-log plot of $\rho(y)$ versus y. Of course, data for $y > D/4$ are affected by the saturation of the profile in the center of the film and have to be excluded (one should

only use data far outside the range of the repulsive wall potential).

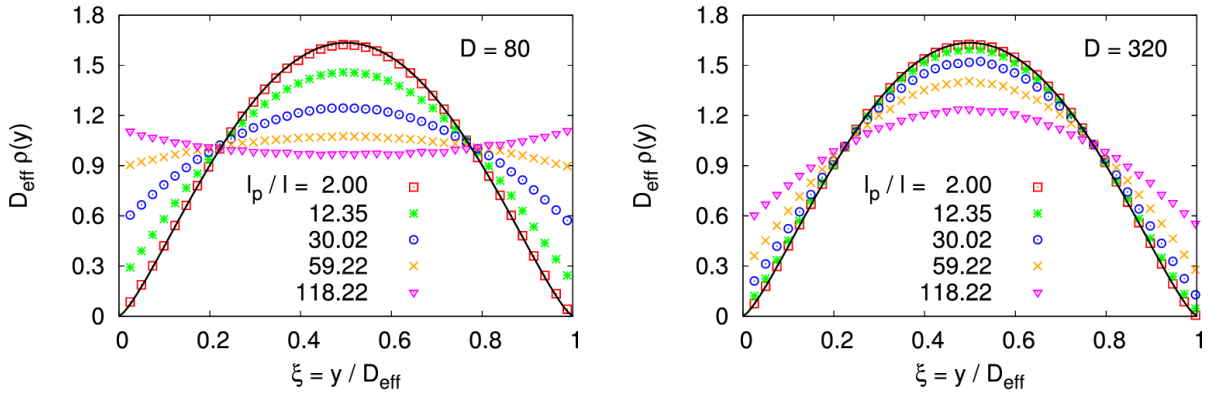

Figure 4.12: Rescaled monomer density profile $D_{\rm eff}\rho(y)$ versus $\xi = y/D_{\rm eff}$ for the case $D = 80$ (a) and $D = 320$ (b), according to the MC model. Several choices of ℓ_p/ℓ are included, as indicated. Full curves show the theoretical prediction, Eqn. 4.17, with the constant C fitted as $C = 10.38$. Here, $D_{\rm eff} = D + 1$.

One sees that in the intermediate regime, the MD data indeed are consistent with a crossover of the effective exponent, defined in terms of the apparent slope where a straight line can be fitted to the data of the log-log plot near $y \approx 10$ from 4/3 (for flexible chains) to 2/3 (for very stiff chains). This finding hence is compatible with Semenovs prediction, Eqn. 4.19. Here, the possibility of small bond angles implicit in the Kratky-Porod model is a crucial feature, and hence, it is not so surprising that for the lattice model Eqn. 4.19 does not hold. Of course, very close to the wall the actual wall potential matters, and hence, the power laws are expected to hold only for $y \gg \ell$, see Eqn. 4.19.

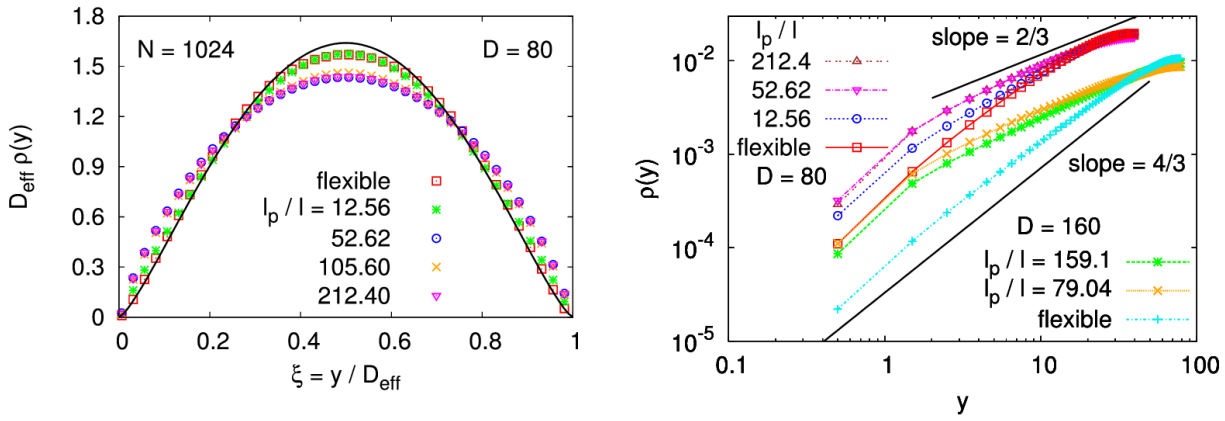

Figure 4.13: (a) Plot of the scaled monomer density $D_{\rm eff}\rho(y)$ as a function of $\xi = y/D_{\rm eff}$ for the continuum model of semiflexible chains with $N = 1024$, as obtained from MD simulations, for a strip of width $D_{\rm eff} = D = 80$, and several choices of the persistence length ℓ_p/ℓ, as indicated. The solid curve shows the fit to Eqn. 4.17 for the fully flexible case, with the constant C being $C = 10.41$. (b) Log-log plot of the monomer density $\rho(y)$ versus y for $N = 1024$, $D = 80$ and 160, and various stiffnesses as indicated by the choices for ℓ_p/ℓ. The solid straight lines indicate the theoretical power laws $\rho(y) \propto y^{4/3}$ for the flexible and $\rho(y) \propto y^{2/3}$ for Kratky-Porod chains, respectively.

Very interesting is also the behavior of the end monomer distribution $\rho_e(y)$. For flexible chains, the scaling prediction is [140]

$$\rho_e(y) = \frac{1}{D_{\rm eff}} C_e \left[\xi(1-\xi)\right]^{25/48}, \tag{4.20}$$

and indeed this (empirical) function provides a very good fit of the MD data for flexible chains ($\kappa = 0$), with the constant $C_e \approx 2.71$ being of the same order as for the SAW model on the square lattice [140] ($C_e = 2.85$).

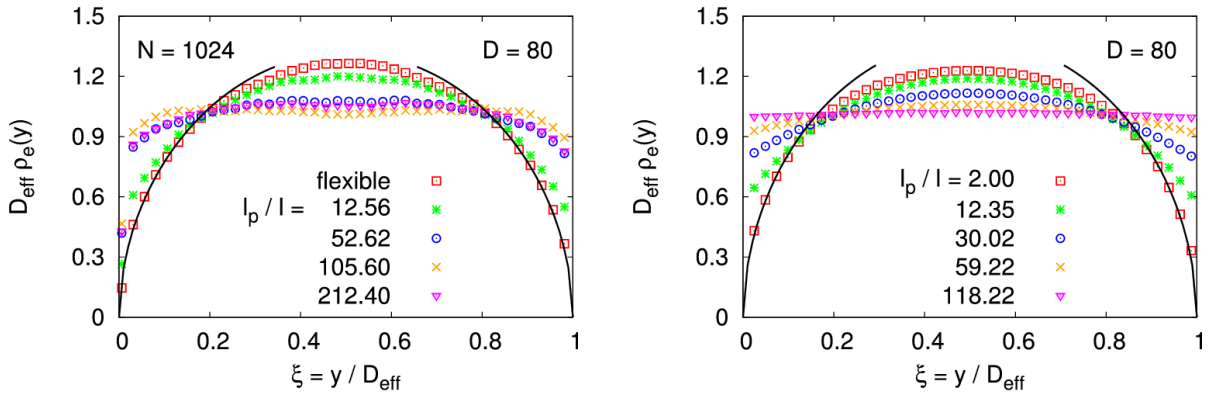

Figure 4.14: Scaled end monomer density profiles $\rho_e(\xi)D_{\rm eff}$ Deff as a function of $\xi = y/D_{\rm eff}$ for the continuum model of semiflexible chains with $N = 1024$, as obtained from MD simulations (a), and for the lattice model of chains with $50000 < N < 200000$ (b). Note that $D_{\rm eff} = D$ was chosen for the off-lattice model but $D_{\rm eff} = D + 1$ for the lattice model, and several choices of the persistence length are shown as indicated. The full curve shows a fit of Eqn. 4.20 for the fully flexible case, with the constant C_e being $C_e = 2.71$ for the continuum, and $C_e = 2.85$ for the lattice.

Again one sees that with increasing stiffness, the end monomer density near the walls gets enhanced, and for very stiff chains a limiting behavior $\rho_e(y) \approx const$ seems to be reached (apart from a small region $\xi < 0.1$ or $1 - \xi < 0.1$, where ρ_e is slightly depressed, but this could be a residual effect from the nonzero range of the repulsive wall potentials). Thus, we speculate that for semiflexible chains (in the limit $N \to \infty$ and then $\ell_p \to \infty$ in a semi-infinite dilute solution), there is no analogue of the power law for the monomer density, Eqn. 4.19, when one considers the density of end monomers instead. In the lattice model, also an essentially constant distribution of $\rho_e(y)$ across the strip was found (Fig. 4.14(b)).

While in the regime $D_{\text{eff}} < \ell_p$ the behavior of $\rho(y)$ and $\rho_e(y)$ for the lattice model is very similar, this is not true for the bead-spring model of semiflexible chains in the continuum.

4.4 Conclusions

We now proceed by summarizing the central findings of the present work. We have simulated two rather different coarse-grained models of semiflexible polymers in two space dimensions, over a wide range of chain lengths and persistence lengths, under good solvent conditions, both in the bulk and under confinement in a strip of width D with repulsive boundaries. One model is a self-avoiding walk on the square lattice, where stiffness is controlled by the energy cost ϵ_b if the walk makes a kink of $\pm 90°$. The density of the kinks for large ϵ/k_BT decreases exponentially with this energy cost, proportional to $\exp(-\epsilon/k_BT)$, and the persistence length ℓ_p then is essentially the inverse of the kink density, $\ell_p \propto \exp(\epsilon/k_BT)$, and can also be interpreted as the average length of straight sequences of bonds between two neighboring kinks along the chain contour. The other model is the standard Grest-Kremer [19] bead-spring model, amended by the standard cosine potential $U_b(\theta) = \epsilon_b(1-\cos\theta)$ [Eqn. 4.3)] between neighboring bonds. For large ϵ_b/k_BT, this potential essentially becomes $U_b(\theta) = (\epsilon_b/2)\theta^2$, and hence, the model (apart from excluded volume) can be considered as a discretization of the well-known Kratky-Porod model of wormlike chains, Eqn. 4.2, so b simply corresponds to the bending rigidity κ_{KP} of that model. Then the persistence length simply is proportional to ϵ_b/k_BT, and this is confirmed by the simula-

tions (see, e.g., Fig. 4.7(a)). Note that in the presence of excluded volume, a valid definition of the persistence length always is derived from $\langle \cos\theta \rangle$, the average cosine of the angle between neighboring bonds; this is a meaningful measure of local chain stiffness, unlike the asymptotic decay of bond vector correlations for bonds that are far separated along the chain contour (this asymptotic decay is controlled by excluded volume effects, ignored in Eqn. 4.2).

We have obtained the mean square end-to-end distance of both models in the bulk, applying Monte Carlo methods for the lattice model and molecular dynamics (with a Langevin thermostat) for the off-lattice model. We find that the crossover from the rod-like regime (for contour lengths $L < \ell_p$) to the self-avoiding walk-like regime (described by Eqn. 4.8) is qualitatively similar in both models, when one studies these linear dimensions as functions of the scaling variable L/ℓ_p (Fig. 4.3). The amplitude prefactors of the power laws in the asymptotic scaling regime for both models differ slightly, as expected, since only exponents are universal, but not amplitude prefactors. Since in the rod regime the data trivially are model-independent ($\langle R_N^2 \rangle = L^2$ for $L \ll \ell_p$), it follows that crossover scaling functions of both models cannot be identical (Fig. 4.3(b)). In fact, if the asymptotic power law is scaled out, one finds in the crossover scaling functions in the regime $1 < L/\ell_p < 10$ a nontrivial maximum, and there is no universality of these crossover scaling functions. However, when one considers the reduced transverse fluctuation (Fig. 4.4), one finds in the crossover scaling plot a maximum, whose position is universal, at least within the accuracy of the present estimations, namely, it occurs at $\ln(L/\ell_p) \approx 1$. Providing such a plot from the analysis of

experimental AFM pictures of semiflexible polymers adsorbed at planar substrates could be an alternative to the experimental estimation of ℓ_P from the Kratky-Porod formula for the mean square end-to-end distance, which is questionable due to its neglect of excluded volume effects (it describes a crossover to Gaussian coil behavior, which in reality cannot occur). Thus, our comparison of the two studied models is not just an academic exercise but could be a useful guide in practice.

While the disparity of local chain conformations between both models hence has only minor consequences, as far as the bulk properties are concerned, this is no longer true when one considers confinement in strips with $D < \ell_p$. One interesting feature is that in the lattice model, the effective persistence length $\ell_p(D)$ gets renormalized, while for the continuum model, it remains unchanged (Fig. 4.7). This discrepancy can be understood from the fact that on the lattice straight sequences of bonds along the y axis get more and more suppressed (Fig. 4.2(c)), while in the continuum bending of the chain (on scales less than the deflection length λ, cf. Figs. 4.2(a) and 4.5) is not affected. A second very interesting discrepancy between both models is that in the continuum model entropic depletion of monomers near the repulsive walls always occurs (Fig. 4.13), while there is no such depletion for rather stiff lattice chains (Fig. 4.12). For flexible chains, both on the lattice and in the continuum, near a repulsive boundary depletion does occur, $\rho(y) \propto y^{4/3}$ for $\ell \ll y \ll D$, and the monomer density profile across the strip exhibits a scaling, which is almost universal (again, a simple model-dependent amplitude factor occurs, cf. Eqn. 4.17)). However, for rather stiff chains in the continuum a different power law has been predicted on the basis of the Kratky-

Porod model by Semenov [159], and our data (Fig. 4.13(b)) seem to be compatible with this prediction. However, while for flexible chains, the chain ends also show an entropic depletion effect, but described by different exponents (Eqn. 4.20), and this prediction has been verified by both the lattice and the continuum model, no such depletion effect can be detected for semiflexible chains. For $D \ll \ell_p$, the end monomer profile is almost constant across the strip, both for the lattice and the continuum model (Fig. 4.14). A third discrepancy is the fact that for the semiflexible bead-spring model, the concept of Odijk [78] of a deflection length (Fig. 4.2(a)) obviously is applicable for strongly confined chains in the continuum (Fig. 4.5) but meaningless for the lattice model. We also have discussed the possibility to extract the distribution function $P(\lambda)$ of deflection lengths directly from a statistical analysis of configurations of confined chains in the continuum model. We have shown that after a suitable further coarse-graining of the chain contours, necessary to remove small scale structure, both the average deflection length $\bar{\lambda}$ and the fluctuation $\Delta\lambda \equiv \left(\bar{\lambda^2} - \bar{\lambda}^2\right)$ could be obtained. Both $\bar{\lambda}$ and $\Delta\lambda$ are of the same order as predicted (Eqn. 4.1).

However, for less extreme confinement ($D > \ell_p$) again a remarkable similarity between both models is found: there is a crossover from rods (for $L < \ell_p$) to self-avoiding walks (for chains that are short enough that a single blob fits into the strip) and further to the Daoud-De Gennes string of blobs. For the Monte Carlo results, where a very wide range of L for every choice of ℓ_p is spanned, these three regimes can be easily seen (Fig. 4.10(b)), but for the MD results, they can also be inferred for appropriate choices of ℓ_p and D. The scaling predictions resulting from the string of blob picture are nicely verified for both models (Fig. 4.11).

We also note that the snapshot pictures in the regime $\ell_p < D < 3\ell_p$, where well-developed blobs do not yet fit into the strip, clearly reveal hairpin formation, as proposed by Odijk [104] who also has estimated that hairpin formation involves the crossing of a free energy barrier that is proportional to ℓ_p for $D \ll \ell_P$. However, in the regime $D \ll \ell_P$ where the theory applied, hardly any hairpins could be observed, and hence, our simulations are not suited to test this theory. For the three-dimensional case, a pioneering study of the effects of hairpins on confinement of semiflexible polymers can be found in Ref. [166].

Of course, for addressing experiments, an extension of our study to three dimensions (quasi-one-dimensional confinement in tubes with square, rectangular, or circular cross section) would be very desirable but must be left to future work. We note that in this case several additional complications arise, such as the intermediate Gaussian regime of chain conformational statistics, and knot formation for very long chains.

However, the goal of this study was not to contribute directly to the analysis of experiments but rather to understand how different general assumptions implicit in the choice of particular coarse-grained models do affect the physical properties of the studied macromolecular systems. In particular, we have found in the bulk that the difference in local chain conformations between lattice and continuum models does no longer matter much, when one compares data for the same choice of persistence length (although the dependence of ℓ_p on the energy parameters is very different). Under confinement, the absence of monomer depletion for rather stiff lattice chains shows that discrete bond angles lead to a different physics in comparison to continuous bond angles as possible for the off-lattice model. We

have argued, however, that both chains may be physically relevant since different types of mechanisms for chain rigidity occur for cases such as alkane-type polymers or dsDNA.

CHAPTER 5
A HETEROGENEOUS SEMI-FLEXIBLE CHAIN MODEL OF dsDNA

As one of the the most important biopolymers, DNA has been drawing longstanding interests for decades both in theoretical modeling and simulation studies. DNA is a complex molecule which is essentially built on two intertwined single strands. Under physiological conditions these two strands are bound together by hydrogen bonding between complementary base pairs (bps), namely, adenine thymine (AT) pair and guanine cytosine (GC) pair. With this main structure itself DNA already offers both rich mechanical and thermodynamic properties. First of all, when compared to a single stranded DNA (ssDNA) whose persistence length is ~ 3 nm under most experimental conditions, a double stranded DNA (dsDNA) with its persistence length one order of magnitude greater (~ 50 nm) is much stiffer, where the rigidity is mainly due to the base pairing interaction and the stacking interaction among adjacent base pairs, although the precise manner also depends on the dsDNA architecture and solvent details. Further, it is the sequence specificity that encodes the genetic information which in turn controls its biological function in the cell, one of the main aspects about this heterogeneity is that there are two hydrogen bonds (HBs) between AT pair while GC pair has three. On average the binding strength per base pair is in the order of k_BT [167], where k_B is the Boltzmann constant and T is the temperature, although

GC pair is more stable than AT pair due to an additional hydrogen bond. Therefore at high enough temperatures the hydrogen bonding can be broken by the thermal energy that the two strands in dsDNA completely dissociate from each other, undergoing a denaturation process. However, even at physiological temperatures the thermal fluctuations may disrupt the local structure of dsDNA (e.g. the AT rich region) introducing bubbles along the sequence. Recently, the advances in nanofluidics experiments have demonstrated that by putting dsDNA into nanochannels and combining fluorescence microscopy technique, optical barcodes can be obtained and mapped to the local denaturation of dsDNA along its extension under confinement [85, 93]. While the newly developed experimental techniques have offered possibilities towards performing analysis on a single molecule level, in the mean time considerably challenging questions have also arisen. For example, when a dsDNA is partially melted into two single strands the local stiffness is also altered, therefore the unmelted regions and the bubbles from the melted region will make the dsDNA exhibit another form of heterogeneity regarding the bending rigidity. It is expected that thermodynamic and mechanical properties will both play significant roles and feedback to each other in determining the global DNA conformations and dynamics. Attempts to address these challenges and provide answers are not only meaningful in giving insights to experiments from theoretical side, but also ensure more reliable and reproducible single molecule analysis. Thus models which incorporates both the thermodynamic and mechanical aspects about DNA yet still has the capability of reaching the experiment length scale would be very helpful.

Historically, models studying the melting statistics of dsDNA have been developed and still widely used in the literature. The most notable one is due to Poland and Scheraga (PS) [168, 169, 170], where the dsDNA is described as a one-dimensional sequence of bound complementary base pairs separated by loops (unbound base pairs) formed by complementary single strands of the same length. For a given sequence, temperature and solvent conditions, the melting probabilities for each base pair of a dsDNA can be calculated from the the partition function which is essentially accounted by the energy of the bounded pairs and the entropy of the loops. It has been shown that the transition nature of the DNA denaturation depends on the loop size distribution, which in turn depends on the space dimensions and the importance of the excluded volume (EV) interactions. The theoretical analysis by Kafri *et al.* revealed that in three dimensions DNA denaturation is a first order transition, which has been later confirmed by lattice Monte Carlo simulation studies. The most important advantage of PS model is that the computation of the melting profiles can be done algorithmically and indeed efficient computer routines have been developed [171, 172], and very long sequences even the entire human genome can be analyzed in this framework, nevertheless, the major drawback of PS model is that it is Ising-like in nature and chain configurations and dynamics can't be inferred. Another more recent model which accounts for the bubble dynamics and bubble lifetime has been proposed by Peyrard, Dauxious and Bishop (PBD) [173, 174]. Unlike the two-state PS model, a partially melted dsDNA was described by a continuous variable — the separation distance of the base pair — which is also the only coordinate variable entering the model's Hamiltonian. In addition to a base pairing interaction, the key

feature of the PBD Hamiltonian is that the stacking interaction among neighboring bases are represented by a nonlinear term which introduces *cooperativity* in bubble formation and propagation. Langevin dynamics and Monte Carlo simulations have been carried out using PBD model to study a variety of topics including the connections between bubble dynamics and specific sequences, protein-DNA binding sites of transcription factors, however, this model is still intrinsically one dimensional thus configurations of dsDNA can not be visualized limiting its use in studying the interplay of the bubble dynamics and chain conformations.

Different from previous models, mesoscopic models of dsDNA have also been developed by several groups recently. In this category, by using a top-down approach different groups of atoms in the DNA molecule are identified and coarse grained into beads as the basic building elements to reconstruct the duplex structure, also with effective interactions introduced among the beads. Notably, the 3SPN (three sites per nucleotide) model developed by de Pablo *et al.* has made a number of successes [175, 176, 177, 178, 179, 180, 181]. As the name suggested, a nucleotide is represented by three beads corresponding to the phosphate group, sugar group and the base of the DNA molecule. Under several later improvements by the same group [176, 177, 178, 179], with thoughtfully designed interactions among the beads the 3SPN model has been able to recover detailed structural aspects of dsDNA such as stable major grooves, minor grooves and correct bending rigidities both for dsDNA and ssDNA. The 3SPN model has been mainly used to study processes such as DNA oligomer hybridization, DNA-histone interactions, which both are intrinsically sensitive to the local structure details of the participating molecules and the surrounding solution condi-

tions [178, 179, 180, 181]. DNA melting has also been studied by 3SPN in terms of calculating the melting temperatures of short oligomers, but bubble statistics for long sequences have not been shown. However, as already pointed out in [178], the ssDNA in the 3SPN model is constructed on the reference of the B-DNA, which may limit sampling the natural random coil like configurations of ssDNA, thus studying bubble statistics of long sequences within 3SPN should be proceeded with cautions.

However, on the other hand much simpler models of dsDNA are still being used in the literature [136, 133, 56, 103, 182], specifically, they are Kremer-Grest type bead-spring model, lattice self-avoiding walk model, discrete wormlike chain (WLC) model, etc. Strictly speaking, these models are not particularly designed for DNA but can be generally used for other types of polymers also. Nevertheless, these highly coarse grained models have been successful in explaining the linear dimensions of DNA confined in nanochannels with regard to both analytical and experimental results [136, 133, 56, 103, 182].

Apparently, the models just mentioned only include the mechanical aspects of DNA and are not sufficient to interpret any that results from dsDNA melting behaviors. On the other hand, the 3SPN model at first glance may seem to be a good candidate for modeling the interplay of the mechanical and thermodynamic properties of DNA, however, the interactions included in 3SPN like the electrostatic may have the potential to unnecessarily complicate the basic physics picture, moreover, the consequences of the current treatment of ssDNA in 3SPN are still not clear. Therefore the gap between polymer type like bead-spring models and coarse grained type like 3SPN models needs to be bridged. Efforts towards this direction

have been made. Notably, Sung *et al.* have developed a semiflexible chain model of dsDNA, where the double strands are described by two paired semiflexible chains, each of which is a homogeneous bead-spring polymer [183, 184, 185]. In the present paper, we address the shortcomings of all above mentioned models by extending Sung's model to incorporate both base pair heterogeneity and EV interaction. The sequence heterogeneity is a critical feature for DNA which fundamentally conveys to its biological functions. The EV effect is also important in determining the bubble size distribution and the transition order of DNA denaturation.

5.1 The model

The two strands of a dsDNA are modeled as two paired semiflexible chains, with each chain is a bead-spring polymer, where the beads are of uniform size and each represents one nucleotide. The Hamiltonian of the model is given as

$$H = U_{\rm EV} + U_{\rm FENE} + U_{\rm Bend} + U_{\rm BP}, \tag{5.1}$$

where the EV interaction between any two nucleotides of the dsDNA are modeled by a short range purely repulsive Morse potential $U_{\rm EV}$ which has a cutoff $r_{\rm cut}$ at its minimum

$$U_{\rm EV} = \sum_{i>j}^{2N} D_0 \left[\left(e^{-a_0(r_{ij}-r_{\rm cut})} - 1 \right)^2 - 1 \right], \quad r_{ij} > r_{\rm cut} \tag{5.2}$$

with N being the number of nucleotides in each strand, D_0 is the potential strength, a_0 controls the width of the potential and r_{ij} is the distance between any two nucleotides.

The connectivity between consecutive beads along each strand is described by the Finitely Extensible Nonlinear Elastic (FENE) potential

$$U_{\text{FENE}} = \sum_{s=1}^{2} \sum_{i=1}^{N-1} -\frac{1}{2} k R_0^2 \ln(1 - b_{s,i}^2 / R_0^2), \tag{5.3}$$

where k is the spring constant, $b_{s,i}$ is the length of the i_{th} bond in strand s, R_0 is the allowed maximum distance between neighboring nucleotides. The two strands in a dsDNA are bound by the corresponding base pairs in each strand, here the base pairing potential U_{BP} takes the full form of Morse potential

$$U_{\text{BP}} = \sum_{i=1}^{N} D \left[\left(e^{-a(d_i - d_0)} - 1 \right)^2 - 1 \right] \tag{5.4}$$

where $d_i = |\mathbf{r}_{1i} - \mathbf{r}_{2i}|$ is the distance between the position vector of the i_{th} complementary base in each strand, d_0 is the equilibrium distance for base pairs and D describes the strength of the hydrogen bonding and is different between AT pair (two HBs) and GC pair (three HBs), here for simplicity we have used $D_{\text{GC}} = 1.5 D_{\text{AT}}$ although we are aware of studies showing that the binding energy for each individual HB is not uniformly the same [186].

The stiffness for each strand is described by an angle dependent interaction between successive bonds as

$$U_{\text{Bend}} = \sum_{s=1}^{2} \sum_{i=1}^{N-2} \kappa \left(d_i \right) \left(1 - \cos \theta_{s,i} \right), \tag{5.5}$$

where $\theta_{s,i}$ is the angle made by the bond vectors $\mathbf{b}_{s,i-1}$ and $\mathbf{b}_{s,i}$ on strand s, Eqn. 5.5 is the discrete form of the well known WLC model, whose bending energy is written as Eqn. 1.7. It can be shown that in three dimensions the persistence length for each strand $\ell_p = \kappa / k_B T$, where k_B is the Boltzmann constant and T is the temperature. By rewriting Eqn. 1.7

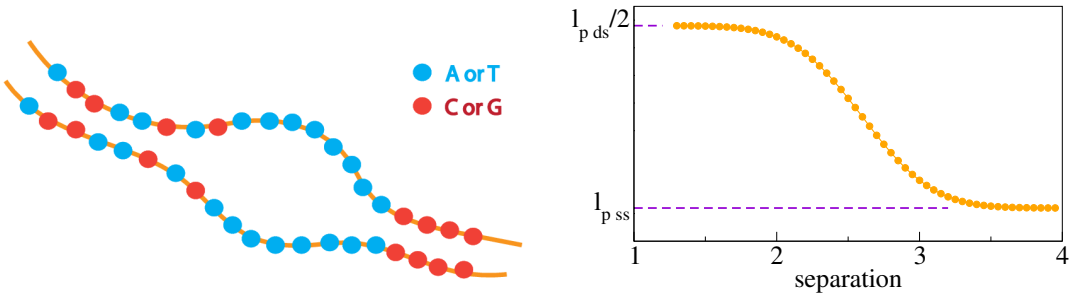

Figure 5.1: A heterogeneous semiflexible chain model of dsDNA.

in terms of the position for the center of mass (COM) of the complementary base pairs, $\mathbf{r}_{\mathrm{COM},i} = (\mathbf{r}_{1,i} + \mathbf{r}_{2,i})/2$, it is easy to show that the persistence length for the two strands (i.e., calculated from the coordinates $\mathbf{r}_{\mathrm{COM},i}$) $L_p = 2\ell_p$. Unlike the common treatment of taking the bending rigidity κ of each strand as a constant in WLC, for a real dsDNA under most experimental conditions of interest, due to thermal fluctuations the two strands are subject to local denaturation thus the persistence length is no longer uniform along the contour and interpolates between those for ssDNA and dsDNA, thus in Eqn. 5.5, we have made the bending parameter $\kappa(d_i)$ dependent upon the separation of the complementary base pairs, as have been done by Sung *et al.* [184]. The exact expression of $\kappa(d_i)$ is given as

$$\kappa(d_i) = \frac{1}{2}\kappa_{\mathrm{ds}} - (\frac{1}{2}\kappa_{\mathrm{ds}} - \kappa_{\mathrm{ss}})\Theta(d_i - r_{1/2}), \tag{5.6}$$

where κ_{ds} and κ_{ss} are the bending rigidities for dsDNA and ssDNA under the physiological condition, respectively. And $\Theta(r) = (1 + \mathrm{erf}(r/c))/2$ is a step function taking values between 0 and 1 for $-\infty < r < \infty$, with c being the width and $r_{1/2}$ the middle point of the step function. With the aid of Eqn. 5.6, it is easy to see that depending on the separation of the complementary base pairs the stiffness $\kappa(d_i)$ ranges between κ_{ss} and κ_{ds}, and if the two

strands are fully bound together the persistence length of those $L_p = \kappa_{\rm ds}/k_BT$, while for one single completely unbound strand, the persistence length of that is $\ell_p = \kappa_{\rm ss}/k_BT$.

We have performed Langevin dynamics simulations based on the model developed above. During the simulation we have taken all nucleotides to be of uniform size with $\sigma = 3.4$ Å and uniform mass with $m = 300$ amu. We have chosen σ, m as the units of length and mass, respectively, for numeric stability the unit of energy ϵ is taken as 0.025 ev. The friction coefficient $\gamma = 0.05\text{ps}^{-1}$ according to reference [173, 174]. For the EV interaction, we have chosen $D_0 = 1.0\epsilon$, $a_0 = 5.4\sigma^{-1}$, $r_{\rm cut} = 1.22\sigma$, for the spring interaction, $k = 30.0\epsilon$, $R_0 = 7.5\sigma$. This choice of parameters for the EV potential along with the FENE potential ensures the average bond length $\langle b \rangle = 0.99$ regardless of the separation of the base pairs. The parameters for the base pairing potential are calibrated to have the resulted melting temperatures to fall in the same range of those determined in experiments for short sequences of dsDNA, in the simulation we have used for $U_{\rm BP}$, $D_{\rm AT} = 1.32\epsilon$, $D_{\rm GC} = 1.5D_{\rm AT}$, $a_{\rm AT} = 10.0\sigma$ and $a_{\rm GC} = 14.0\sigma$.

Fig. 5.2(a) shows the fraction of the melted base pairs as a function of temperature for sequences A, G, AG, all of the same length, as expected, our model captures the basic trend that the melting temperature depends on base pair composition and is higher for sequences with higher GC content. For the bending potential, we have used $\kappa_{\rm ds} = 156\epsilon$, $\kappa_{\rm ss} = 12\epsilon$ to have the persistence lengths at the physiological condition agree with the mostly reported values in the literature, i.e., for dsDNA $L_p = 50$nm, and for ssDNA $\ell_p \simeq 4$ nm. Fig. 5.2(b) shows the persistence length calculated from coordinates $\mathbf{r}_{{\rm COM},i}$ for various sequences at

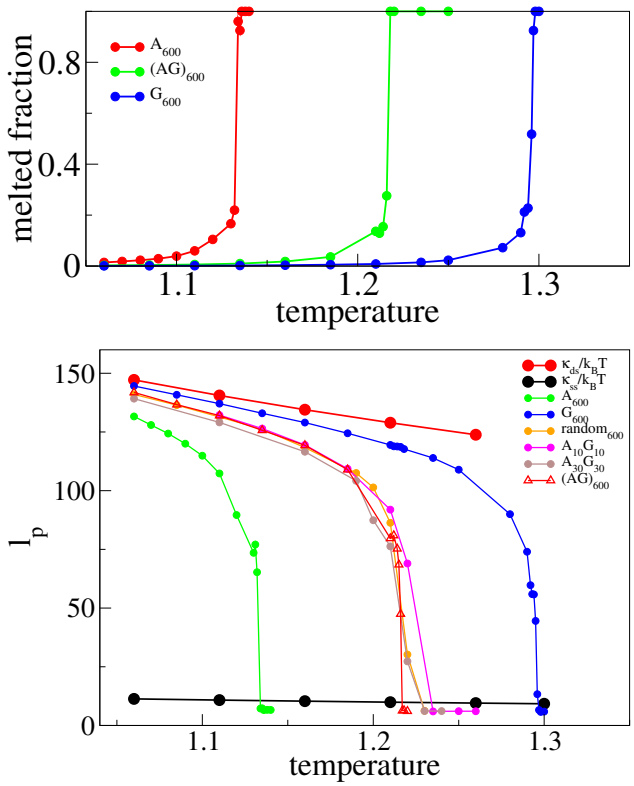

Figure 5.2: Melting profile

different temperatures. It can be seen that at low temperatures, the persistence length is relatively the same for all sequences, and as the temperature increases the persistence length starts to decrease due to local denaturation, it is also shown that the persistence length for sequences with equal GC/AT content (random or periodic pattern) follow almost the same decreasing path, which of course falls in the middle of two extremes –AT and GC.

5.2 Results and discussions

As discussed previously, due to thermal fluctuations, the base pairs of dsDNA are subject to dissociation which results in bubbles along the strands, and it has been found that the size distribution of the bubbles is related to the phase transition order of dsDNA denaturation. Starting from the partition function of PS model, Poland and Scheraga [169, 170] has shown that the distribution of bubbles of length l follow

$$P(l) \sim \frac{s^l}{l^c}, \tag{5.7}$$

where s is a non-universal geometric factor, and c is the loop exponent. The transition order is only determined by the the loop exponent c: for $c < 1$, there is no phase transition, for $1 < c < 2$ a continuous transition occurs, while for $c > 2$ a first order transition will take place. Early studies [169, 170] for ideal random loops showed $c = d/2$, where d is the dimension of the space, by considering the excluded volume effect, later Fisher [187] showed that c should be modified to $c = d\nu$, where ν is the Flory exponent, since c is still smaller than 2 both in 2 and 3 dimensions, the transition is still continuous but becomes shaper. However, the previous derivations of c value [169, 170, 187] didn't consider the interaction between the loop and the rest of the DNA chain, by including this interaction, Kafri *et al.* [188] showed that Eqn. 5.7 still holds and the transition order is still determined by c, but in $d = 2, 3$ dimensions c is greater than 2.0, which in fact proves that the DNA denaturation is a first order transition. However, it is important to note that the previous conclusions about the value of c only apply to homogeneous DNA, where the binding strength is the same

for all the base pairs without make a difference between AT pair and GC pair. Fig. 5.3(a) shows that for a dsDNA made of all GC pairs, at the critical temperature (determined from the melting profile Fig. 5.2(a)) our simulation indeed agrees with that the bubble size distribution follows a power law decay with an exponent $c = 2.1$. More interestingly, for dsDNAs with both AT and GC pairs present along the sequence we have found that, as shown in Fig. 5.3(b), for random sequences and alternative AT and GC regions of relatively small size the loop exponent still takes the value 2.1, however, as the periodic size for the AT and GC regions increases, the loop exponent starts to decrease for bubbles of length at the order of 10, and at greater length scales (of order 100) the bubble size distribution is no longer a power law decay and has showed peaks expressing the sequence pattern, which provides evidences that for real dsDNAs with heterogeneous base pairs, the loop exponent more depends on the specific sequence and in some cases it can be smaller than 2.1 indicating that the denaturation is not a first order transition any more.

It is rather interesting to note that during the denaturation process, the strand ends of dsDNA tend to get separated more easily than the strands in the middle. This can be explained by that the fork length distribution follows $p(l) \sim 1/l^{c'}$ as can be derived using the scaling theory for polymer networks of arbitrary topology, and $c' = 0.09$ indicating a very weak dependence on the sizes of forks, This is also demonstrated by our simulation results in Fig. 5.4, where it is shown that near the melting temperature the probabilities of forming forks of different lengths are almost equal.

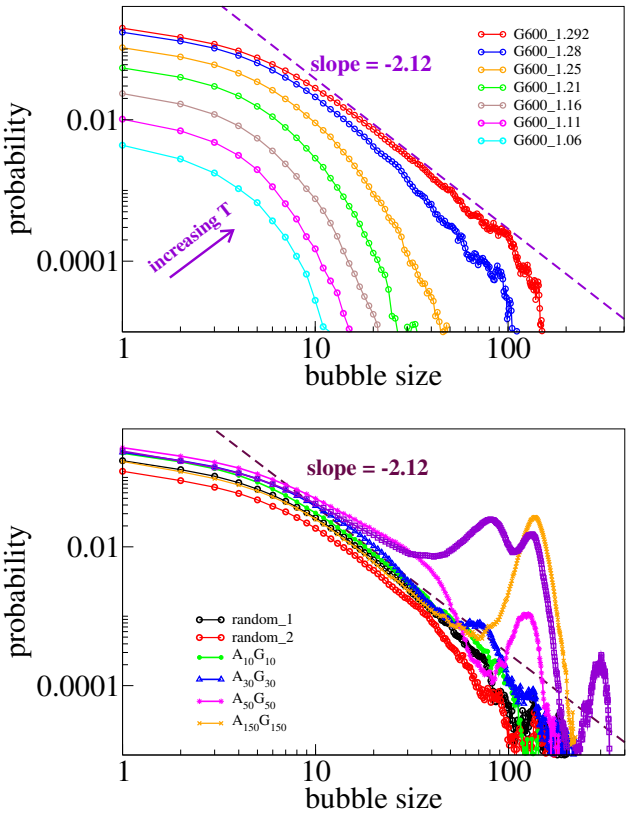

Figure 5.3: Bubble size distribution for a dsDNA G600 at various temperatures. (b) Bubble size distribution for random and periodic sequences at the melting temperature.

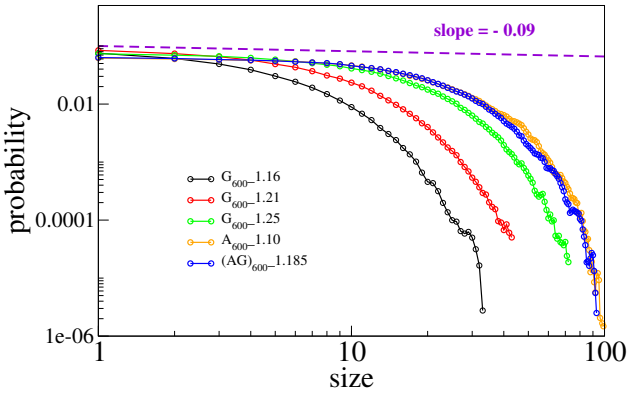

Figure 5.4: Fork length distribution

5.3 Summary and conclusions

To summarize, we have developed a coarse grained model capturing the interplay of the thermodynamic and the mechanic characteristics for dsDNA. In this model, the two strands are modeled as two semiflexible bead-spring polymer chains, in which the heterogeneity are introduced by the same pairing potential of different strengths for AT and GC base pairs. The stiffness of each strand has been implemented with the bending constant as a sigmoid function of the separation of the base pairs. We have performed Langevin dynamics simulations and calibrated the model to recover the melting temperatures to agree with the experimental ranges for various sequences, and as the temperature increased from the physiological condition to the melting temperature, the persistence length varies from that of dsDNA to that of ssDNA. Compared to the recently developed CG models for DNA, our model does not provide a helix structure but has an advantage of studying long sequences yet still preserving many intrinsic properties about DNA.

We further studied the bubble size distribution based our model. We have shown that for a homogeneous dsDNA made of only AT or GC pairs, our simulation results agree with the previous conclusion of first order transition, however, for sequences of periodic AT and GC regions, when the periodic size is relatively large compared to the sequence length, we show that the bubble size distribution exhibits peaks expressing the sequence pattern, and more importantly, the denaturation is no longer a first order transition.

CHAPTER 6
CONCLUSIONS AND OUTLOOK

In this dissertation, we have carried out an extensive study on the equilibrium properties and dynamical characteristics for two-dimensional swollen semi-flexible polymers in the bulk and under channel confinement. We also developed a three-dimensional model of dsDNA in which both mechanical and thermodynamic aspects of dsDNA have been incorporated.

We first developed a new scaling theory of monomer dynamics for semi-flexible polymers in 2D, which is also confirmed by our molecular dynamics simulation results. Our theory predicts novel crossover dynamics at an intermediate time when the fluctuations of the monomers become greater than ℓ_p. Around this time the monomer dynamics becomes the same as that of a fully flexible chain characterized by $t^{2\nu/(2\nu+1)} = t^{0.6}$ in 2D. The theory expands the existing scaling theory for monomer dynamics for a WLC and that of a fully flexible chain to include the effect of the chain persistence length. Fully flexible chains are self similar objects, while a polymer segment up to its own persistence length is not. Therefore, it is expected that for a length scale up to ℓ_p the dynamics will have different characteristics due to bending modes arising out of the chain stiffness. Our theory elucidates the exact role of chain persistence length neither contained in the WLC model nor seen before.

Our study on the end-to-end distance of semi-flexible polymers disapproved the validity of the well-known WLC theory due to severe excluded volume effect in two dimensions, our results show that when not in the rod limit, the RMS end-to-end distance for chains of different contour length and persistence length follows the scaling relation derived by Schaefer, Joanny, and Pincus [59] and Nakanishi [74]. We generalized the understanding of transverse fluctuations for which analytical results only existed for only extremely stiff chains, our numerical results show that the normalized transverse fluctuations for chains in the whole range of stiffness collapse onto one master plot and show non-monotonic behavior with the maximum occurring at $L \gtrapprox \ell_p$.

Chapter 3 studies the elongation of a semi-flexible polymer confined in a two-dimensional strip. Depending on the interplay of the chain length, the persistence length and the width of the strip, different scaling regimes for the elongation exist. Starting from a scaling ansatz proposed by Jun, Thirumalai, and Ha [106], we have summarized and presented scaling relations of the extension for general dimensions. Our simulation results have showed that the controversial extended de Gennes regime is vanishingly small in two dimensions, and analogous to the counterpart in the bulk, the newly discovered Gauss-de Gennes regime by Dorfman [103] due to ideal chain behavior in three dimensions is also absent in a two-dimensional confinement.

In chapter 4 we have compared our results in preceding chapters to results obtained by Monte Carlo simulations on a lattice polymer model. The bead-spring model in continuum space describes natural biopolymers for which the stiffness arises from continuous variations

of the bond angles, and the lattice model depicts more suitably for synthetic polymers where only a limited number of discrete angles are allowed. We have showed that, despite the disparity of local chain conformations between both models, the results for bulk properties are in a good agreement. For confinement in strips with $\ell_p < D$, we have demonstrated that two significant differences exist: (i) The persistence length in the lattice model has a dependence on D thus resulting in a renormalization compared to that in the bulk; (ii) the monomer density profiles near repulsive walls for semi-flexible polymers follow a power law proposed by Semenov [159] in the continuum model, while for the lattice case the same profile tends to a nonzero constant across the strip. And also importantly, for the continuum model we reported direct estimates for the well-know Odjik deflection length and its distributions.

Chapter 6 presents a semi-flexible chain model of dsDNA which is a generalization of the model by Sung *et al.* by including excluded volume effect and heterogeneity. We have demonstrated that depending on the temperature, the persistence length in our model ranges from that of dsDNA to that of ssDNA. In addition, the simulation results from our model confirmed the existing theory for the bubble size probability distribution function for homogeneous sequences and discovered new patterns for heterogeneous sequences.

Up to now, most of this dissertation and majority of the research in the literature have devoted to studying semi-flexible polymers under the equilibrium state, however, from the perspective of gaining insights on processes in an active biological environment such as inside the cell and developing related technological applications, understanding how semi-flexible polymers behave in non-equilibrium states is essential. Indeed, initial efforts have been made

recently towards this direction. Notably, Reisner's group has performed experiments where a single DNA molecule confined and equilibrated inside a nanochannel is compressed from one end of the molecule by a dynamically sliding gasket [189]. The gasket is realized by an optically trapped bead which behaves like a nano-dozer. Interestingly, the monomer concentration profiles at different stages of compression have been studied, and differential equations have been set up in the case that the persistence length ℓ_p of the DNA is much smaller than the channel width D, it is found that depending on the sliding speed of the bead relative to the DNA molecule, different scaling regimes exist for the monomer concentration profile. In a more recent work by the same group [190], the monomer concentration profiles and evolutions of the extension of the molecule are also studied when the sliding bead is being retracted. Despite the initial exploration by Reisner, many areas of interest still remain to be investigated, e.g., it is expected that the differential equation will fail in the case of $\ell_p < D$, thus leading to questions that how the DNA molecule behave when compressed in a narrow channel and how the behavior should be quantified and understood. Another interesting question is how the hydrodynamic effect plays its role when different sliding speeds are applied. Some of these aspects are being studied by us, which will be reported in separate publications.

LIST OF REFERENCES

[1] M. Rubinstein and R. H. Colby, *Polymer Physics*. Oxford University Press, 2003.

[2] R. Phillips, J. Kondev, and J. Theriot, *Physical Biology of the Cell*. Garland Science, 2009.

[3] M. A. Dichtl and E. Sackmann, "Colloidal probe study of short time local and long time reptational motion of semiflexible macromolecules in entangled networks," *New Journal of Physics*, vol. 1, no. 1, p. 18, 1999.

[4] K. Rechendorff, G. Witz, J. Adamcik, and G. Dietler, "Persistence length and scaling properties of single-stranded dna adsorbed on modified graphite," *The Journal of Chemical Physics*, vol. 131, no. 9, 2009.

[5] S. S. Sheiko, B. S. Sumerlin, and K. Matyjaszewski, "Cylindrical molecular brushes: Synthesis, characterization and properties," *Progress in Polymer Science*, vol. 33, no. 7, pp. 759 – 785, 2008.

[6] N. Gunari, M. Schmidt, , and A. Janshoff, "Persistence length of cylindrical brush molecules measured by atomic force microscopy," *Macromolecules*, vol. 39, no. 6, pp. 2219–2224, 2006.

[7] O. Kratky and G. Porod, "Diffuse small-angle scattering of x-rays in colloid systems," *Journal of Colloid Science*, vol. 4, no. 1, pp. 35 – 70, 1949.

[8] O. Kratky and G. Porod, "Rntgenuntersuchung gelster fadenmolekle," *Recueil des Travaux Chimiques des Pays-Bas*, vol. 68, no. 12, pp. 1106–1122, 1949.

[9] M. Doi and S. F. Edwards, *Theory of Polymer Dynamics*. Clarendon Press, Oxford, 1986.

[10] L. D. Landau and E. M. Lifshitz, *Statistical Physics, Part 1, 3rd ed.* Pergamon Press, 1988.

[11] L. Harnau, R. G. Winkler, and P. Reineker, "On the dynamics of polymer melts: Contribution of rouse and bending modes," *EPL (Europhysics Letters)*, vol. 45, no. 4, p. 488, 1999.

[12] R. G. Winkler, "Deformation of semiflexible chains," *The Journal of Chemical Physics*, vol. 118, no. 6, pp. 2919–2928, 2003.

[13] H. Yamakawa, *Modern Theory of Polymer Solution*. Harper & Row Publisher, 1971.

[14] J. Wilhelm and E. Frey, "Radial distribution function of semiflexible polymers," *Phys. Rev. Lett.*, vol. 77, pp. 2581–2584, Sep 1996.

[15] R. Granek, "From semi-flexible polymers to membranes: Anomalous diffusion and reptation," *J. Phys. II France*, vol. 7, no. 12, pp. 1761–1788, 1997.

[16] E. Farge and A. C. Maggs, "Dynamic scattering from semiflexible polymers," *Macromolecules*, vol. 26, no. 19, pp. 5041–5044, 1993.

[17] K. Kroy and E. Frey, "Dynamic scattering from solutions of semiflexible polymers," *Phys. Rev. E*, vol. 55, pp. 3092–3101, Mar 1997.

[18] J. T. Bullerjahn, S. Sturm, L. Wolff, and K. Kroy, "Monomer dynamics of a wormlike chain," *EPL (Europhysics Letters)*, vol. 96, no. 4, p. 48005, 2011.

[19] G. S. Grest and K. Kremer, "Molecular dynamics simulation for polymers in the presence of a heat bath," *Phys. Rev. A*, vol. 33, pp. 3628–3631, 1986.

[20] W. van Gunsteren and H. Berendsen, "Algorithms for brownian dynamics," *Molecular Physics*, vol. 45, no. 3, pp. 637–647, 1982.

[21] T. Odijk, "Polyelectrolytes near the rod limit," *Journal of Polymer Science: Polymer Physics Edition*, vol. 15, no. 3, pp. 477–483, 1977.

[22] T. Odijk, "The statistics and dynamics of confined or entangled stiff polymers," *Macromolecules*, vol. 16, no. 8, pp. 1340–1344, 1983.

[23] P. de Gennes, "Polymers at an interface; a simplified view," *Advances in Colloid and Interface Science*, vol. 27, no. 3, pp. 189 – 209, 1987.

[24] G. Fleer, M. Cohen-Stuart, J. Scheutjens, T. Cosgrove, and B. Vincent, *Polymers at Interfaces*. Chapman & Hall, London, 1993.

[25] E. Eisenriegler, *Polymers Near Surfaces*. World Scientific, Singapore, 1993.

[26] R. R. Netz and D. Andelman, "Neutral and charged polymers at interfaces," *Physics Reports*, vol. 380, no. 12, pp. 1 – 95, 2003.

[27] T. Takebayashi, Y. Morita, and F. Oosawa, "Electronmicroscopic investigation of the flexibility of f-actin," *Biochimica et Biophysica Acta (BBA) - Protein Structure*, vol. 492, no. 2, pp. 357 – 363, 1977.

[28] B. T. Stokke, A. Elgsaeter, G. Skjrak-Brjek, and O. Smidsrd, "The molecular size and shape of xanthan, xylinan, bronchial mucin, alginate, and amylose as revealed by electron microscopy," *Carbohydrate Research*, vol. 160, pp. 13 – 28, 1987.

[29] S. Trachtenberg and I. Hammel, "The rigidity of bacterial flagellar filaments and its relation to filament polymorphism," *Journal of Structural Biology*, vol. 109, no. 1, pp. 18 – 27, 1992.

[30] J. Bednar, P. Furrer, V. Katritch, A. Stasiak, J. Dubochet, and A. Stasiak, "Determination of {DNA} persistence length by cryo-electron microscopy. separation of the static and dynamic contributions to the apparent persistence length of {DNA}," *Journal of Molecular Biology*, vol. 254, no. 4, pp. 579 – 594, 1995.

[31] R. Schoenauer, P. Bertoncini, G. Machaidze, U. Aebi, J.-C. Perriard, M. Hegner, and I. Agarkova, "Myomesin is a molecular spring with adaptable elasticity," *Journal of Molecular Biology*, vol. 349, no. 2, pp. 367 – 379, 2005.

[32] P. Papadopoulos, , G. Floudas*, I. Schnell, , I. Lieberwirth, T. Q. Nguyen, , and H.-A. Klok, "Thermodynamic confinement and -helix persistence length in poly(-benzyl-l-glutamate)-b-poly(dimethyl siloxane)-b-poly(-benzyl-l-glutamate) triblock copolymers," *Biomacromolecules*, vol. 7, no. 2, pp. 618–626, 2006. PMID: 16471939.

[33] X. E. Li, K. C. Holmes, W. Lehman, H. Jung, and S. Fischer, "The shape and flexibility of tropomyosin coiled coils: Implications for actin filament assembly and regulation," *Journal of Molecular Biology*, vol. 395, no. 2, pp. 327 – 339, 2010.

[34] H. G. Hansma and J. H. Hoh, "Biomolecular imaging with the atomic force microscope," *Annual Review of Biophysics and Biomolecular Structure*, vol. 23, no. 1, pp. 115–140, 1994.

[35] N. Yoshinaga, K. Yoshikawa, and S. Kidoaki, "Multiscaling in a long semiflexible polymer chain in two dimensions," *The Journal of Chemical Physics*, vol. 116, no. 22, pp. 9926–9929, 2002.

[36] F. Valle, M. Favre, P. De Los Rios, A. Rosa, and G. Dietler, "Scaling exponents and probability distributions of dna end-to-end distance," *Phys. Rev. Lett.*, vol. 95, p. 158105, Oct 2005.

[37] J. Moukhtar, E. Fontaine, C. Faivre-Moskalenko, and A. Arneodo, "Probing persistence in dna curvature properties with atomic force microscopy," *Phys. Rev. Lett.*, vol. 98, p. 178101, Apr 2007.

[38] N. Mcke, K. Klenin, R. Kirmse, M. Bussiek, H. Herrmann, M. Hafner, and J. Langowski, "Filamentous biopolymers on surfaces: Atomic force microscopy images compared with brownian dynamics simulation of filament deposition," *PLoS ONE*, vol. 4, p. e7756, 11 2009.

[39] J. Moukhtar, C. Faivre-Moskalenko, P. Milani, B. Audit, C. Vaillant, E. Fontaine, F. Mongelard, G. Lavorel, P. St-Jean, P. Bouvet, F. Argoul, and A. Arneodo, "Effect of genomic long-range correlations on dna persistence length: From theory to

single molecule experiments," *The Journal of Physical Chemistry B*, vol. 114, no. 15, pp. 5125–5143, 2010.

[40] B. Maier and J. O. Rädler, "Conformation and self-diffusion of single dna molecules confined to two dimensions," *Phys. Rev. Lett.*, vol. 82, pp. 1911–1914, Mar 1999.

[41] B. Maier, , and J. O. Rdler*, "Dna on fluid membranes: A model polymer in two dimensions," *Macromolecules*, vol. 33, no. 19, pp. 7185–7194, 2000.

[42] P. G. de Gennes, *Scaling Concepts in Polymer Physics*. Cornell-University Press, Ithaca, 1979.

[43] A. D. Sokal, *Monte Carlo and Molecular Dynamics Simulations in Polymer Science, edited by K. Binder, Chapter 2*. Oxford University Press, New York, 1995.

[44] P. J. Flory, *Statistical Mechanics of Chain Molecules*. Hanser, New York, 1989.

[45] A. Y. Grosberg and A. R. Khokhlov, *Statistical Physics of Macromolecules*. AIP Press, New York, 2004.

[46] D. A. D. Parry and E. N. Baker, "Biopolymers," *Reports on Progress in Physics*, vol. 47, no. 9, p. 1133, 1984.

[47] H.-P. Hsu, W. Paul, and K. Binder, "Standard definitions of persistence length do not describe the local intrinsic stiffness of real polymer chains," *Macromolecules*, vol. 43, no. 6, pp. 3094–3102, 2010.

[48] K. Binder, *Monte Carlo and Molecular Dynamics Simulations in Polymer Science, edited by K. Binder, Chapter 1*. Oxford University Press, New York, 1995.

[49] C. Hyeon and D. Thirumalai, "Capturing the essence of folding and functions of biomolecules using coarse-grained models," *Nature Communications*, vol. 2, no. 487, 2011.

[50] H.-P. Hsu, W. Paul, and K. Binder, "Understanding the multiple length scales describing the structure of bottle-brush polymers by monte carlo simulation methods," *Macromolecular Theory and Simulations*, vol. 20, no. 7, pp. 510–525, 2011.

[51] O. Kratky and G. Porod, "Diffuse small-angle scattering of x-rays in colloid systems," *Journal of Colloid Science*, vol. 4, no. 1, pp. 35 – 70, 1949.

[52] R. A. Harris and J. E. Hearst, "On polymer dynamics," *The Journal of Chemical Physics*, vol. 44, no. 7, pp. 2595–2602, 1966.

[53] H.-P. Hsu, W. Paul, and K. Binder, "Breakdown of the kratky-porod wormlike chain model for semiflexible polymers in two dimensions," *EPL (Europhysics Letters)*, vol. 95, no. 6, p. 68004, 2011.

[54] H.-P. Hsu and K. Binder, "Stretching semiflexible polymer chains: Evidence for the importance of excluded volume effects from monte carlo simulation," *The Journal of Chemical Physics*, vol. 136, no. 2, 2012.

[55] H.-P. Hsu, W. Paul, and K. Binder, "Scattering function of semiflexible polymer chains under good solvent conditions," *The Journal of Chemical Physics*, vol. 137, no. 17, 2012.

[56] H.-P. Hsu and K. Binder, "Semi-flexible polymer chains in quasi-one-dimensional confinement: a monte carlo study on the square lattice," *Soft Matter*, vol. 9, pp. 10512–10521, 2013.

[57] P. Grassberger, "Pruned-enriched rosenbluth method: Simulations of θ polymers of chain length up to 1 000 000," *Phys. Rev. E*, vol. 56, pp. 3682–3693, Sep 1997.

[58] H.-P. Hsu and P. Grassberger, "A review of monte carlo simulations of polymers with perm," *Journal of Statistical Physics*, vol. 144, no. 3, pp. 597–637, 2011.

[59] D. W. Schaefer, J. F. Joanny, and P. Pincus, "Dynamics of semiflexible polymers in solution," *Macromolecules*, vol. 13, no. 5, pp. 1280–1289, 1980.

[60] L. Harnau, R. G. Winkler, and P. Reineker, "Dynamic structure factor of semiflexible macromolecules in dilute solution," *The Journal of Chemical Physics*, vol. 104, no. 16, pp. 6355–6368, 1996.

[61] R. Shusterman, S. Alon, T. Gavrinyov, and O. Krichevsky, "Monomer dynamics in double- and single-stranded dna polymers," *Phys. Rev. Lett.*, vol. 92, p. 048303, Jan 2004.

[62] E. P. Petrov, T. Ohrt, R. G. Winkler, and P. Schwille, "Diffusion and segmental dynamics of double-stranded dna," *Phys. Rev. Lett.*, vol. 97, p. 258101, Dec 2006.

[63] M. Hinczewski and R. R. Netz, "Global cross-over dynamics of single semiflexible polymers," *EPL (Europhysics Letters)*, vol. 88, no. 1, p. 18001, 2009.

[64] M. Hinczewski, X. Schlagberger, M. Rubinstein, O. Krichevsky, and R. R. Netz, "End-monomer dynamics in semiflexible polymers," *Macromolecules*, vol. 42, no. 3, pp. 860–875, 2009.

[65] M. Hinczewski and R. R. Netz, "Dynamics of dna: Experimental controversies and theoretical insights," *Physica A: Statistical Mechanics and its Applications*, vol. 389, no. 15, pp. 2993 – 2996, 2010.

[66] M. O. Steinhauser, J. Schneider, and A. Blumen, "Simulating dynamic crossover behavior of semiflexible linear polymers in solution and in the melt," *The Journal of Chemical Physics*, vol. 130, no. 16, 2009.

[67] A. Winkler, P. Virnau, K. Binder, R. G. Winkler, and G. Gompper, "Hydrodynamic mechanisms of spinodal decomposition in confined colloid-polymer mixtures: A multiparticle collision dynamics study," *The Journal of Chemical Physics*, vol. 138, no. 5, 2013.

[68] A. Huang, R. Adhikari, A. Bhattacharya, and K. Binder, "Universal monomer dynamics of a two-dimensional semi-flexible chain," *EPL (Europhysics Letters)*, vol. 105, no. 1, p. 18002, 2014.

[69] *Here we use the same notation as previously used by others to describe the monomer dynamics of the chain [19]-[83].*

[70] L. Schäfer, A. Ostendorf, and J. Hager, "Scaling of the correlations among segment directions of a self-repelling polymer chain," *Journal of Physics A: Mathematical and General*, vol. 32, no. 45, p. 7875, 1999.

[71] P. Cifra, "Differences and limits in estimates of persistence length for semi-flexible macromolecules," *Polymer*, vol. 45, no. 17, pp. 5995 – 6002, 2004.

[72] S. Redner and V. Privman, "Persistency of two-dimensional self-avoiding walks," *Journal of Physics A: Mathematical and General*, vol. 20, no. 13, p. L857, 1987.

[73] L. Schäfer and K. Elsner, "Calculation of the persistence length of a flexible polymer chain with short-range self-repulsion," *The European Physical Journal E*, vol. 13, no. 3, p. 225, 2004.

[74] Nakanishi, H., "Flory approach for polymers in the stiff limit," *J. Phys. France*, vol. 48, no. 6, pp. 979–984, 1987.

[75] J. Moon and H. Nakanishi, "Onset of the excluded-volume effect for the statistics of stiff chains," *Phys. Rev. A*, vol. 44, pp. 6427–6442, Nov 1991.

[76] H.-P. Hsu, W. Paul, and K. Binder, "Polymer chain stiffness vs. excluded volume: A monte carlo study of the crossover towards the worm-like chain model," *EPL (Europhysics Letters)*, vol. 92, no. 2, p. 28003, 2010.

[77] H. Yamakawa and M. Fujii, "Wormlike chains near the rod limit: Path integral in the wkb approximation," *The Journal of Chemical Physics*, vol. 59, no. 12, pp. 6641–6644, 1973.

[78] T. Odijk, "The statistics and dynamics of confined or entangled stiff polymers," *Macromolecules*, vol. 16, no. 8, pp. 1340–1344, 1983.

[79] A. Caspi, M. Elbaum, R. Granek, A. Lachish, and D. Zbaida, "Semiflexible polymer network: A view from inside," *Phys. Rev. Lett.*, vol. 80, pp. 1106–1109, Feb 1998.

[80] A.-L. Barabasi and H. E. Stanley, *Fractal Concepts in Surface Growth*. Cambridge University Press, 1995.

[81] I. Gerroff, A. Milchev, K. Binder, and W. Paul, "A new offlattice monte carlo model for polymers: A comparison of static and dynamic properties with the bondfluctuation model and application to random media," *The Journal of Chemical Physics*, vol. 98, no. 8, pp. 6526–6539, 1993.

[82] A. Milchev, W. Paul, and K. Binder, "Offlattice monte carlo simulation of dilute and concentrated polymer solutions under theta conditions," *The Journal of Chemical Physics*, vol. 99, no. 6, pp. 4786–4798, 1993.

[83] K. Binder and W. Paul, "Monte carlo simulations of polymer dynamics: Recent advances," *Journal of Polymer Science, Part B*, vol. 35, no. 1, p. 1, 1997.

[84] L. Le Goff, O. Hallatschek, E. Frey, and F. m. c. Amblard, "Tracer studies on f-actin fluctuations," *Phys. Rev. Lett.*, vol. 89, p. 258101, Dec 2002.

[85] W. Reisner, J. N. Pedersen, and R. H. Austin, "Dna confinement in nanochannels: physics and biological applications," *Reports on Progress in Physics*, vol. 75, no. 10, p. 106601, 2012.

[86] B. Teague, M. S. Waterman, S. Goldstein, K. Potamousis, S. Zhou, S. Reslewic, D. Sarkar, A. Valouev, C. Churas, J. M. Kidd, S. Kohn, R. Runnheim, C. Lamers, D. Forrest, M. A. Newton, E. E. Eichler, M. Kent-First, U. Surti, M. Livny, and D. C. Schwartz, "High-resolution human genome structure by single-molecule analysis," *Proceedings of the National Academy of Sciences*, vol. 107, no. 24, pp. 10848–10853, 2010.

[87] M. Krishnan, I. Mnchand, and P. Schwille, "Spontaneous stretching of dna in a two-dimensional nanoslit," *Nano Letters*, vol. 7, no. 5, pp. 1270–1275, 2007.

[88] D. J. Bonthuis, C. Meyer, D. Stein, and C. Dekker, "Conformation and dynamics of dna confined in slitlike nanofluidic channels," *Phys. Rev. Lett.*, vol. 101, p. 108303, Sep 2008.

[89] W. Reisner, K. J. Morton, R. Riehn, Y. M. Wang, Z. Yu, M. Rosen, J. C. Sturm, S. Y. Chou, E. Frey, and R. H. Austin, "Statics and dynamics of single dna molecules confined in nanochannels," *Phys. Rev. Lett.*, vol. 94, p. 196101, May 2005.

[90] Y. Kim, K. S. Kim, K. L. Kounovsky, R. Chang, G. Y. Jung, J. J. dePablo, K. Jo, and D. C. Schwartz, "Nanochannel confinement: Dna stretch approaching full contour length," *Lab Chip*, vol. 11, pp. 1721–1729, 2011.

[91] J. O. Tegenfeldt, C. Prinz, H. Cao, S. Chou, W. W. Reisner, R. Riehn, Y. M. Wang, E. C. Cox, J. C. Sturm, P. Silberzan, and R. H. Austin, "The dynamics of genomic-length dna molecules in 100-nm channels," *Proceedings of the National Academy of Sciences of the United States of America*, vol. 101, no. 30, pp. 10979–10983, 2004.

[92] C. H. Reccius, J. T. Mannion, J. D. Cross, and H. G. Craighead, "Compression and free expansion of single dna molecules in nanochannels," *Phys. Rev. Lett.*, vol. 95, p. 268101, Dec 2005.

[93] W. Reisner, N. B. Larsen, A. Silahtaroglu, A. Kristensen, N. Tommerup, J. O. Tegenfeldt, and H. Flyvbjerg, "Single-molecule denaturation mapping of dna in nanofluidic channels," *Proceedings of the National Academy of Sciences*, vol. 107, no. 30, pp. 13294–13299, 2010.

[94] T. Su, S. K. Das, M. Xiao, and P. K. Purohit, "Transition between two regimes describing internal fluctuation of dna in a nanochannel," *PLoS ONE*, vol. 6, p. e16890, 03 2011.

[95] E. R. Mardis, "A decades perspective on dna sequencing technology," *Nature*, vol. 470, p. 198, 2011.

[96] F. Sanger and A. Coulson, "A rapid method for determining sequences in {DNA} by primed synthesis with {DNA} polymerase," *Journal of Molecular Biology*, vol. 94, no. 3, pp. 441 – 448, 1975.

[97] F. Sanger, S. Nicklen, and A. R. Coulson, "Dna sequencing with chain-terminating inhibitors," *Proceedings of the National Academy of Sciences*, vol. 74, no. 12, pp. 5463–5467, 1977.

[98] Y. Yang, T. W. Burkhardt, and G. Gompper, "Free energy and extension of a semiflexible polymer in cylindrical confining geometries," *Phys. Rev. E*, vol. 76, p. 011804, Jul 2007.

[99] C. Manneschi, E. Angeli, T. Ala-Nissila, L. Repetto, G. Firpo, and U. Valbusa, "Conformations of dna in triangular nanochannels," *Macromolecules*, vol. 46, no. 10, pp. 4198–4206, 2013.

[100] Y. Wang, D. R. Tree, and K. D. Dorfman, "Simulation of dna extension in nanochannels," *Macromolecules*, vol. 44, no. 16, pp. 6594–6604, 2011.

[101] A. Huang, R. Adhikari, A. Bhattacharya, and K. Binder, "Universal monomer dynamics of a two-dimensional semi-flexible chain," *EPL (Europhysics Letters)*, vol. 105, no. 1, p. 18002, 2014.

[102] Daoud, M. and De Gennes, P.G., "Statistics of macromolecular solutions trapped in small pores," *J. Phys. France*, vol. 38, no. 1, pp. 85–93, 1977.

[103] D. R. Tree, Y. Wang, and K. D. Dorfman, "Extension of dna in a nanochannel as a rod-to-coil transition," *Phys. Rev. Lett.*, vol. 110, p. 208103, May 2013.

[104] T. Odijk, "Scaling theory of dna confined in nanochannels and nanoslits," *Phys. Rev. E*, vol. 77, p. 060901, Jun 2008.

[105] L. Dai, J. J. Jones, J. R. C. van der Maarel, and P. S. Doyle, "A systematic study of dna conformation in slitlike confinement," *Soft Matter*, vol. 8, pp. 2972–2982, 2012.

[106] S. Jun, D. Thirumalai, and B.-Y. Ha, "Compression and stretching of a self-avoiding chain in cylindrical nanopores," *Phys. Rev. Lett.*, vol. 101, p. 138101, Sep 2008.

[107] *In this case one can use the same free energy expression of Eqn. 3.2 replacing* $D \rightarrow H$ *[103].*

[108] *This result is valid both in two and three dimensions as can be seen fron the expansion of various averages for worm like chains near the rod limit [77, 13].*

[109] *Analytic calculations [98] for a cylindrical/square channel supported by numerical calculations indicate that this prefactor A is universal, although there is no general proof. Our results in this letter also support this claim.*

[110] T. W. Burkhardt, Y. Yang, and G. Gompper, "Fluctuations of a long, semiflexible polymer in a narrow channel," *Phys. Rev. E*, vol. 82, p. 041801, Oct 2010.

[111] K. Jo, D. M. Dhingra, T. Odijk, J. J. de Pablo, M. D. Graham, R. Runnheim, D. Forrest, and D. C. Schwartz, "A single-molecule barcoding system using nanoslits for dna analysis," *Proceedings of the National Academy of Sciences*, vol. 104, no. 8, pp. 2673–2678, 2007.

[112] K. Shin1, S. Obukhov, J.-T. Chen, J. Huh, Y. Hwang, S. Mok, P. Dobriyal, P. Thiyagarajan, and T. P. Russell, "Tenhanced mobility of confined polymers," *Nature Materials*, vol. 6, pp. 961 – 965, 2007.

[113] P.-K. Lin, K. hui Lin, C.-C. Fu, K.-C. Lee, P.-K. Wei, W.-W. Pai, P.-H. Tsao, Y.-L. Chen, and W. S. Fann, "One-dimensional dynamics and transport of dna molecules in a quasi-two-dimensional nanoslit," *Macromolecules*, vol. 42, no. 5, pp. 1770–1774, 2009.

[114] J. Tang, S. L. Levy, D. W. Trahan, J. J. Jones, H. G. Craighead, and P. S. Doyle, "Revisiting the conformation and dynamics of dna in slitlike confinement," *Macromolecules*, vol. 43, no. 17, pp. 7368–7377, 2010.

[115] H. Uemura, M. Ichikawa, and Y. Kimura, "Crossover behavior in static and dynamic properties of a single dna molecule from three to quasi-two dimensions," *Phys. Rev. E*, vol. 81, p. 051801, May 2010.

[116] K. D. Dorfman, D. Gupta, A. Jain, A. Muralidhar, and D. R. Tree, "Hydrodynamics of dna confined in nanoslits and nanochannels," *The European Physical Journal Special Topics*, vol. 223, no. 14, pp. 3179–3200, 2014.

[117] W. F. Reinhart, J. G. Reifenberger, D. Gupta, A. Muralidhar, J. Sheats, H. Cao, and K. D. Dorfman, "Distribution of distances between dna barcode labels in nanochannels close to the persistence length," *The Journal of Chemical Physics*, vol. 142, no. 6, 2015.

[118] T. Odijk, "Similarity applied to the statistics of confined stiff polymers," *Macromolecules*, vol. 17, no. 3, pp. 502–503, 1984.

[119] T. Odijk, "Theory of lyotropic polymer liquid crystals," *Macromolecules*, vol. 19, no. 9, pp. 2313–2329, 1986.

[120] T. W. Burkhardt, "Free energy of a semiflexible polymer in a tube and statistics of a randomly-accelerated particle," *Journal of Physics A: Mathematical and General*, vol. 30, no. 7, p. L167, 1997.

[121] G. Morrison and D. Thirumalai, "The shape of a flexible polymer in a cylindrical pore," *The Journal of Chemical Physics*, vol. 122, no. 19, 2005.

[122] J. Z. Y. Chen and D. E. Sullivan, "Free energy of a wormlike polymer chain confined in a slit: crossover between two scaling regimes," *Macromolecules*, vol. 39, no. 22, pp. 7769–7773, 2006.

[123] Y. Jung, S. Jun, and B.-Y. Ha, "Self-avoiding polymer trapped inside a cylindrical pore: Flory free energy and unexpected dynamics," *Phys. Rev. E*, vol. 79, p. 061912, Jun 2009.

[124] F. Throff, F. Wagner, and E. Frey, "The effect of internal and global modes on the radial distribution function of confined semiflexible polymers," *EPL (Europhysics Letters)*, vol. 91, no. 3, p. 38004, 2010.

[125] F. Thüroff, B. Obermayer, and E. Frey, "Longitudinal response of confined semiflexible polymers," *Phys. Rev. E*, vol. 83, p. 021802, Feb 2011.

[126] Y.-L. Chen, M. D. Graham, J. J. de Pablo, G. C. Randall, M. Gupta, and P. S. Doyle, "Conformation and dynamics of single dna molecules in parallel-plate slit microchannels," *Phys. Rev. E*, vol. 70, p. 060901, Dec 2004.

[127] P. Cifra, "Channel confinement of flexible and semiflexible macromolecules," *The Journal of Chemical Physics*, vol. 131, no. 22, 2009.

[128] P. Cifra, Z. Benkov, and T. Bleha, "Chain extension of dna confined in channels," *The Journal of Physical Chemistry B*, vol. 113, no. 7, pp. 1843–1851, 2009.

[129] P. Cifra, "Weak-to-strong confinement transition of semi-flexible macromolecules in slit and in channel," *The Journal of Chemical Physics*, vol. 136, no. 2, 2012.

[130] J. Z. Y. Chen, "Free energy and extension of a wormlike chain in tube confinement," *Macromolecules*, vol. 46, no. 24, pp. 9837–9844, 2013.

[131] L. Dai and P. S. Doyle, "Comparisons of a polymer in confinement versus applied force," *Macromolecules*, vol. 46, no. 15, pp. 6336–6344, 2013.

[132] H.-P. Hsu and K. Binder, "Semiflexible macromolecules with discrete bond angles confined in nanoslits: A monte carlo test of scaling concepts," *Macromolecules*, vol. 46, no. 19, pp. 8017–8025, 2013.

[133] A. Huang and A. Bhattacharya, "Dna confined in a two-dimensional strip geometry," *EPL (Europhysics Letters)*, vol. 106, no. 1, p. 18004, 2014.

[134] A. Muralidhar, D. R. Tree, Y. Wang, and K. D. Dorfman, "Interplay between chain stiffness and excluded volume of semiflexible polymers confined in nanochannels," *The Journal of Chemical Physics*, vol. 140, no. 8, 2014.

[135] L. Dai, J. van der Maarel, and P. S. Doyle, "Extended de gennes regime of dna confined in a nanochannel," *Macromolecules*, vol. 47, no. 7, pp. 2445–2450, 2014.

[136] Z. Benkova, P. Namer, and P. Cifra, "Stripe to slab confinement for the linearization of macromolecules in nanochannels," *Soft Matter*, vol. 11, pp. 2279–2289, 2015.

[137] K. Kremer and K. Binder, "Dynamics of polymer chains confined into tubes: Scaling theory and monte carlo simulations," *The Journal of Chemical Physics*, vol. 81, no. 12, pp. 6381–6394, 1984.

[138] A. Milchev, W. Paul, and K. Binder, "Polymer chains confined into tubes with attractive walls: A monte carlo simulation," *Macromolecular Theory and Simulations*, vol. 3, no. 2, pp. 305–323, 1994.

[139] P. Sotta, A. Lesne, and J. M. Victor, "Monte carlo simulation of a grafted polymer chain confined in a tube," *The Journal of Chemical Physics*, vol. 112, no. 3, pp. 1565–1573, 2000.

[140] H.-P. Hsu and P. Grassberger, "2-dimensional polymers confined in a strip," *The European Physical Journal B - Condensed Matter and Complex Systems*, vol. 36, no. 2, pp. 209–214, 2003.

[141] R. M. Jendrejack, E. T. Dimalanta, D. C. Schwartz, M. D. Graham, and J. J. de Pablo, "Dna dynamics in a microchannel," *Phys. Rev. Lett.*, vol. 91, p. 038102, Jul 2003.

[142] R. M. Jendrejack, D. C. Schwartz, M. D. Graham, and J. J. de Pablo, "Effect of confinement on dna dynamics in microfluidic devices," *The Journal of Chemical Physics*, vol. 119, no. 2, pp. 1165–1173, 2003.

[143] H.-P. Hsu, K. Binder, L. I. Klushin, and A. M. Skvortsov, "What is the order of the two-dimensional polymer escape transition?," *Phys. Rev. E*, vol. 76, p. 021108, Aug 2007.

[144] H.-P. Hsu, K. Binder, L. I. Klushin, and A. M. Skvortsov, "Escape transition of a polymer chain from a nanotube: How to avoid spurious results by use of the force-biased pruned-enriched rosenbluth algorithm," *Phys. Rev. E*, vol. 78, p. 041803, Oct 2008.

[145] L. I. Klushin, A. M. Skvortsov, H.-P. Hsu, and K. Binder, "Dragging a polymer chain into a nanotube and subsequent release," *Macromolecules*, vol. 41, no. 15, pp. 5890–5898, 2008.

[146] A. Milchev, L. Klushin, A. Skvortsov, and K. Binder, "Ejection of a polymer chain from a nanopore: Theory and computer experiment," *Macromolecules*, vol. 43, no. 16, pp. 6877–6885, 2010.

[147] J. C. Le Guillou and J. Zinn-Justin, "Critical exponents from field theory," *Phys. Rev. B*, vol. 21, pp. 3976–3998, May 1980.

[148] T. Odijk, "Dna confined in nanochannels: Hairpin tightening by entropic depletion," *The Journal of Chemical Physics*, vol. 125, no. 20, 2006.

[149] C. Bustamante, J. Marko, E. Siggia, and S. Smith, "Entropic elasticity of lambda-phage dna," *Science*, vol. 265, no. 5178, pp. 1599–1600, 1994.

[150] J. T. Titantah, C. Pierleoni, and J.-P. Ryckaert, "Single chain elasticity and thermoelasticity of polyethylene," *The Journal of Chemical Physics*, vol. 117, no. 19, pp. 9028–9036, 2002.

[151] M. Rawiso, R. Duplessix, and C. Picot, "Scattering function of polystyrene," *Macromolecules*, vol. 20, no. 3, pp. 630–648, 1987.

[152] J. S. Pedersen and P. Schurtenberger, "Static properties of polystyrene in semidilute solutions: A comparison of monte carlo simulation and small-angle neutron scattering results," *EPL (Europhysics Letters)*, vol. 45, no. 6, p. 666, 1999.

[153] T. Norisuye and H. Fujita, "Excluded-volume effects in dilute polymer solutions. xiii. effects of chain stiffness," *Polymer Journal*, vol. 14, pp. 143–147, 1982.

[154] G. Maurstad, S. Danielsen, and B. T. Stokke, "Analysis of compacted semiflexible polyanions visualized by atomic force microscopy: influence of chain stiffness on the morphologies of polyelectrolyte complexes," *The Journal of Physical Chemistry B*, vol. 107, no. 32, pp. 8172–8180, 2003.

[155] A. R. Khokhlov and A. N. Semenov, "Liquid-crystalline ordering in solutions of semiflexible macromolecules with rotational-isomeric flexibility," *Macromolecules*, vol. 17, no. 12, pp. 2678–2685, 1984.

[156] F. Latinwo and C. M. Schroeder, "Model systems for single molecule polymer dynamics," *Soft Matter*, vol. 7, pp. 7907–7913, 2011.

[157] R. G. Winkler, P. Reineker, and L. Harnau, "Models and equilibrium properties of stiff molecular chains," *The Journal of Chemical Physics*, vol. 101, no. 9, pp. 8119–8129, 1994.

[158] T. Vogel, T. Neuhaus, M. Bachmann, and W. Janke, "Thermodynamics of tubelike flexible polymers," *Phys. Rev. E*, vol. 80, p. 011802, Jul 2009.

[159] A.N. Semenov, "Adsorption of a semiflexible wormlike chain," *Eur. Phys. J. E*, vol. 9, no. 4, pp. 353–363, 2002.

[160] A. Huang, A. Bhattacharya, and K. Binder, "Conformations, transverse fluctuations, and crossover dynamics of a semi-flexible chain in two dimensions," *The Journal of Chemical Physics*, vol. 140, no. 21, 2014.

[161] L. F. Liu, L. Perkocha, R. Calendar, and J. C. Wang, "Knotted dna from bacteriophage capsids," *Proceedings of the National Academy of Sciences*, vol. 78, no. 9, pp. 5498–5502, 1981.

[162] V. V. Rybenkov, N. R. Cozzarelli, and A. V. Vologodskii, "Probability of dna knotting and the effective diameter of the dna double helix," *Proceedings of the National Academy of Sciences*, vol. 90, no. 11, pp. 5307–5311, 1993.

[163] D. Reith, H. Meyer, and F. Mller-Plathe, "Mapping atomistic to coarse-grained polymer models using automatic simplex optimization to fit structural properties," *Macromolecules*, vol. 34, no. 7, pp. 2335–2345, 2001.

[164] W. Humphrey, A. Dalke, and K. Schulten, "Vmd: Visual molecular dynamics," *Journal of Molecular Graphics*, vol. 14, no. 1, pp. 33 – 38, 1996.

[165] E. Eisenriegler, K. Kremer, and K. Binder, "Adsorption of polymer chains at surfaces: Scaling and monte carlo analyses," *The Journal of Chemical Physics*, vol. 77, no. 12, pp. 6296–6320, 1982.

[166] A. Muralidhar, D. R. Tree, and K. D. Dorfman, "Backfolding of wormlike chains confined in nanochannels," *Macromolecules*, vol. 47, no. 23, pp. 8446–8458, 2014.

[167] E. T. Kool, "Hydrogen bonding, base stacking, and steric effects in dna replication," *Annual Review of Biophysics and Biomolecular Structure*, vol. 30, no. 1, pp. 1–22, 2001.

[168] D. Poland and H. A. Scheraga, *Theory of Helix-Coil Transition.* Academic Press, New York, 1970.

[169] D. Poland and H. A. Scheraga, "Phase transitions in one dimension and the helix-coil transition in polyamino acids," *The Journal of Chemical Physics*, vol. 45, no. 5, pp. 1456–1463, 1966.

[170] D. Poland and H. A. Scheraga, "Occurrence of a phase transition in nucleic acid models," *The Journal of Chemical Physics*, vol. 45, no. 5, pp. 1464–1469, 1966.

[171] R. D. Blake and S. G. Delcourt, "Thermal stability of dna," *Nucleic Acids Research*, vol. 26, no. 14, pp. 3323–3332, 1998.

[172] R. D. Blake, J. W. Bizzaro, J. D. Blake, G. R. Day, S. G. Delcourt, J. Knowles, K. A. Marx, and J. SantaLucia, "Statistical mechanical simulation of polymeric dna melting with meltsim.," *Bioinformatics*, vol. 15, no. 5, pp. 370–375, 1999.

[173] M. Peyrard and A. R. Bishop, "Statistical mechanics of a nonlinear model for dna denaturation," *Phys. Rev. Lett.*, vol. 62, pp. 2755–2758, Jun 1989.

[174] T. Dauxois, M. Peyrard, and A. R. Bishop, "Dynamics and thermodynamics of a nonlinear model for dna denaturation," *Phys. Rev. E*, vol. 47, pp. 684–695, Jan 1993.

[175] T. A. Knotts, N. Rathore, D. C. Schwartz, and J. J. de Pablo, "A coarse grain model for dna," *The Journal of Chemical Physics*, vol. 126, no. 8, 2007.

[176] E. Sambriski, D. Schwartz, and J. de Pablo, "A mesoscale model of {DNA} and its renaturation," *Biophysical Journal*, vol. 96, no. 5, pp. 1675 – 1690, 2009.

[177] G. S. Freeman, D. M. Hinckley, and J. J. de Pablo, "A coarse-grain three-site-per-nucleotide model for dna with explicit ions," *The Journal of Chemical Physics*, vol. 135, no. 16, 2011.

[178] D. M. Hinckley, G. S. Freeman, J. K. Whitmer, and J. J. de Pablo, "An experimentally-informed coarse-grained 3-site-per-nucleotide model of dna: Structure, thermodynamics, and dynamics of hybridization," *The Journal of Chemical Physics*, vol. 139, no. 14, 2013.

[179] D. M. Hinckley, J. P. Lequieu, and J. J. de Pablo, "Coarse-grained modeling of dna oligomer hybridization: Length, sequence, and salt effects," *The Journal of Chemical Physics*, vol. 141, no. 3, 2014.

[180] G. S. Freeman, D. M. Hinckley, J. P. Lequieu, J. K. Whitmer, and J. J. de Pablo, "Coarse-grained modeling of dna curvature," *The Journal of Chemical Physics*, vol. 141, no. 16, 2014.

[181] G. S. Freeman, J. P. Lequieu, D. M. Hinckley, J. K. Whitmer, and J. J. de Pablo, "Dna shape dominates sequence affinity in nucleosome formation," *Phys. Rev. Lett.*, vol. 113, p. 168101, Oct 2014.

[182] D. R. Tree, A. Muralidhar, P. S. Doyle, and K. D. Dorfman, "Is dna a good model polymer?," *Macromolecules*, vol. 46, no. 20, pp. 8369–8382, 2013.

[183] J.-H. Jeon, W. Sung, and F. H. Ree, "A semiflexible chain model of local denaturation in double-stranded dna," *The Journal of Chemical Physics*, vol. 124, no. 16, 2006.

[184] J.-Y. Kim, J.-H. Jeon, and W. Sung, "A breathing wormlike chain model on dna denaturation and bubble: Effects of stacking interactions," *The Journal of Chemical Physics*, vol. 128, no. 5, 2008.

[185] O.-c. Lee, J.-H. Jeon, and W. Sung, "How double-stranded dna breathing enhances its flexibility and instability on short length scales," *Phys. Rev. E*, vol. 81, p. 021906, Feb 2010.

[186] H. Szatyowicz and N. Sadlej-Sosnowska, "Characterizing the strength of individual hydrogen bonds in dna base pairs," *Journal of Chemical Information and Modeling*, vol. 50, no. 12, pp. 2151–2161, 2010.

[187] M. E. Fisher, "Effect of excluded volume on phase transitions in biopolymers," *The Journal of Chemical Physics*, vol. 45, no. 5, pp. 1469–1473, 1966.

[188] Y. Kafri, D. Mukamel, and L. Peliti, "Why is the dna denaturation transition first order?," *Phys. Rev. Lett.*, vol. 85, pp. 4988–4991, Dec 2000.

[189] A. Khorshid, P. Zimny, D. Tétreault-La Roche, G. Massarelli, T. Sakaue, and W. Reisner, "Dynamic compression of single nanochannel confined dna via a nanodozer assay," *Phys. Rev. Lett.*, vol. 113, p. 268104, Dec 2014.

[190] A. Khorshid, S. Amin, Z. Zhang, T. Sakaue, and W. W. Reisner, "Nonequilibrium dynamics of nanochannel confined dna," *Macromolecules*, vol. 0, no. 0, p. null, 0.